Characterization and control of biofilm and biofluid microstructure and rheology

Goldina Kwandou

A thesis in fulfilment of the requirements for the degree of

Doctor of Philosophy

School of Chemical Engineering

Faculty of Engineering

August 2018

Thesis/Dissertation Sheet

Surname/Family Name	:	**KWANDOU**
Given Name/s	:	**Goldina**
Abbreviation for degree as give in the University calendar	:	**PhD**
Faculty	:	**Engineering**
School	:	**School of Chemical Engineering**
Thesis Title	:	**Characterization and control of biofilm and biofluid microstructure and rheology**

Abstract

Bacterial cells can sometimes form and thrive within biofilms, a community of cells embedded in a self-produced extracellular polysaccharide (EPS) matrix. The EPS gives biofilms three-dimensional structures, protecting cells in biofilms by making them more resistant to chemical and physical attack. It is thought that the proper characterisation of biofilms is important to design treatments for their removal. The main problem is that biofilms are very complex and often heterogeneous, making them difficult to characterise and model. In addition, the restructuring of biofilms can be a result of changes in their growth environments or even removal treatments, complicating characterisation.

This thesis aims to understand how environments or treatments can change the structural features of a biofilm and also to expand the knowledge of structural heterogeneity they possess. A literature review on structural heterogeneity in different systems of biofluids summarises current knowledge in the field. The first part of the project focuses on development of a model biofilm with controlled heterogeneity, using natural polysaccharide derived from *S. elodea* biofilm. Here, it was found that although heterogeneity can be controlled, it can be highly variable in the relevant length scale. In the second part of the project, an *E.coli* biofilm was exposed to plasma treatment, a common disinfection approach. Plasma rearranges biofilm structure by local dehydration, making biofilm more resistant to subsequent treatments. Lastly, the project evaluates the effect of environmental change on the microstructure of *A. xylinum* biofilm by increasing viscosity of its growth medium. This biofilm produces a thick cellulose pellicle, but instead of being harmful, its properties are actually useful for many applications for example, as a scaffold in tissue engineering. Addition of alginate changes the pellicle microstructure, making it denser in an analogous effect to that of the plasma treatment studied earlier, but does not affect its actual growth process.

The thesis summarises the insights gained into characterisation, modification, and engineering of biofilm properties and points to opportunities for future research and development in this area.

ORIGINALITY STATEMENT

‘I hereby declare that this submission is my own work and to the best of my knowledge it contains no materials previously published or written by another person, or substantial proportions of material which have been accepted for the award of any other degree or diploma at UNSW or any other educational institution, except where due acknowledgement is made in the thesis. Any contribution made to the research by others, with whom I have worked at UNSW or elsewhere, is explicitly acknowledged in the thesis. I also declare that the intellectual content of this thesis is the product of my own work, except to the extent that assistance from others in the project's design and conception or in style, presentation and linguistic expression is acknowledged.’

Signed …….....

Date ……30/8/2018……

COPYRIGHT STATEMENT

AUTHENTICITY STATEMENT

INCLUSION OF PUBLICATION STATEMENT

UNSW is supportive of candidates publishing their research results during their candidature as detailed in the UNSW Thesis Examination Procedure.

Publications can be used in their thesis in lieu of a Chapter if:

- The student contributed greater than 50% of the content in the publication and is the "primary author", ie. the student was responsible primarily for the planning, execution and preparation of the work for publication
- The student has approval to include the publication in their thesis in lieu of a Chapter from their supervisor and Postgraduate Coordinator.
- The publication is not subject to any obligations or contractual agreements with a third party that would constrain its inclusion in the thesis

Please indicate whether this thesis contains published material or not.

☐ *This thesis contains no publications, either published or submitted for publication (if this box is checked, you may delete all the material on page 2)*

☐ *Some of the work described in this thesis has been published and it has been documented in the relevant Chapters with acknowledgement (if this box is checked, you may delete all the material on page 2)*

☒ *This thesis has publications (either published or submitted for publication) incorporated into it in lieu of a chapter and the details are presented below*

CANDIDATE'S DECLARATION

I declare that:

- I have complied with the Thesis Examination Procedure
- where I have used a publication in lieu of a Chapter, the listed publication(s) below meet(s) the requirements to be included in the thesis.

Name	Signature	Date (dd/mm/yy)
Goldina Kwandou		30/8/2018

Postgraduate Coordinator's Declaration (to be filled in where publications are used in lieu of Chapters)

I declare that:

- the information below is accurate
- where listed publication(s) have been used in lieu of Chapter(s), their use complies with the Thesis Examination Procedure
- the minimum requirements for the format of the thesis have been met.

PGC's Name	PGC's Signature	Date (dd/mm/yy)

For each publication incorporated into the thesis in lieu of a Chapter, provide all of the requested details and signatures required

Details of publication #1:
Full title: *Atmospheric air plasma induces increased cell aggregation during the formation of* Escherichia coli *biofilms*

Authors: *Goldina Kwandou, Anne Mai-Prochnow, Stuart W. Prescott, Patrick T. Spicer, Patrick J. Cullen*

Journal or book name: *Plasma Processes and Polymers*

Volume/page numbers: 2018, e1700212

Date accepted/ published*: 6th May 2018*

Status	*Published*		*Accepted and In press*	***x***	*In progress (submitted)*	

The Candidate's Contribution to the Work
The candidate did the experiment, analysed the data and wrote the paper

Location of the work in the thesis and/or how the work is incorporated in the thesis:
Chapter 4

Primary Supervisor's Declaration
I declare that:
- the information above is accurate
- this has been discussed with the PGC and it is agreed that this publication can be included in this thesis in lieu of a Chapter
- All of the co-authors of the publication have reviewed the above information and have agreed to its veracity by signing a 'Co-Author Authorisation' form.

Supervisor's name	***Supervisor's signature***	***Date (dd/mm/yy)***

Acknowledgements

First of all, I would like to thank my dearest supervisor - Patrick Spicer for his valuable time and patience to guide and help me throughout my PhD. His constant support and encouragement helped me to grow as a better researcher and even better person. I am also grateful to my ex-supervisor PJ Cullen, for teaching me everything about plasma. I would like also to thank my co-supervisor Stuart Prescott, for his knowledge in polymer science and his essential help with Python.

I would like to thank our collaborator, Anne-Mai Prochnow from CSIRO who taught me microbiology and how to grow biofilm.

Also, I would like to thank BMIF staffs at UNSW for their help with the various confocal microscopes.

I would also like to give a special thanks to the Post Doc in our group - Firoozeh Babayekhorasani for her passion for microrheology, and all the other lessons I learnt from her.

I would also like to thank my friends in Complex Fluids group – Haiqiao, who helped me by giving me ideas when I was stuck during these years; Jie, for your immense help at the beginning of my PhD, I will always be grate to you; Zengyi, for your help with all lab issues and Isaac, for your help with matplotlib plotting. And also I would like to thank the newer members of Complex Fluids group – Haoda, Zhiwei and Wenjia for the friendship the past year. I also would like to thank the visiting students from America in the group that I met during my PhD, Abby, Jerome and Tamas and from France, Vincent for the friendship. Thank you to our previous Pot Doc, Vincent for his help in the lab and also the friendship.

I would to express my special thanks to Matthew, who is also a visiting student in the group who is now my good friend, I will not forget all the sushi dinners we had and the “crazy things” we did when you were here. I’m hoping the best for your study in Spain. I also want to thank my collaborator turned friend, Rhiannon

who also taught me more about polymers and also helped correct my writing; I hope all the best for you in Germany.

Thank you to my office mates: Kak Dilla, Hassan and Florence. Thank you for all the chats and even consultations you guys gave me when I'm very much stressed.

I would like to thank my best friend Evelyn, for all the support you gave me and the constant reminder to take care of my health and even when you offered to bring me food when I was too busy and skipping my meals. Thank you to James, for being an amazing friend since my pre-uni (foundation) year.

I would like to express my gratitude to Michele Pozzoli – who constantly gives me his love, support, and even scientific help. I am so grateful to have you in my life.

Last but not least, I would like to thank my family – my mom, my dad, and also my sister, who has always supported me, believed in me even prayed for my success. Thank you to my grandpa who motivates me to even start a PhD, without him I would not even get to this point in my life.

Table of Contents

Originality statement ii
Copyright statement iii
Authenticity statement iii
Inclusion of Publication statement iv
Acknowledgements vi
Table of Contents viii
List of Figures xii
List of Tables xvi
List of Abbreviations xvii
Thesis Abstract xviii
Chapter 1 1
1.1 Background 2
1.2 Aim and objectives 2
1.3 Thesis summary 3
Chapter 2 4
2.1 Introduction to biofluids 5
2.1.1 | Definition of biofluids and their functions 5
2.1.2 | Biofluid rheology and heterogeneity 7
2.2 The origins of biofluids microstructural heterogeneity 9
2.2.1 | Role of interaction between fluid components 9
2.2.2 | Effect of change in chemical environment 13
2.2.3 | Effect of change in physical environment 15
2.3 Quantification of biofluid heterogeneity 16
2.3.1 | Microscopic features 16
2.3.2 | Molecular Transport 16
2.3.3 | Mechanical properties 19
2.4 Structural heterogeneity and transport into biofluids 20
2.5 Structural heterogenity and properties of biofluids 23
2.5.1 | Effect on biopolymer gelation 23

2.5.2 | Effect to mechanical properties 24
2.5.3 | Effects of behaviour and properties of cells in ECM matrix 24
2.6 Conclusions 26
2.7 References 27
Chapter 3 38
3.1 Introduction 39
3.2 Materials and methods 43
3.2.1 | Gellan gel preparation 43
3.2.2 | Bulk rheology experiment 44
3.2.3 | Microrheology experiments 44
3.3 Results and discussions 45
3.3.1 | Effect of salts on gellan rheology 45
3.3.2 | Heterogeneity of gellan gels with different mixture of salts 47
3.3.3 | Heterogeneity of two mixed gellan gels 50
3.3.4 | Heterogeneity of gellan gels in a capillary 57
3.4 Conclusions 60
3.5 References 62
Chapter 4 66
4.1 Introduction 67
4.2 Materials and methods 68
4.2.1 | Preparation of biofilm sample 68
4.2.2 | Plasma setup 69
4.2.3 | Plasma-biofilm treatment conditions 70
4.2.3.1 | Direct treatment 70
4.2.3.2 | Indirect (liquid) treatment 71
4.2.4 | Confocal Laser Scanning Microscopy (CLSM) 72
4.2.5 | Image analysis 72
4.2.6 | Hydrogen peroxide (H_2O_2) measurement 73
4.3 Results and discussions 73
4.3.1 | The effect of plasma treatment on biofilm structure 73
4.3.2 | Regrowth of surviving bacteria 78

4.3.3 | The effect of plasma-induced biofilm structure on subsequent treatment 79
4.3.4 | The effect of plasma chemicals on biofilm structure 81
4.3.5 | Dilution effect on biofilm structure 85
4.3.6 | Explanation of structure formation 88
4.4 Conclusions 90
4.5 References 91
Chapter 5 95
5.1 Introduction 96
5.2 Materials and methods 99
5.2.1 | Preparation of alginate solution 99
5.2.2 | Bacterial cellulose production 99
5.2.3 | Preparation of cellulose dispersion 100
5.2.4 | Measurement of pellicle properties 100
5.2.5 | Rheological measurement 100
5.2.6 | Zeta potential measurement 101
5.2.7 | Confocal Laser Scanning Microscopy (CLSM) 101
5.2.8 | Calculation of intermolecular forces 101
5.2.9 | Calculation of cellulose surface area exposed to alginate 103
5.3 Results and discussions 103
5.3.1 | The growth of bacterial cellulose pellicle 103
5.3.2 | Effect of growth medium rheology on properties of pellicle 105
5.3.3 | Effect of medium viscosity on mechanical properties of a cellulose pellicle 109
5.3.4 | Time-dependent properties of pellicles during growth 111
5.3.5 | The attraction between alginate and cellulose, and its effect on pellicle final structure 113
5.4 Conclusions 117
5.5 References 118
CHAPTER 6 121
6.1 General Conclusion 122
6.2 Recommendations for future study 123
Appendices 125

List of Figures

FIGURE 2.1 Heterogeneity in different biological systems. Pictures were taken from references [1, 8-13]. 7

FIGURE 2.2 Type of interactions commonly occurring in biofluids. Pictures were taken from reference [29, 30] 9

FIGURE 2.3 Sources of interaction in biofluids. Pictures were taken from reference [1, 33] 10

FIGURE 2.4 van-Hove correlation functions of particles diffusing in a) homogeneous medium, b) heterogeneous medium. Pictures were reproduced from ref [86] with permission 18

FIGURE 2.5 The permeability of a biofluid barrier. Picture was taken from reference [106] 22

FIGURE 3.1 Bulk rheology of 0.25% gellan with two different salts; a) Stress sweep results at 1Hz, b) calculated tan δ. Closed symbol indicates storage modulus (G'), while open symbol indicates loss modulus (G") 46

FIGURE 3.2 a) Storage modulus of gels with different proportions of KCl and NaCl, b) Loss modulus of gels with different proportion KCl and NaCl, c) Tan δ of gels with different proportion KCl and NaCl 47

FIGURE 3.3 a) Particle diffusive trajectories in gels with different proportion of KCl and NaCl, b) The average MSDs of particles diffusing in gels with different proportions of salts (black line indicates slope equals to 1), c) van Hove correlation of gels with different proportion of NaCl and KCl at t = 0.5s. 49

FIGURE 3.4 Bulk appearance of the gels used in the experiments; a) 100% hard gel, b) 100% soft gel (0% hard gel) 51

FIGURE 3.5 Bulk rheology of hard gels, soft gels, and their mixtures at a range of concentrations of the hard gel. a) Flow curves of gels and gel mixtures, the n here indicates flow index, b) Storage modulus (G') obtained from stress sweep .....**Error! Bookmark not defined.**

FIGURE 3.6 a) Representative particle trajectories in gels with different proportions, b) Average mean square displacement of particles diffusing in different gels 53

FIGURE 3.7 Bulk and microscale moduli as a function of hard gel concentration at ω=1 rad/s. a) Bulk rheology, b) Microrheology 54

FIGURE 3.8 Plots of van-Hove correlation of gellan samples at short (0.029s) and at long time (0.29s). a) 0% hard gel, b) 20% hard gel, c) 40% hard gel, d) 60% hard gel, e) 80% hard gel, f) 100% hard gel..... 56

FIGURE 3.9 a) Cartoons showing location of observed particle locations in capillary, b) MSD of particle at different location when fresh and aged..... 57

FIGURE 3.10 Plots of van-Hove correlation of particles at different positions in capillary (t=0.29s) for both fresh and aged sample at 15 hrs; a) hard side of capillary, b) middle side of capillary, c) soft side of capillary, d) collated data of all positions..... 59

FIGURE 4.1 a) DBD design incorporating the glass bottom imaging dish containing the growing biofilm within the discharge gap, b) Schematic of air discharge in contact with liquid and addition of PAL to growing biofilm.... 70

FIGURE 4.2 Effect of treatment time on biofilm structure a) Confocal images of biofilm structure before and after plasma treatment, b) quantification of dead cells (symbol ●) and cell clumps larger than 20 μm^2 (symbol ■) 75

FIGURE 4.3 Effect of biofilm maturity on plasma clumping a) confocal images of 24-h and 48-h of untreated and plasma treated biofilm, b) percentage of clumps bigger than 20 μm^2, c) quantification of red cells ... **Error! Bookmark not defined.**

FIGURE 4.4 a) Confocal images of untreated 72-h biofilm and biofilm grown for 72-h but exposed to 30 s plasma treatment at different biofilm ages, where it is shown that biofilms retain their aggregated structure after those plasma treatments, b) percentage of clumps bigger than 10 μm^2, c) quantification of red cells ..... **Error! Bookmark not defined.**

FIGURE 4.5 a) Confocal imaging of plasma-treated samples that were imaged right after treatment where fewer cells are killed after treated twice, b) the percentage of aggregates bigger than 10 μm^2, c) quantification of dead cells 81

FIGURE 4.6 a) Calibration curve for H_2O_2 by spectrometer at 610 nm, b) The H_2O_2 concentration in plasma treated liquid 83

FIGURE 4.7 A) Confocal images of untreated biofilm, incubated with 30 μM H2O2 and incubated with plasma liquid treated for 60 s, b) percentage of aggregates bigger than 10 μm^2, c) red cells quantification of samples..... 84

FIGURE 4.8 The effect of liquid volume covering biofilm during plasma treatment on aggregation and cell death a) confocal images of different structures observed, b) quantification of dead cells (symbol ●) and cell clumps larger than 10 μm^2 (symbol ■) 87

FIGURE 4.9 a) Circular pattern ring structure formed by bacteria after plasma treatment, b) Compact structure formed by bacteria after plasma treatment, c) pattern rings formed by surface-deposited bacteria after plasma treatment reproduced from ref [25] with permission.....**Error! Bookmark not defined.**

FIGURE 4.10 The drying effect on structure of biofilm by oven at 50 °C for different treatment time. a) Treated for 30 s, b) treated for 60 s, c) treated for 90 s.....**Error! Bookmark not defined.**

FIGURE 5.1 a) Early incubation, and bacterial multiplication, b) Formation of fibrous masses, c) Flotation of fibrous masses to air-liquid interface and full coverage of the interface, d) Formation of pellicle starter, e) Compaction of fibrous masses below pellicle starter, f) Thickening of pellicle. 104

FIGURE 5.2 Viscosities of alginate solution at the different concentrations used in pellicle growth experiments..... 106

FIGURE 5.3 a) Top view of wet and dry pellicles; b) The change of thickness of wet pellicles with alginate concentration; c) The dry weight of pellicles with alginate concentration..... 107

FIGURE 5.4 The change in a) water weight retained in each pellicle with alginate concentration, b) pellicle density with viscosity of alginate solutions 108

FIGURE 5.5 The change in elastic or storage modulus (G') of pellicles as a function of strain for pellicles grown with different alginate concentrations. 109

FIGURE 5.6 a) The appearance of pellicles grown in TRIS and 1% alginate at different days; b) the change of dry weight in respect to incubation time (days); c) the change of wet thickness as a function of incubation time. 111

FIGURE 5.7 a) Change in tan δ of cellulose dispersion with alginate concentration, b) Change in storage modulus and yield stress of cellulose dispersion with alginate concentration. 113

FIGURE 5.8 The calculation of intermolecular forces in the system with different concentration of alginate, a) 0% alginate, b) 0.2% alginate, c) 0.4% alginate, d) 0.6% alginate, e) 0.8% alginate, f) 1% alginate. The insets show zoom-in area of the part of figures in the red squares. 114

FIGURE 5.9 a) The change zeta potential in respect of ratio of moles of alginate to surface area of cellulose fibers (data from dispersed fibers), b) The change of ratio of alginate to surface area of cellulose fibers in respect to days of growth (data from dry weight of pellicles grown in 1% alginate)..... 116

FIGURE 5.10 Confocal images of the structure of pellicles grown in medium with different viscosity. Increasing alginate levels constrain growth and increase attraction between fibers, leading to increased alignment at higher concentrations, though the random nature of pellicle folding, assembly, and continued growth can make quantification difficult. Scale bar is 10 μm. ... 117

List of Tables

TABLE 4.1 Design of regrowth experiment where U indicates untreated and T treated samples 72

TABLE 4.2 The amount of water removed by plasma treatment 85

List of Abbreviations

A.xylinum	*Acetobacter xylinum*
AFM	Atomic Force Microscope
DBD	Dielectric Barrier Discharge
DNA	Deoxyribonucleic acid
E.coli	*Escherichia coli*
ECM	Extracellular matrix
EPS	Extracellular polymer substance
MSD	Mean square displacement
NAC	N-Acetylcysteine
OES	Optical emission spectra
P. aeruginosa	*Pseudomonas aeruginosa*
PBS	Phosphate buffered saline
PEG	Poly (ethylene) glycol
PI	Propidium iodide
PVP	Poly (vinyl pyridine)
S. aureus	*Staphylococcus aureus*
SEM	Scanning Electron Microscope

Thesis Abstract

Bacterial cells can sometimes form and thrive within biofilms, a community of cells embedded in a self-produced extracellular polysaccharide (EPS) matrix. The EPS gives biofilms three-dimensional structures, protecting cells in biofilms by making them more resistant to chemical and physical attack. It is thought that the proper characterisation of biofilms is important to design treatments for their removal. The main problem is that biofilms are very complex and often heterogeneous, making them difficult to characterise and model. In addition, the restructuring of biofilms can be a result of changes in their growth environments or even removal treatments, complicating characterisation.

This thesis aims to understand how environments or treatments can change the structural features of a biofilm and also to expand the knowledge of structural heterogeneity they possess. A literature review on structural heterogeneity in different systems of biofluids summarises current knowledge in the field. The first part of the project focuses on development of a model biofilm with controlled heterogeneity, using natural polysaccharide derived from *S. elodea* biofilm. Here, it was found that although heterogeneity can be controlled, it can be highly variable in the relevant length scale. In the second part of the project, an *E.coli* biofilm was exposed to plasma treatment, a common disinfection approach. Plasma rearranges biofilm structure by local dehydration, making biofilm more resistant to subsequent treatments. Lastly, the project evaluates the effect of environmental change on the microstructure of *A. xylinum* biofilm by increasing viscosity of its growth medium. This biofilm produces a thick cellulose pellicle, but instead of being harmful, its properties are actually useful for many applications for example, as a scaffold in tissue engineering. Addition of alginate changes the pellicle microstructure, making it denser in an analogous effect to that of the plasma treatment studied earlier, but does not affect its actual growth process.

The thesis summarises the insights gained into characterisation, modification, and engineering of biofilm properties and points to opportunities for future research and development in this area.

Chapter 1

Introduction

1.1 BACKGROUND

Complex commercial and biological fluids have interesting rheological properties that dictate their flow, function, and performance. The rheology of mucus, for example, allows its removal by cell cilia, while diseased mucus can be viscous thus normal respiratory processes cannot remove it. Another example is biofilms, bacterial communities where the viscosity of a fluid matrix causes drug delivery to be slow or minimal when compared to more dilute bacterial suspension. Characterisation and understanding of complex biofluid structure, rheology, and response will be useful for applications like drug delivery design.

There have been a number of studies of the bulk flow properties of biofluids, but the complex microstructures are not always best characterised using bulk techniques. A key property that dictates the rheology of a biofluid is their three - dimensional microstructure, which can be the result of complex interactions between the fluid components like cells, biopolymers, and external chemical and stresses. As a result, biofluid structures can be significantly heterogeneous in nature, making new approaches to study, characterisation, control, and modification biofluids difficult.

1.2 AIM AND OBJECTIVES

The main aim of this thesis is to improve understanding of biofluid heterogeneity by studying specific examples of model fluids, natural biofilms that have been treated by novel mitigation methods and biofilms that have distinct interactions with their environment.

1.3 THESIS SUMMARY

The thesis will be structured as follows:

Chapter 1 introduces the subjects under study.

Chapter 2 provides a literature review of current work on microstructural heterogeneity of biological fluids. The work summarises how microstructural heterogeneity occurs, how it can be studied, and how knowledge of microstructural heterogeneity can be applied in various fields.

Chapter 3 deals with development of a model heterogeneous biopolymer gel using a mixture of cross-linkers as well as a mixture of two gels with distinct bulk and microrheological properties.

Chapter 4 studies the effects of incomplete plasma eradication of *Escherichia coli* biofilm and the effects of subsequent structural regrowth and recovery on response to later plasma treatments.

Chapter 5 examines the effect of growth medium viscosity on the growth process, microstructure, and bulk properties of an *Acetobacter xylinus* biofilm. Specifically, the chapter examines how changing biopolymer interactions can alter biofilm microstructure.

Finally, Chapter 6 provides general conclusions to the research and recommends future study needed in this area.

Chapter 2

Literature Review

2.1 INTRODUCTION TO BIOFLUIDS

2.1.1 | Definition of biofluids and their functions

Many prokaryotic and eukaryotic cells and tissues are made of, or surrounded by, a layer of a fluid matrix. Some prominent examples of these matrices include: the actin network of the cytoskeleton, the extracellular polymer matrix (EPS) that covers bacterial aggregates in biofilms, the extracellular matrix (ECM) of both animal and plant cells, and various other fluids such as cartilage synovial fluid, the vitreous humour in eyes and the mucus found in respiratory, gastrointestinal, reproduction tract. These fluids are made up of mainly water (>90%) [1, 2] and their unique matrix structure is made up of biopolymers, such as polysaccharides and proteins [2], that are excreted by the cells they protect.

The protection of a fluid matrix allows small molecules such as nutrients and waste products to pass through, while selectively eliminating large molecules, hence acting as a natural sieve. In some systems, for example in *B. subtilis* & *E.coli* biofilms, the presence of water channels has been observed to help transport materials into the interior of the biofilms [3, 4]. In addition, the presence of biopolymers increases the viscosity of the fluid permeating the matrix, so the diffusivity of molecules in these fluids is lower. In most cases, many of these biopolymers are also charged, thus when charged molecules pass through the networks there could be an interaction that further slows down their diffusion [5]. In some systems containing mucus, the mucus layer is continuously renewed by removing the old mucus layer *via* ciliary clearance, thus also removing the trapped molecules within their structure [6].

The fluid matrix also performs another important role: providing structural support to cells by acting as a scaffold to regulate their mechanical properties. An example is the vitreous humour, which helps the eye maintain its spherical shape. Biofilm EPS and eukaryotic ECM matrices resist deformation to the system, protecting the cells inside. These matrices also play important roles in mediating the communication between the cells inside.

Some fluid matrices also act as lubricants. The presence of synovial fluid in between the articular cartilages of synovial joints prevents them sticking to each other [7]. Mucus found in gastrointestinal and reproductive tracts helps the movement of food and sperm, respectively, to move forward to the next steps of digestion and reproduction.

A key element of many of the functions, and malfunctions, of the above biofluids is their mechanical properties, as these affect diffusion, flow, and friction during biological processes. Historically, biofluids have been studied as relatively homogeneous materials but a broad range of recent work indicates the importance of heterogeneity. We review here the origins, characterisation, and applications of biofluids with heterogeneous structures.

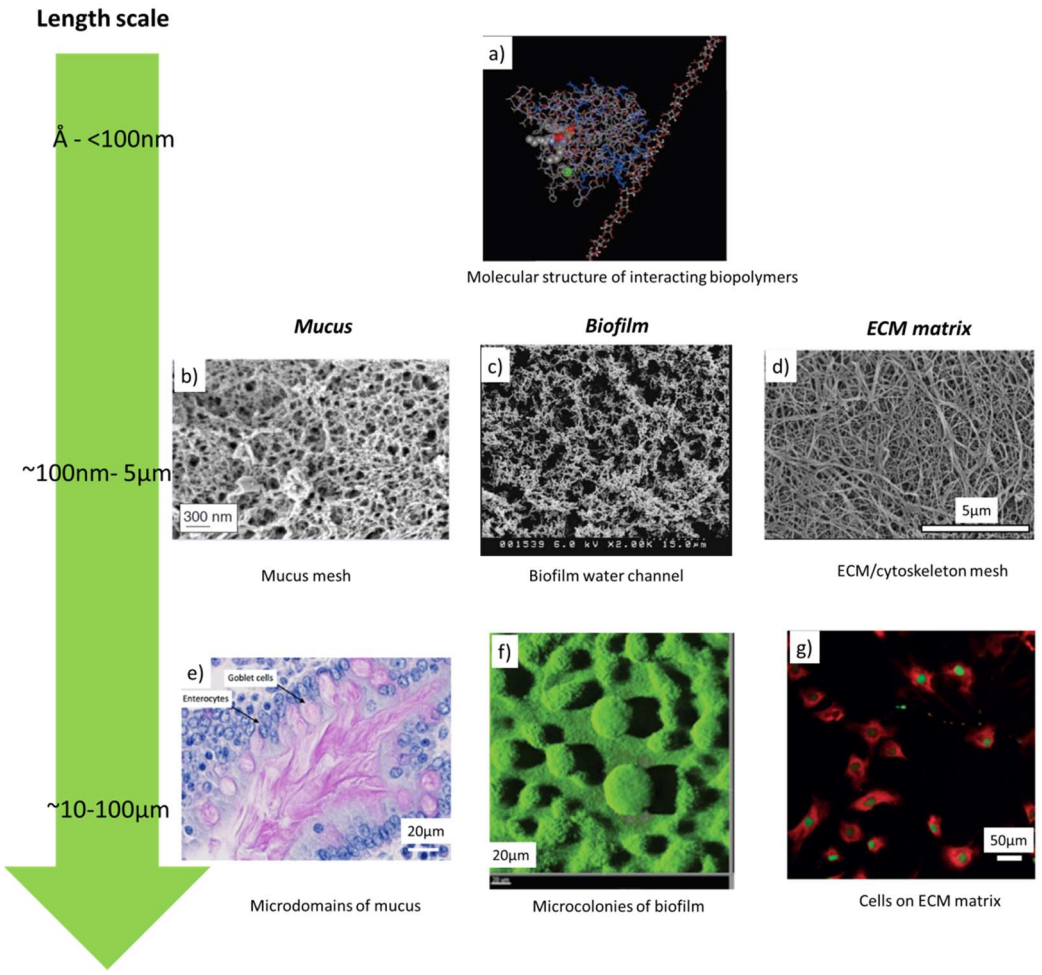

FIGURE 2.1 Heterogeneity in different biological systems. Pictures were taken from references [1, 8-13].

2.1.2 | Biofluid rheology and heterogeneity

In general, biofluids are highly heterogeneous systems. The actual definition of biofluid heterogeneity varies between different fields and different biofluids, but heterogeneity usually stems from the existence of populations of components like cells, polymers, and proteins that can create microenvironments with very different properties. An example in cell biology is the occurrence of subpopulations of mutant cells that have significantly different phenotypic expression of proteins, polysaccharides, DNA, and other macromolecules when compared to the majority of cells present [14, 15]. Self-assembly of a macromolecule into a 3D-structure, such as protein folding, can occur through

heterogeneous pathways depending on folding conditions [16]. This interaction can occur between similar and different macromolecules, resulting in heterogeneous macromolecular interaction [17]. Characterisation of the networks and environments formed after such synthesis and self-assembly can be understood using concepts from polymer science that explain effects of variations in polymer side chains or charge [18], conformations [19], molecular weight [20, 21], or contour length [22].

Rheology deals with characterisation of flow properties of a fluid. Many biological fluid flow behaviours are distinct from Newtonian fluids, like water. The flow behaviours of biological fluids are the results of the three-dimensional structure formed by their building blocks. Just as the structure of biological fluids is often heterogeneous, the rheological response of biofluid systems can be as well. In this review, heterogeneity is defined as rheological heterogeneity in a biological fluid as a result of structural variation.

Rheological heterogeneity is dependent on the length scale of the relevant structure. The range of structural length scales might vary slightly depending on the system, but typically is around 100 nm – 5 μm for biological networks (Figure 2.1). The mesh is a result of entanglement, cross-linking, bundling and aggregation of polymer and its cellular units (Figure 2.2). Bacterial cells in biofilms have been modelled as colloidal particles which can affect structure and rheology [23]. Specific arrangements of cells can occur, as observed in biofilm microcolonies where the cells are oriented at certain angles or separated by certain distances [24, 25]. Their interaction might also cause variations in density (Figure 2.2).

On larger length scales, around 10 μm-100 μm, some biological fluids still have heterogeneity (Figure 2.1). In mucus and biofilms for example, there are regions that can contain discrete domains with high or low concentrations of polymers [11, 26, 27]. As polymer network length scales are much smaller, the difference in polymer concentration causes rheological heterogeneity, forming regions of fluid that behave as a viscous fluid permeating an elastic polymer network. The

difference in the fluid viscosity can also result in lower cross-link density [27, 28], but with higher thickness means a larger volume.

Studying heterogeneity of biological fluids is useful to understand barrier properties, which can have a profound effect on drug transport. Rheological heterogeneity can also be indicative of disease and other health variations, so measurement and quantification is essential.

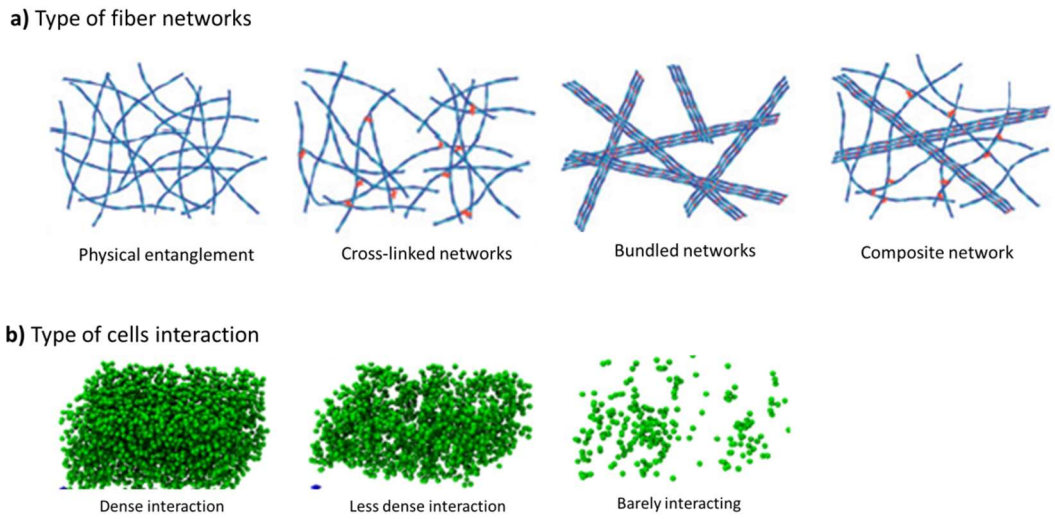

FIGURE 2.2 Type of interactions commonly occurs in biofluids. Pictures were taken from references [29, 30]

2.2 THE ORIGINS OF BIOFLUIDS MICROSTRUCTURAL HETEROGENEITY

2.2.1 | Role of interaction between fluid components

The origins of microstructural heterogeneity in biofluids are broadly variable. The production of biopolymers is actually regulated on the molecular level. Initially, the precursors of these biopolymers are produced inside the cells and then undergo various modifications during their polymerization. Polymer modifications and polymerization are regulated by gene mutations or deletions before being released outside the cells, affecting the final properties of the

biopolymers. Alginate, for example, a polysaccharide that is important in the formation of *P. aeruginosa* biofilms, may undergo epimerization by the AlgG gene from D-mannuronate to L-guluronate, which will affect the final alginate gelling ability and the binding ability to calcium ions [31]. Another example is the initial polymerization of mucins, where the Agr2 gene is needed so later these mucins can be further polymerized in the Golgi to form branched networks [32]. Heterogeneity amongst the cell subpopulations can produce biologically distinct functions [14], and further diversify the cellular production of biopolymers.

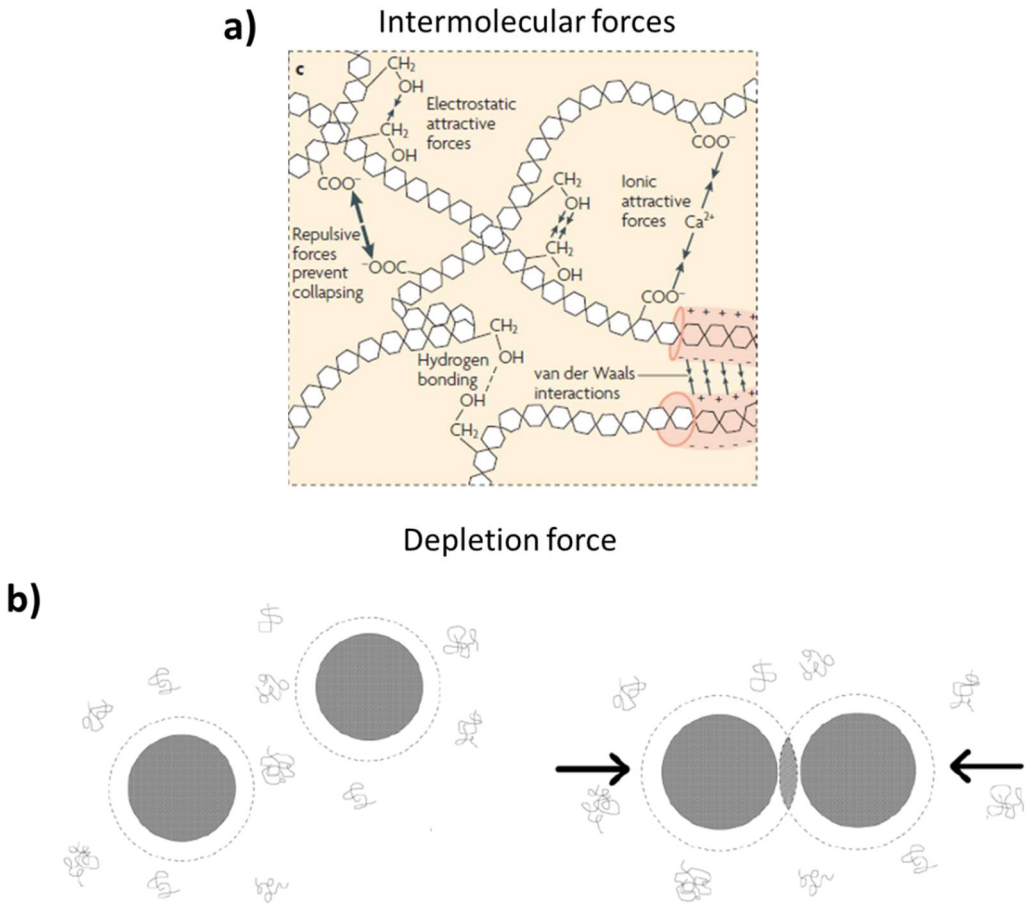

FIGURE 2.3 Sources of interaction in biofluids. Pictures were taken from references [1, 33]

Biopolymers interact with each other *via* self-assembly to form a microstructure, which is dictated by the types of biopolymers and their properties. On the length scale where these interactions occur, one molecule might exhibit different interactions that can form heterogeneous microstructures, as explained in the previous section. These interactions are usually dominated by intermolecular forces such as van der Waals forces and hydrogen bonding (Figure 2.3a) or can occur through hydrophobic interactions. Mucins, for example, are known to cross-link with each other through hydrophobic interactions to form a mucus gel [34], but are also known to form physical entanglements [11]. Physical entanglements between biopolymers can be enhanced through electrostatic and hydrogen bonding. Mucus gel is also built from mucins and non-mucin proteins *via* electrostatic or covalent interactions [34, 35]. As the polymer interactions are an important factor determining gel structure, changes in the composition of certain molecules building the system will change the final three-dimensional structure of a biological fluid [36].

Heterogeneity forms as soon as any interaction between biopolymers becomes relevant, which is denoted by overlap concentration (c*) [37]. Below this concentration, the interaction between polymer chains is considered negligible. Overlap concentration occurs when there are enough polymer chains in the system where these polymer chains can overlap with each other or even creating chain-to-chain contact. Above this critical overlap concentration, polymer chains transition from dilute to semi-dilute regimes [38]. Concentration of polymer in the solutions is thus an important variable. Below the overlap concentration, many biopolymer systems show homogeneity [37, 39], as interactions are less frequent. Studies on actin, the main biopolymer in cytoskeletons, shows that with increasing concentration of biopolymers in solution, there is also an increase in their heterogeneity [40-42]. An increase in interactions is usually followed by an increase in magnitude of the bulk rheological/mechanical properties of the biofluid [43, 44].

In complex biological systems such as biofilms, cells are important components that build the fluid structure [45]. As cells are usually charged , they also can form

interactions with biopolymers through electrostatic interaction/hydrogen bonding [46], thus they can also act as cross-linker in biofluid structure [30, 47]. This will change the overall structural heterogeneity of the fluid structure, especially with regions with high concentration of cells, as well as increase the modulus of the biofluid gels [48].

Biofluid structure can evolve over time as biological systems usually release polymers at different times and even at different locations, as found in *Vibrio cholera* biofilms [49]. During their later life cycle, it is also found that there is a progressive increase of protein production in a biofilm [50]. In addition, other biopolymers can still occur concurrently and might have different distributions within biofluid. Concentration of biofilm polysaccharides usually increases with the increase in depth [51].

Other than intermolecular forces, other attractive forces such as depletion can increase the interaction between components (Figure 2.3b). Although less common, the depletion force has been proven an important force that drives cellular organization [33]. Depletion force happens when molecules or particles are suspended in a solution of non-absorbent smaller molecules that act as a depletant. When two large molecules are approaching each other, these non-absorbent molecules will create a difference in osmotic pressure between the large molecules. This will exclude the depletant molecules in the space in between the two large molecules, creating excluded volume. Due to this, a depletion force will be created and push the two larger molecules to interact. When this happens, a phase separation will occur [52]. As a result, there are usually regions with high and low concentrations of biopolymers. This has been observed in many biological systems such as human lamin networks [53] or mucus [54], which will create somehow a heterogeneous system with two microenvironments. The extent of depletion will be increased by depletant concentration [55].

Depletion force has been used to explain how cells in microcolonies are separated from the EPS matrix [56, 57] because the EPS biopolymers act as depletant. The increase in depletant concentration causes the bacterial cells to become more

aggregated [58, 59], thus bacterial strains that overproduce EPS polymers will have enhanced aggregation [60].

2.2.2 | Effect of change in chemical environment

The heterogeneity of a structure is affected by the rate of transport of nutrients into the structure, for example in biofilms or ECM. This can be caused by the slowing down of transport rates by high viscosities or structural barriers by the fluid matrix. The growth of a biofilm that is far from a nutrient source is shown to be retarded [61]. The slower penetration rate of drugs into biofilms can be a reason why the bacterial cells in biofilms develop resistance to drugs, as the bacterial cells near the bottom have time to undergo metabolic changes enabling resistance [62].

In addition, as explained in section 2.1, the presence of chemicals that can change any electrostatic interactions or covalent bonding can change the extent of heterogeneity. The presence of salts will change the electrostatic interactions of biopolymer structures. Different ion types and charges have been observed to induce changes and the addition of lithium, sodium, potassium, magnesium and calcium reduced viscosity of biofilms by reducing cross-links [63]. In addition, growing biofilms in the presence of high salt concentrations produces biofilms with more homogeneous connections [64]. However, in mucus gels it is found the change of interaction due to increased salt concentration is not followed by an increase in the degree of heterogeneity [54].

Fluid pH can also change the interaction of biopolymers and cells. When the pH of a fluid environment is reduced, and the pH is lower than the pKa of the polymers, there will be an increase in the polymer aggregation. It is observed that the microstructure of biofilms can be degraded by changing the pH where instability occurs [30]. Mucin undergoes conformational change from an isotropic random coil to anisotropic conformation when pH is reduced [34]. It is also observed that a combination of acetic acid and N-acetylcysteine (NAC) can penetrate a biofilm and kill 100% of the cells by reducing the cross-links formed

between polymers and cells [47]. The decrease in pH of mucus gels from 7 to 2 increases the structural heterogeneity by causing a mesoscopic phase separation [54].

The presence of surfactant can also change the interaction of biofluids. Lungs naturally produce surfactant that reduces surface tension at the alveolar air/liquid interface [65]. Similar to other molecules, surfactant can be charged, possibly interacting with other biofluid components through electrostatic forces or depletion effects. Many studies have shown that there is a change of structure with addition of surfactants. The addition of surfactant caused vaginal mucus to condense and bundle, reducing overall pore size [66] and reducing heterogeneity, in agreement with another study that found surfactant reduces structural heterogeneity of mucus [54].

The structure of biofluids can also be changed by the addition of certain polymers that interact with biofluid components [67], though polymeric diffusion is much slower than small molecule transport. Depending on the type and charge of the polymers, different effects on biofluid structure can be observed. For example, the addition of poly(ethylene glycol) (PEG) is shown to cause mucin fibres to bundle while also forming smaller areas of low fibre density close to the bundles [68]. These two areas have different microstructures and rheological properties, which likely causes an increase in mucin network heterogeneity. Willits & Saltzmann observed [68] that poly(vinyl pyridine) (PVP) also alters mucus structure, forming a region with lower fiber density as well as regions with almost no fibers.

The microstructure of fluids can change by addition of drugs and enzymes that can degrade biofluid mesh structure. Drugs usually have a specific target action, where a change in heterogeneity depends on each drug's mechanism. Mannitol for example, which increases the hydration of mucus samples, does not change the interaction of the mucin structure, but only dilutes the mucus. The dilution of is shown to only swell the mucus gel, which decreases its fiber density [67]. This means that in this case, heterogeneity should not change as connections stay the same. NAC and Pulmozyme (DNAse), which target the hydrogen bonding in the mucus structure (disulphide bond and phosphodiester linkage, respectively) [69]

will change the interaction of the mucus chains, also changing the heterogeneity. Studies with these kinds of drugs have been shown to both increase [8] and decrease [70, 71] the structural heterogeneity.

Other than drugs, enzymes can also degrade microstructure of a biofluid through similar mechanism where they cleave the bond of specific molecules. The addition of trypsin to a biofilm degrades its structure, increasing its mesh size and increasing its heterogeneity [72]. In some natural settings, structural degradation can occur only at one specific area in the overall fluid structure. A common example is caused by the enzymes released by eukaryotic cells when they are migrating. In addition, it is also found that the degradation occurs heterogeneously as the cells release enzymes to the area furthest away from its original location while areas directly next to the cell remain elastic [73].

2.2.3 | Effect of change in physical environment

Many biopolymers respond to physical cues from the environment, such as temperature, for them to self-assemble. Examples are polysaccharides such as gellan which starts to self-assemble after an increase in the temperature of the solution [74], meaning temperature should be able to change structural heterogeneity. Collagen, for example, has been shown to form a more homogeneous microstructure when structure formation occurs at an increased temperature [75].

The assembled structure of a biofluid can also be altered by shear. *P. aeruginosa* biofilm preferentially grows in regions with highest fluid flow rates [76]. High shear stress causes biofilms to detach [77], and if there is a difference in the strength of the network, the structure will be rearranged, which will increase the extent of structural heterogeniety [78].

2.3 QUANTIFICATION OF BIOFLUID HETEROGENEITY

2.3.1 | Microscopic features

The use of dye with optical or confocal microscopy is the most commonly used technique for characterisation of micrometre length scales. Usually, a dye selectively (or semi-selectively) binds with macromolecules of interest. For example, Periodic acid-Schiff (PAS)/alcian blue staining is used to stain mucin [79]. The heterogeneous domains in mucus can be highlighted by different colour intensity correlated to mucin density [11]. The dye is usually a fluorescing molecule that is excited by laser illumination at certain wavelengths. The increase in fluorescence might indicate a denser network, which can be caused by bundling of polymers.

The use of dyes can also help to differentiate structural heterogeneities in the fluid. Due to the presence of different building blocks, different dyes might be used in order to differentiate this. To observe the heterogeneities within a biofilm, it is common to employ at least two dyes: one for the bacterial cells, a common example is the SYTO9 or propidium iodide (PI), and the other an EPS dye. As different biofilm EPS could be made from different types of polysaccharides, various dyes need to be used. When higher resolution is needed, other techniques such as scanning electron microscopy (SEM) will be used.

Measurements are later quantified using image analysis. Variation of structural features of a biofilm, such as size of microcolonies [80], or mesh size, can be analysed by looking at spatial arrangement of light and dark regions in the images, which can give the range of mesh sizes. Multiple microscopy techniques are often used to observe the entire structure [81]

2.3.2 | Molecular Transport

The heterogeneity of molecular transport in biofluids is commonly studied using particle tracking, also known as passive microrheology. As the name suggests, the technique depends on tracking the diffusive movement of small colloidal

particles in a fluid for a period of time. The location of the particles is then used to calculate its mean squared displacement (MSD), which is defined as:

Equation 2.1 $$MSD(\tau) = \langle \Delta r(\tau)^2 \rangle = \langle [r(t+\tau) - r(t)]^2 \rangle$$

where $r(t)$ is the position of the particle at time t, and τ is the lag time between the two positions of a particle during calculation of its MSD.

In a heterogeneous fluid, the MSD varies significantly. This is why simple statistical analysis has been used to quantify heterogeneity. The statistical analysis is usually done for MSD values at a given lag time, which includes the measure of MSD normalized standard deviation, the difference of the maximum and minimum values, and also the normalized skewness of data [40]. The histogram of MSD data for homogeneous fluids, such as glycerol, is normally distributed so that the peak is at the mean value. Standard deviation measures the variation of data from the mean, so a larger the standard deviation means a higher degree of heterogeneity. Skewness is a measure of the symmetry of a distribution and will be close to zero for a homogeneous system. The MSD distribution of a heterogeneous fluid will be skewed, as there are values that are concentrated on a certain side of the histogram while the spread of data is large. In many cases, when there is a higher degree of heterogeneity, the value of skewness will also increase [40, 41]. Although it is simple, this method is very sensitive to outliers, which can affect the final analysis [82].

Quantification of heterogeniety has also been performed by a method called bin-partition analysis. In this method, the MSD values are sorted and the contributions of 10%, 25% and 50% of the highest MSD values to the ensemble/averaged MSD are evaluated [83, 84]. For homogeneous solutions, the contribution of MSD values to the ensemble should be very close to 10%, 25% and 50% at the lag times assesed. An increase in the contribution usually indicates a higher extent of heterogeniety [85].

A qaulitative way to detect heterogeniety is by plotting the van Hove correlation function. The basis of the idea is that the total distance tracer particles travel during a time interval must be the same if they are travelling in a homogenoeus

medium [86]. As such, the van-Hove correlation is used to show whether the distribution of the particle displacements can be fitted to a Gaussian functional form, meaning the system is homogeneous. When the tracer particles are travelling in a heterogeneous medium, the function usually has to be fitted with two distinct Gaussian functional forms.

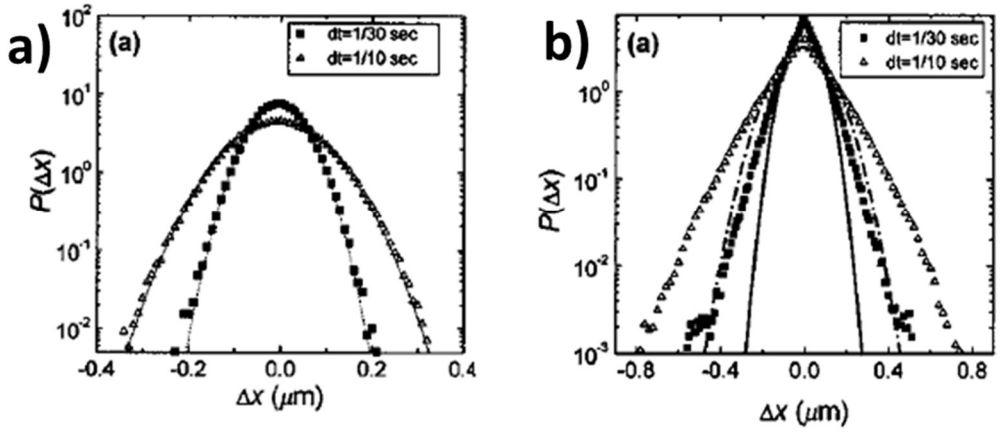

FIGURE 2.4 van-Hove correlation functions of particles diffusing in a) homogeneous medium, b) heterogeneous medium. Pictures were reproduced from reference [86] with permission

To complement the technique, some papers have also calculated the HR ratio (N) [87, 88], defined as:

Equation 2.2 $$\text{N (HR ratio)} = \frac{\langle \Delta x^4 \rangle}{3\langle \Delta x^2 \rangle^2} - 1$$

Where Δx^4 is the fourth moment, while Δx^2 is the second moment of displacement data at a defined lag time. Homogeneity usually results in an HR ratio that is very close to 0. Excess kurtosis of the displacement value at a lag time has also been used to calculate heterogeneity [89], which is defined as:

Equation 2.3 $$Excess\ kurtosis = \left(\frac{\sum_{i=1}^{i=n}(x_i - \bar{x})^4}{(n-1)\sigma^4}\right) - 3$$

Similar to the HR ratio, for increasingly heterogeneous systems, the excess kurtosis increases as well.

The HR ratio and excess kurtosis are good approximations of the increase in heterogeneity with a given variable, such as concentration of biopolymers. In some cases it is also useful to calculate an F-value for each pair of particles [86].

2.3.3 | Mechanical properties

In terms of quantification of micromechanical properties of a biological fluid, a few techniques have been used. Most of the techniques are based on the application of force to a sample, measuring the response from the material. The first technique is the use of the Atomic Force Microscope (AFM). Young's modulus can be calculated by fitting the force-indentation data with a relevant mechanical model, such as the Hertzian model [90]. This model defines the load (F) as:

Equation 2.4 $$F = \frac{4ER^{1/2}}{3(1-\sigma^2)}\delta^{3/2}$$

Where F is the load, δ is the indentation, R is the probe's radius of curvature, E is the Young's modulus, and σ is the Poisson's ratio of the elastic solid. In addition, there is an assumption that the sample is a semi-infinite homogeneous elastic solid. However, care has to be taken as it has been shown that AFM probe tip shape and tip radius will affect the measurement. Worn out probes can overestimate the hardness value of a material [91]. Just like the MSD, here heterogeneity is determined by plotting the spatial distribution of Young's modulus [90].

Other techniques that can be used to measure micromechanical properties of a biofluid are through magnetic or optical tweezer microrheology. In a way, these two techniques are similar to passive microrheology as they also use probe particles. However, active techniques apply an external force that is generated

through magnetic field or laser radiation instead of Brownian motion as passive microrheology does[92].

Brillouin scattering is a technique which depends on the interaction of laser light with thermal vibrations in the sample, thus it is regarded as a non-invasive measurement compared to the other methods mentioned before. The interaction produces backscattered light that is shifted relative to the laser wavelength, known as Brillouin frequency shifts (v_B) [93]. This v_B can be used to calculate elastic modulus through the below equation [94]:

Equation 2.5 $$v_B = \frac{2n}{\lambda} V \cos\left(\frac{\theta}{2}\right)$$

V is the acoustic velocity defined as $V=\sqrt{E/\rho}$, where E is the Elastic modulus, ρ is the density, n is the refractive index, λ is the optical wavelength and θ is the scattering angle. The method measures the shifts at few different areas in the sample, which correlate directly to elastic modulus. Thus, heterogeneity in mechanical properties of the sample can be resolved. With this technique, it is found that there is a difference in mechanics of a biofilm microcolony [95] or the crystalline lens [94] between its exterior and interior, where the centre is stiffer than the edges.

2.4 STRUCTURAL HETEROGENEITY AND TRANSPORT INTO BIOFLUIDS

Cells and tissues need nutrients such as sugars, amino acids and ions for normal cell functioning, all of which need to be transported to their specific location. Similarly, the same mechanism is also used for drug molecules needed to reach specific target cells and tissues. The transport rate of molecules is governed by their diffusion rate through the cell/tissue barrier matrices. As these barrier structures are made up of biopolymers, this should increase the overall fluid viscosity. A difference in viscosity changes diffusion transport rates greatly, so transport is much slower in high viscosity fluids. It is observed that the same size antibiotic molecules travel to the bottom of an *S. aureus* biofilm ten times slower than travelling in water with free flowing bacterial cells [62].

The nutrient or drug molecules are usually small, so the transport rate is not only governed by the viscosity, but also any hindrance provided by fluid structures. The interaction between biopolymers in biofluids usually produces a 3D mesh structure with a characteristic mesh size that can vary between different systems. The relative size of molecules/particles diffusing through biofluid is an important factor. In general, molecules smaller than 50 nm can pass through biofilms, mucus, and the extracellular matrix barrier [96-99] because their length scale is smaller than the mesh sizes of these systems. Under certain circumstances, bacteria are able to modify the biofilm structure, which leads to a change in mesh size of the polymer matrix. Such changes affect the diffusivity of molecules through the new mesh. For example, biofilms of three different types of bacteria, grown in the presence of 0.01mM Fe(III), completely hindered the diffusivity of 50 nm particles [96].

The mesh sizes of biofluids are often quite heterogeneous. In many systems, the distribution of MSD and diffusion coefficient is very large, with respiratory mucus for example, the MSD ranges between 10^{-4} to 10^{2} μm^2 [100]. The diffusion coefficient within a single biofilm was found to vary by up to 4 orders of magnitude [101]. Heterogeneity, in general, will slow down particle diffusion in polymer gels [102]. The diffusivity of 5 nm particles in a *P. fluorescens* biofilm is slowed down by 15% compared to when they are diffusing in water [96] due to viscosity and confining effects.

Olmsted *et al* [97] found that charged polystyrene particles diffuse much slower in mucus than do viruses of comparable size, indicating the charged particles are interacting with the biofluids. Particles that have opposite charges to the network matrix will be attracted *via* electrostatic interactions, causing particles to stick and slowing their diffusion [103]. As a result, the particle size is less of a factor in diffusion rate. de Beer et al [104] observed that the non-specific binding of TRITC-IgG with biofilm cell clusters slows down its diffusion compared to phycoerythrin, even though their size is smaller.

Understanding charge distribution within a single system might help to design particle transport through fluid barriers. Biofilms have a charge density that can

vary with biofilm height, which also changes over the progression of their growth [4]. In general, particles that are not charged, such as PEG-coated particles, will have better diffusivity through the barrier and will vary depending on PEG molecular weight and coating density [105].

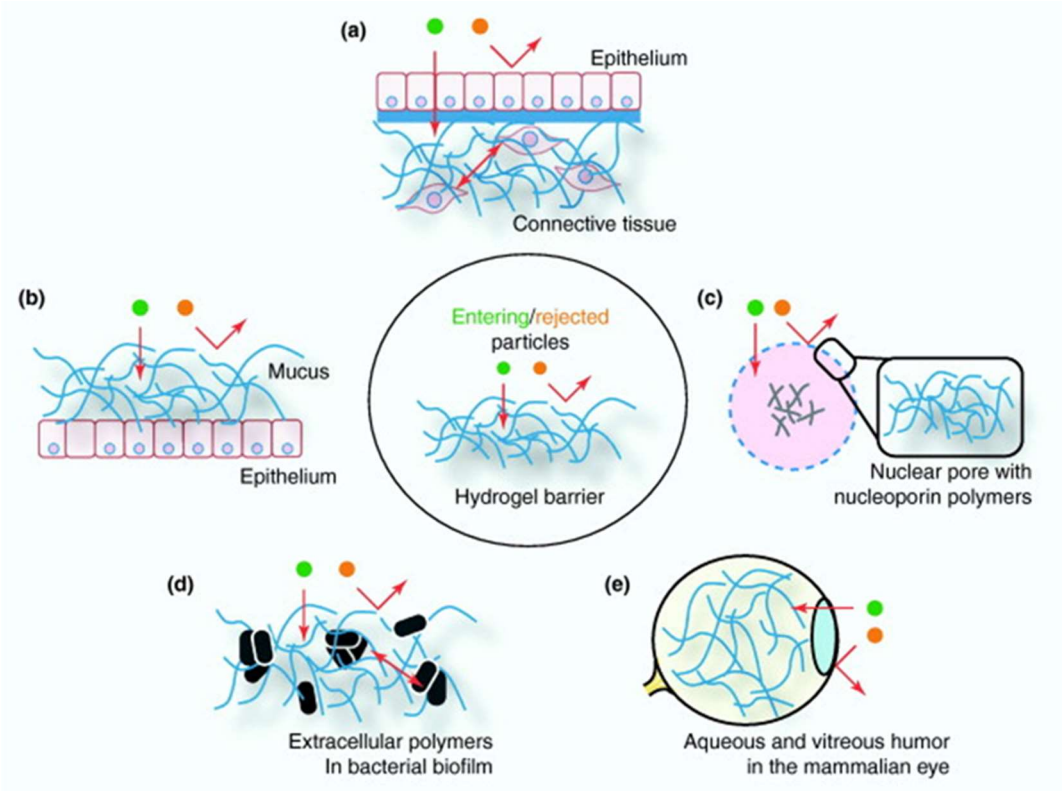

FIGURE 2.5 The permeability of a biofluid barrier. Picture was taken from reference [106] with permission.

The presence of heterogeneity in biofluids is not always disadvantageous. The flow profiles into a biofilm can vary depending on the structure, allowing bulk movement or flow between cell aggregates [107]. Beads can diffuse through biofilms and become distributed throughout it because its rough surface of water-filled pores aids diffusion [108]. In the water-filled pores, colloidal particles can travel freely [3], with a calculated diffusivity value identical to that in water [104].

The rate of particle transport through piglet mucus with heterogeneous structures is also increased in channels with large pore size [109]

2.5 STRUCTURAL HETEROGENITY AND PROPERTIES OF BIOFLUIDS

2.5.1 | Effect on biopolymer gelation

The moment when storage, or elastic, modulus (G') exceeds the loss, or viscous, modulus (G") is an indicator of gelation, where there is a transition of polymeric viscous fluid to a gel with a complex 3D structure that has elasticity. However, to be kept in mind, this transition does not actually define the actual gel point, where it has to satisfy Winter and Chambon criteria. According to Winter and Chambon at the gel point [126], the viscoelastic moduli of the network should exhibit power law scaling with frequency $G' \sim G'' \sim \omega^n$. This is important as heterogeneity might have a strong effect on the gelation properties of a biofluid.

In the case where the final gel with measurable bulk properties is heterogeneous, the presence of heterogeneity helps to increase gelation rate. Microrheology measurements can show the presence of a sort of elastic nucleation point, compared to bulk rheology that could not detect it. This phenomenon has been observed in 2% barley β-glucan solutions, where there is a change from diffusive to sub-diffusive behaviour within 60 minutes, however in bulk the storage modulus can be detected only after 110 mins [110].

On the other hand, in the case of actin gelation, a key component in cellular structure and locomotion, an initial high level of heterogeneity can prolong the actual gelation time [82]. Solutions with higher concentration of actin (14 mM) form a more heterogeneous structure compared than lower concentration samples [40]. This might negatively affect the cellular response to external stress.

Another example is when infections of *S.epidermidis* bacteria cause the microstructure of fibrin to become more heterogeneous instead of forming a quite

uniform network needed for its gelation [111]. This is again is found to increase gelation time and the likelihood of fibrin gel rupture.

2.5.2 | Effect to mechanical properties

The presence of structural heterogeneity will affect the mechanical properties at the microscale. Recently, this effect of heterogeneity was shown in many biological systems. In single biofilm microcolonies [95] or even eye lenses [112], it is common that their centre is stiffer than their edges. The actual value of elasticity in a single *E. coli* biofilm is found to vary by up to three orders of magnitude, ranging between 0.5-200 Pa [113], with larger values at increasing depths [95].

Different microstructure in similar systems can affect the mechanical properties. Structural heterogeneity causes amyloid fibrils to have a wide range of measured Young's moduli [90].

Microstructure of a fluid will affect its bulk properties. Disrupted microstructure of an intact biofilm can reduce its bulk modulus by two orders of magnitude [114]. Thus, the presence of microscale heterogeneity can affect the overall bulk properties. In alginate gels [115] it is found that the presence of heterogeneity decreases bulk modulus, but in other cases such as cystic fibrosis sputum [70], the presence of structural heterogeneity actually increases the bulk modulus. This will be problematic in the case of biofilm or mucus removal from a surface.

2.5.3 | Effects of behaviour and properties of cells in ECM matrix

The structure of biofluids does not only affect the transport or mechanics, but can also affect the behaviour of living cells in the fluid. Many of these observations were made with eukaryotic cells in the ECM. Cells can sense the properties of the matrix surrounding them. In fact, cells grown in gels with different properties can differentiate heterogeneously [116, 117]. Enhanced matrix stiffness is shown to increase cell proliferation, but cross-links prepared with different chemicals like glutaraldehyde (GTA) and 1-Ethyl-3-3-dimethyl aminopropyl carbodiimide

(EDAC) show differences in cellular retention [118]. Cells can also sense matrix stiffness, in fact the gradient of the matrix stiffness can guide them during cell migration, a phenomenon called durotaxis [119]. Thus, cell behaviour can be modulated with matrix mechanical properties.

In addition to cell behaviour, the mechanical properties of the ECM matrix can also affect the cells mechanical properties. The internal modulus of cells increased with increasing ECM matrix stiffness, accompanied by an increase of the cell area [120]. As a result, it has been found that continuous exposure of healthy cells to a stiff matrix can induce the formation of a malignant tumour, which has stiffer internal mechanics [121].

The importance of heterogeneity is recognised not only for fluid bulk properties that affect cell behaviours, but studies indicate the actual microstructure plays a vital role, as this can also be sensed by the cells. ECM structure with bundled fibrils shows enhanced local adhesion scale stiffness [122]. Invasiveness of cells increased and clustering decreased with increased fibril diameter, and also the bending stiffness of single fibrils [123].

The presence of structural heterogeneity can affect cell behaviour, encouraging invasive cell migration. Two studies mimic matrix heterogeneity by putting two gels with different properties next to the other, or use the same gel but create an interface that gives defects in the gel [124, 125]. Both studies show that cells can sense these differences in the matrix and behave differently than in a homogeneous environment. In a system where two gels with different properties are placed next to each other, cells switch morphology straight after they pass the interface [124]. In the second example, a surface defect was created between two identical gels, which resulted in structural heterogeneity. Invading cells preferentially moved at that interface along the defect area (softer matrix) before they spread towards the homogeneous part of the matrix [125].This behaviour is not seen in the gel with a homogeneous microstructure and stiff matrix, where they try to degrade the gel but fail to invade it [125].

2.6 CONCLUSIONS

Heterogeneity of biofluids may have a different definition by different fields that study them. However, in this review, heterogeneity is defined as the structural heterogeneity that impacts rheological properties of a biofluid. Despite some differences, the understanding of heterogeneity in different fields cannot be overlooked as it has importance in determining the interaction between biopolymers and their interaction with cells. From the production of biopolymers that might be affected by cellular heterogeneity, or even the chemistry of the biopolymer, all can eventually affect structural heterogeneity.

Heterogeneity can also differ from system to system, however there are many common aspects in terms of the range of relevant length scales. At smaller length scales, in between 100nm to 5μm, the structural heterogeneity is more about the connection between the building blocks that results in varying mesh size. In larger length scales, biofluids usually have different micro-domains where there will be two very different rheological response.

Heterogeneity can be affected by factors that will affect biopolymer assembly. This includes chemical factors such as pH, ionic strength, or even drugs or enzymes and might likely be affected by physical factors such as temperature and shear.

Understanding of heterogeneity will be crucial as it affects the transport rate of molecules such nutrients or drugs. Heterogeneity also affects how cells behave, which will be an important factor in determining cell migration, possibly aiding to understand cancer migration, for example.

In conclusion, knowledge of biofluid heterogeneity will help to understand the complexity of their structure. This will unlock key mechanisms of the origin of biofluids unique properties, which could be used to engineer their production and properties. This will be the basis of studies performed in the next chapters of this thesis.

2.7 REFERENCES

1. Flemming, H.-C. and J. Wingender, *The biofilm matrix.* Nat Rev Micro, 2010. **8**(9): p. 623-633.

2. Schnaare;, R.L., L.H. Block;, and L.C. Rohan;, *Rheology*. Remington: The Science and Practice of Pharmacy, ed. D.B. Troy. Vol. 2. 2006, Baltimore, Maryland: Lippincott Williams & Wilkins.

3. Wilking, J.N., V. Zaburdaev, M. De Volder, R. Losick, M.P. Brenner, and D.A. Weitz, *Liquid transport facilitated by channels in Bacillus subtilis biofilms.* Proceedings of the National Academy of Sciences, 2013. **110**(3): p. 848-852.

4. Birjiniuk, A., N. Billings, E. Nance, J. Hanes, K. Ribbeck, and P.S. Doyle, *Single particle tracking reveals spatial and dynamic organization of the Escherichia coli biofilm matrix.* New Journal of Physics, 2014. **16**(8): p. 085014.

5. Donlan, R.M. and J.W. Costerton, *Biofilms: Survival Mechanisms of Clinically Relevant Microorganisms.* Clinical Microbiology Reviews, 2002. **15**(2): p. 167-193.

6. Girod, S., J. Zahm, C. Plotkowski, G. Beck, and E. Puchelle, *Role of the physiochemical properties of mucus in the protection of the respiratory epithelium.* European Respiratory Journal, 1992. **5**(4): p. 477-487.

7. Tamer, T.M., *Hyaluronan and synovial joint: function, distribution and healing.* Interdisciplinary Toxicology, 2013. **6**(3): p. 111-125.

8. Suk, J.S., S.K. Lai, N.J. Boylan, M.R. Dawson, M.P. Boyle, and J. Hanes, *Rapid transport of muco-inert nanoparticles in cystic fibrosis sputum treated with N-acetyl cysteine.* Nanomedicine, 2011. **6**(2): p. 365-375.

9. Wen, Z.T., H.V. Baker, and R.A. Burne, *Influence of BrpA on Critical Virulence Attributes of Streptococcus mutans.* Journal of Bacteriology, 2006. **188**(8): p. 2983-2992.

10. Holder, A.J., N. Badiei, K. Hawkins, C. Wright, P.R. Williams, and D.J. Curtis, *Control of collagen gel mechanical properties through manipulation of gelation conditions near the sol–gel transition.* Soft Matter, 2018. **14**(4): p. 574-580.

11. Meldrum, O.W., G.E. Yakubov, M.R. Bonilla, O. Deshmukh, M.A. McGuckin, and M.J. Gidley, *Mucin gel assembly is controlled by a collective action of non-mucin proteins, disulfide bridges, Ca2+-mediated links, and hydrogen bonding.* Scientific Reports, 2018. **8**(1): p. 5802.

12. Crusz, S.A., R. Popat, M.T. Rybtke, M. Cámara, M. Givskov, T. Tolker-Nielsen, S.P. Diggle, and P. Williams, *Bursting the bubble on bacterial biofilms: a flow cell methodology.* Biofouling, 2012. **28**(8): p. 835-842.

13. Dingal, P.C.D.P., A.M. Bradshaw, S. Cho, M. Raab, A. Buxboim, J. Swift, and D.E. Discher, *Fractal heterogeneity in minimal matrix models of scars modulates stiff-niche stem-cell responses via nuclear exit of a mechanorepressor.* Nature Materials, 2015. **14**: p. 951.

14. Altschuler, S.J. and L.F. Wu, *Cellular Heterogeneity: Do Differences Make a Difference?* Cell, 2010. **141**(4): p. 559-563.

15. Stewart, P.S. and M.J. Franklin, *Physiological heterogeneity in biofilms.* Nat Rev Micro, 2008. **6**(3): p. 199-210.

16. Udgaonkar, J.B., *Multiple Routes and Structural Heterogeneity in Protein Folding.* Annual Review of Biophysics, 2008. **37**(1): p. 489-510.

17. Cole, J.L., *Analysis of Heterogeneous Interactions.* Methods in enzymology, 2004. **384**: p. 212-232.

18. van Beurden-Lamers, W.M.O., R. Spee-Brand, J. Dekker, and G.J. Strous, *Sulphation causes heterogeneity of gastric mucins.* Biochimica et Biophysica Acta (BBA) - General Subjects, 1989. **990**(3): p. 232-239.

19. Smith, J.L., W.A. Hendrickson, R.B. Honzatko, and S. Sheriff, *Structural heterogeneity in protein crystals.* Biochemistry, 1986. **25**(18): p. 5018-5027.

20. Sheehan, J.K., D.J. Thornton, M. Somerville, and I. Carlstedt, *The Structure and Heterogeneity of Respiratory Mucus Glycoproteins.* American Review of Respiratory Disease, 1991. **144**(3_pt_2): p. S4-S9.

21. Porsch, B., R. Laga, J. Horský, Č. Koňák, and K. Ulbrich, *Molecular Weight and Polydispersity of Calf-Thymus DNA: Static Light-Scattering and Size-Exclusion Chromatography with Dual Detection.* Biomacromolecules, 2009. **10**(11): p. 3148-3150.

22. Round, A.N., M. Berry, T.J. McMaster, S. Stoll, D. Gowers, A.P. Corfield, and M.J. Miles, *Heterogeneity and Persistence Length in Human Ocular Mucins.* Biophysical Journal, 2002. **83**(3): p. 1661-1670.

23. Rogers, S.S., C. van der Walle, and T.A. Waigh, *Microrheology of bacterial biofilms in vitro: Staphylococcus aureus and Pseudomonas aeruginosa.* Langmuir, 2008. **24**(23): p. 13549-55.

24. Gu, H., S. Hou, C. Yongyat, S. De Tore, and D. Ren, *Patterned Biofilm Formation Reveals a Mechanism for Structural Heterogeneity in Bacterial Biofilms.* Langmuir, 2013. **29**(35): p. 11145-11153.

25. Dzul, S.P., M.M. Thornton, D.N. Hohne, E.J. Stewart, A.A. Shah, D.M. Bortz, M.J. Solomon, and J.G. Younger, *Contribution of the Klebsiella pneumoniae Capsule to Bacterial Aggregate and Biofilm Microstructures.* Applied and Environmental Microbiology, 2011. **77**(5): p. 1777-1782.

26. Lim, Y.F., M.A.K. Williams, R.G. Lentle, P.W.M. Janssen, B.W. Mansel, S.A.J. Keen, and P. Chambers, *An exploration of the microrheological environment around the distal ileal villi and proximal colonic mucosa of the possum (Trichosurus vulpecula).* Journal of The Royal Society Interface, 2013. **10**(81).

27. Stewart, P.S., R. Murga, R. Srinivasan, and D. de Beer, *Biofilm structural heterogeneity visualized by three microscopic methods.* Water Research, 1995. **29**(8): p. 2006-2009.

28. Atuma, C., V. Strugala, A. Allen, and L. Holm, *The adherent gastrointestinal mucus gel layer: thickness and physical state in vivo.* American Journal of Physiology-Gastrointestinal and Liver Physiology, 2001. **280**(5): p. G922-G929.

29. Lieleg, O., M.M.A.E. Claessens, and A.R. Bausch, *Structure and dynamics of cross-linked actin networks.* Soft Matter, 2010. **6**(2): p. 218-225.

30. Stewart, E.J., M. Ganesan, J.G. Younger, and M.J. Solomon, *Artificial biofilms establish the role of matrix interactions in staphylococcal biofilm assembly and disassembly.* Scientific Reports, 2015. **5**: p. 13081.

31. Franklin, M.J., D.E. Nivens, J.T. Weadge, and P.L. Howell, *Biosynthesis of the Pseudomonas aeruginosa Extracellular Polysaccharides, Alginate, Pel, and Psl.* Frontiers in Microbiology, 2011. **2**: p. 167.

32. Adler, K., M. Tuvim, and B. Dickey, *Regulated Mucin Secretion from Airway Epithelial Cells.* Frontiers in Endocrinology, 2013. **4**(129).

33. Marenduzzo, D., K. Finan, and P.R. Cook, *The depletion attraction: an underappreciated force driving cellular organization.* The Journal of Cell Biology, 2006. **175**(5): p. 681-686.

34. Cao, X., R. Bansil, K.R. Bhaskar, B.S. Turner, J.T. LaMont, N. Niu, and N.H. Afdhal, *pH-Dependent Conformational Change of Gastric Mucin Leads to Sol-Gel Transition.* Biophysical Journal, 1999. **76**(3): p. 1250-1258.

35. Radicioni, G., R. Cao, J. Carpenter, A.A. Ford, T.T. Wang, Y. Li, and M. Kesimer, *The innate immune properties of airway mucosal surfaces are regulated by dynamic interactions between mucins and interacting proteins: the mucin interactome.* Mucosal Immunology, 2016. **9**: p. 1442.

36. Serra, D.O., A.M. Richter, and R. Hengge, *Cellulose as an Architectural Element in Spatially Structured Escherichia coli Biofilms.* Journal of Bacteriology, 2013. **195**(24): p. 5540-5554.

37. Shayegan, M. and N.R. Forde, *Microrheological Characterization of Collagen Systems: From Molecular Solutions to Fibrillar Gels*. PLOS ONE, 2013. **8**(8): p. e70590.

38. Ying, Q. and B. Chu, *Overlap concentration of macromolecules in solution.* Macromolecules, 1987. **20**(2): p. 362-366.

39. Xu, J., W. Cheng, G.E. Inglett, P. Wu, S. Kim, S.X. Liu, and Y. Tseng, *Micro-heterogeneity of cellulosic fiber biopolymer prepared from corn hulls.* LWT - Food Science and Technology, 2010. **43**(6): p. 977-981.

40. Apgar, J., Y. Tseng, E. Fedorov, M.B. Herwig, S.C. Almo, and D. Wirtz, *Multiple-Particle Tracking Measurements of Heterogeneities in Solutions of Actin Filaments and Actin Bundles.* Biophysical Journal, 2000. **79**(2): p. 1095-1106.

41. Tseng, Y. and D. Wirtz, *Mechanics and Multiple-Particle Tracking Microheterogeneity of α-Actinin-Cross-Linked Actin Filament Networks.* Biophysical Journal, 2001. **81**(3): p. 1643-1656.

42. Shin, J.H., M.L. Gardel, L. Mahadevan, P. Matsudaira, and D.A. Weitz, *Relating microstructure to rheology of a bundled and cross-linked F-actin network in vitro.* Proceedings of the National Academy of Sciences of the United States of America, 2004. **101**(26): p. 9636-9641.

43. Stojković, B., S. Sretenovic, I. Dogsa, I. Poberaj, and D. Stopar, *Viscoelastic Properties of Levan-DNA Mixtures Important in Microbial Biofilm Formation as Determined by Micro- and Macrorheology.* Biophysical Journal, 2015. **108**(3): p. 758-765.

44. Hu, W., L. Li, S. Sharma, J. Wang, I. McHardy, R. Lux, Z. Yang, X. He, J.K. Gimzewski, Y. Li, and W. Shi, *DNA Builds and Strengthens the Extracellular Matrix in Myxococcus xanthus Biofilms by Interacting with Exopolysaccharides.* PLoS ONE, 2012. **7**(12): p. e51905.

45. Hung, C., Y. Zhou, J.S. Pinkner, K.W. Dodson, J.R. Crowley, J. Heuser, M.R. Chapman, M. Hadjifrangiskou, J.P. Henderson, and S.J. Hultgren, *Escherichia coli Biofilms Have an Organized and Complex Extracellular Matrix Structure.* mBio, 2013. **4**(5).

46. Mayer, C., R. Moritz, C. Kirschner, W. Borchard, R. Maibaum, J. Wingender, and H.-C. Flemming, *The role of intermolecular interactions: studies on model systems for bacterial biofilms.* International Journal of Biological Macromolecules, 1999. **26**(1): p. 3-16.

47. Kundukad, B., M. Schussman, K. Yang, T. Seviour, L. Yang, S.A. Rice, S. Kjelleberg, and P.S. Doyle, *Mechanistic action of weak acid drugs on biofilms.* Scientific Reports, 2017. **7**(1): p. 4783.

48. Su, C., M. Padra, M.A. Constantino, S. Sharba, A. Thorell, S.K. Lindén, and R. Bansil, *Influence of the viscosity of healthy and diseased human mucins on the motility of Helicobacter pylori.* Scientific Reports, 2018. **8**(1): p. 9710.

49. Berk, V., J.C.N. Fong, G.T. Dempsey, O.N. Develioglu, X. Zhuang, J. Liphardt, F.H. Yildiz, and S. Chu, *Molecular Architecture and Assembly Principles of Vibrio cholerae Biofilms.* Science, 2012. **337**(6091): p. 236-239.

50. Southey-Pillig, C.J., D.G. Davies, and K. Sauer, *Characterization of Temporal Protein Production in Pseudomonas aeruginosa Biofilms.* Journal of Bacteriology, 2005. **187**(23): p. 8114-8126.

51. Ahimou, F., M.J. Semmens, G. Haugstad, and P.J. Novak, *Effect of Protein, Polysaccharide, and Oxygen Concentration Profiles on Biofilm Cohesiveness.* Applied and Environmental Microbiology, 2007. **73**(9): p. 2905-2910.

52. Tuinier, R., J. Rieger, and C.G. de Kruif, *Depletion-induced phase separation in colloid–polymer mixtures.* Advances in Colloid and Interface Science, 2003. **103**(1): p. 1-31.

53. Panorchan, P., D. Wirtz, and Y. Tseng, *Structure-function relationship of biological gels revealed by multiple-particle tracking and differential interference contrast microscopy: The case of human lamin networks.* Physical Review E, 2004. **70**(4): p. 041906.

54. Wagner, C.E., B.S. Turner, M. Rubinstein, G.H. McKinley, and K. Ribbeck, *A Rheological Study of the Association and Dynamics of MUC5AC Gels.* Biomacromolecules, 2017. **18**(11): p. 3654-3664.

55. Tharmann, R., M.M.A.E. Claessens, and A.R. Bausch, *Micro- and Macrorheological Properties of Actin Networks Effectively Cross-Linked by Depletion Forces.* Biophysical Journal, 2006. **90**(7): p. 2622-2627.

56. Schwarz-Linek, J., A. Winkler, L.G. Wilson, N.T. Pham, T. Schilling, and W.C.K. Poon, *Polymer-induced phase separation in Escherichia coli suspensions.* Soft Matter, 2010. **6**(18): p. 4540-4549.

57. Schwarz-Linek, J., G. Dorken, A. Winkler, L.G. Wilson, N.T. Pham, C.E. French, T. Schilling, and W.C.K. Poon, *Polymer-induced phase separation in suspensions of bacteria.* EPL (Europhysics Letters), 2010. **89**(6): p. 68003.

58. Eboigbodin, K.E., J.R.A. Newton, A.F. Routh, and C.A. Biggs, *Role of Nonadsorbing Polymers in Bacterial Aggregation.* Langmuir, 2005. **21**(26): p. 12315-12319.

59. Ghosh, P., J. Mondal, E. Ben-Jacob, and H. Levine, *Mechanically-driven phase separation in a growing bacterial colony.* Proceedings of the National Academy of Sciences, 2015. **112**(17): p. E2166-E2173.

60. Dorken, G., G.P. Ferguson, C.E. French, and W.C.K. Poon, *Aggregation by depletion attraction in cultures of bacteria producing*

exopolysaccharide. Journal of The Royal Society Interface, 2012. **9**(77): p. 3490-3502.

61. Chang, I., E.S. Gilbert, N. Eliashberg, and J.D. Keasling, *A three-dimensional, stochastic simulation of biofilm growth and transport-related factors that affect structure.* Microbiology, 2003. **149**(10): p. 2859-2871.

62. Jefferson, K.K., D.A. Goldmann, and G.B. Pier, *Use of Confocal Microscopy To Analyze the Rate of Vancomycin Penetration through Staphylococcus aureus Biofilms.* Antimicrobial Agents and Chemotherapy, 2005. **49**(6): p. 2467-2473.

63. Chen, X. and P.S. Stewart, *Role of electrostatic interactions in cohesion of bacterial biofilms.* Applied Microbiology and Biotechnology, 2002. **59**(6): p. 718-720.

64. Stewart, E.J., A.E. Satorius, J.G. Younger, and M.J. Solomon, *Role of Environmental and Antibiotic Stress on Staphylococcus epidermidis Biofilm Microstructure.* Langmuir : the ACS journal of surfaces and colloids, 2013. **29**(23): p. 7017-7024.

65. Johansson, J. and T. Curstedt, *Molecular Structures and Interactions of Pulmonary Surfactant Components.* European Journal of Biochemistry, 2004. **244**(3): p. 675-693.

66. Lai, S.K., Y.-Y. Wang, K. Hida, R. Cone, and J. Hanes, *Nanoparticles reveal that human cervicovaginal mucus is riddled with pores larger than viruses.* Proceedings of the National Academy of Sciences, 2010. **107**(2): p. 598-603.

67. Taylor Nordgård, C. and K.I. Draget, *Oligosaccharides As Modulators of Rheology in Complex Mucous Systems.* Biomacromolecules, 2011. **12**(8): p. 3084-3090.

68. Willits, R.K. and W.M. Saltzman, *Synthetic polymers alter the structure of cervical mucus.* Biomaterials, 2001. **22**(5): p. 445-452.

69. Henke, M.O. and F. Ratjen, *Mucolytics in cystic fibrosis.* Paediatric Respiratory Reviews, 2007. **8**(1): p. 24-29.

70. Dawson, M., D. Wirtz, and J. Hanes, *Enhanced viscoelasticity of human cystic fibrotic sputum correlates with increasing microheterogeneity in particle transport.* The Journal of Biological Chemistry, 2003. **278**(50): p. 50393-401.

71. Reighard, K.P., D.B. Hill, G.A. Dixon, B.V. Worley, and M.H. Schoenfisch, *Disruption and eradication of P. aeruginosa biofilms using nitric oxide-releasing chitosan oligosaccharides.* Biofouling, 2015. **31**(9-10): p. 775-787.

72. Zrelli, K., O. Galy, P. Latour-Lambert, L. Kirwan, J.M. Ghigo, C. Beloin, and N. Henry, *Bacterial biofilm mechanical properties persist upon antibiotic treatment and survive cell death.* New Journal of Physics, 2013. **15**(12): p. 125026.

73. Schultz, K.M., K.A. Kyburz, and K.S. Anseth, *Measuring dynamic cell–material interactions and remodeling during 3D human mesenchymal stem cell migration in hydrogels.* Proceedings of the National Academy of Sciences, 2015. **112**(29): p. E3757-E3764.

74. Morris, E.R., K. Nishinari, and M. Rinaudo, *Gelation of gellan – A review.* Food Hydrocolloids, 2012. **28**(2): p. 373-411.

75. Jones, C.A.R., L. Liang, D. Lin, Y. Jiao, and B. Sun, *The spatial-temporal characteristics of type I collagen-based extracellular matrix.* Soft Matter, 2014. **10**(44): p. 8855-8863.

76. Zhang, W., T.S. Sileika, C. Chen, Y. Liu, J. Lee, and A.I. Packman, *A novel planar flow cell for studies of biofilm heterogeneity and flow–biofilm interactions.* Biotechnology and Bioengineering, 2011. **108**(11): p. 2571-2582.

77. Horn, H., H. Reiff, and E. Morgenroth, *Simulation of growth and detachment in biofilm systems under defined hydrodynamic conditions.* Biotechnology and Bioengineering, 2003. **81**(5): p. 607-617.

78. Jang, H., R. Rusconi, and R. Stocker, *Biofilm disruption by an air bubble reveals heterogeneous age-dependent detachment patterns dictated by initial extracellular matrix distribution.* npj Biofilms and Microbiomes, 2017. **3**(1): p. 6.

79. Pozzoli, M., H.X. Ong, L. Morgan, M. Sukkar, D. Traini, P.M. Young, and F. Sonvico, *Application of RPMI 2650 nasal cell model to a 3D printed apparatus for the testing of drug deposition and permeation of nasal products.* European Journal of Pharmaceutics and Biopharmaceutics, 2016. **107**: p. 223-233.

80. Beyenal, H., C. Donovan, Z. Lewandowski, and G. Harkin, *Three-dimensional biofilm structure quantification.* Journal of Microbiological Methods, 2004. **59**(3): p. 395-413.

81. Alhede, M., K. Qvortrup, R. Liebrechts, N. Høiby, M. Givskov, and T. Bjarnsholt, *Combination of microscopic techniques reveals a comprehensive visual impression of biofilm structure and composition.* FEMS Immunology & Medical Microbiology, 2012. **65**(2): p. 335-342.

82. Tseng, Y., K.M. An, and D. Wirtz, *Microheterogeneity Controls the Rate of Gelation of Actin Filament Networks.* Journal of Biological Chemistry, 2002. **277**(20): p. 18143-18150.

83. Xu, J., T. Chang, G.E. Inglett, S. Kim, Y. Tseng, and D. Wirtz, *Micro-heterogeneity and micro-rheological properties of high-viscosity oat β-glucan solutions.* Food Chemistry, 2007. **103**(4): p. 1192-1198.

84. Xu, J., Y. Tseng, C.J. Carriere, and D. Wirtz, *Microheterogeneity and Microrheology of Wheat Gliadin Suspensions Studied by Multiple-Particle Tracking.* Biomacromolecules, 2002. **3**(1): p. 92-99.

85. Goodman, A., Y. Tseng, and D. Wirtz, *Effect of Length, Topology, and Concentration on the Microviscosity and Microheterogeneity of DNA Solutions.* Journal of Molecular Biology, 2002. **323**(2): p. 199-215.

86. Valentine, M.T., P.D. Kaplan, D. Thota, J.C. Crocker, T. Gisler, R.K. Prud'homme, M. Beck, and D.A. Weitz, *Investigating the microenvironments of inhomogeneous soft materials with multiple particle tracking.* Phys Rev E Stat Nonlin Soft Matter Phys, 2001. **64**(6 Pt 1): p. 061506.

87. Kegel, W.K., B. van, and Alfons, *Direct Observation of Dynamical Heterogeneities in Colloidal Hard-Sphere Suspensions.* Science, 2000. **287**(5451): p. 290-293.

88. Aufderhorst-Roberts, A., W.J. Frith, and A.M. Donald, *Micro-scale kinetics and heterogeneity of a pH triggered hydrogel.* Soft Matter, 2012. **8**(21): p. 5940-5946.

89. Houghton, H.A., I.A. Hasnain, and A.M. Donald, *Particle tracking to reveal gelation of hectorite dispersions.* The European Physical Journal E, 2008. **25**(2): p. 119-127.

90. Guo, S. and B.B. Akhremitchev, *Packing Density and Structural Heterogeneity of Insulin Amyloid Fibrils Measured by AFM Nanoindentation.* Biomacromolecules, 2006. **7**(5): p. 1630-1636.

91. Calabri, L., N. Pugno, C. Menozzi, and S. Valeri, *AFM nanoindentation: tip shape and tip radius of curvature effect on the hardness measurement.* Journal of Physics: Condensed Matter, 2008. **20**(47): p. 474208.

92. Wilson, L.G. and W.C.K. Poon, *Small-world rheology: an introduction to probe-based active microrheology.* Physical Chemistry Chemical Physics, 2011. **13**(22): p. 10617-10630.

93. Elsayad, K., S. Werner, M. Gallemí, J. Kong, E.R. Sánchez Guajardo, L. Zhang, Y. Jaillais, T. Greb, and Y. Belkhadir, *Mapping the subcellular mechanical properties of live cells in tissues with fluorescence emission–Brillouin imaging.* Science Signaling, 2016. **9**(435): p. rs5-rs5.

94. Scarcelli, G. and S.H. Yun, *Confocal Brillouin microscopy for three-dimensional mechanical imaging.* Nature Photonics, 2007. **2**: p. 39.

95. Karampatzakis, A., C.Z. Song, L.P. Allsopp, A. Filloux, S.A. Rice, Y. Cohen, T. Wohland, and P. Török, *Probing the internal micromechanical properties of Pseudomonas aeruginosa biofilms by Brillouin imaging.* npj Biofilms and Microbiomes, 2017. **3**(1): p. 20.

96. Peulen, T.-O. and K.J. Wilkinson, *Diffusion of Nanoparticles in a Biofilm.* Environmental Science & Technology, 2011. **45**(8): p. 3367-3373.

97. Olmsted, S.S., J.L. Padgett, A.I. Yudin, K.J. Whaley, T.R. Moench, and R.A. Cone, *Diffusion of Macromolecules and Virus-Like Particles in Human Cervical Mucus.* Biophysical Journal, 2001. **81**(4): p. 1930-1937.

98. Belli, V., D. Guarnieri, M. Biondi, F. della Sala, and P.A. Netti, *Dynamics of nanoparticle diffusion and uptake in three-dimensional cell cultures.* Colloids and Surfaces B: Biointerfaces, 2017. **149**: p. 7-15.

99. Nance, E.A., G.F. Woodworth, K.A. Sailor, T.-Y. Shih, Q. Xu, G. Swaminathan, D. Xiang, C. Eberhart, and J. Hanes, *A Dense Poly(ethylene glycol) Coating Improves Penetration of Large Polymeric Nanoparticles within Brain Tissue.* Science translational medicine, 2012. **4**(149): p. 149ra119-149ra119.

100. Schuster, B.S., J.S. Suk, G.F. Woodworth, and J. Hanes, *Nanoparticle diffusion in respiratory mucus from humans without lung disease.* Biomaterials, 2013. **34**(13): p. 3439-3446.

101. Vogt, M., H.C. Flemming, and W.S. Veeman, *Diffusion in Pseudomonas aeruginosa biofilms: a pulsed field gradient NMR study.* Journal of Biotechnology, 2000. **77**(1): p. 137-146.

102. Parrish, E., M.A. Caporizzo, and R.J. Composto, *Network confinement and heterogeneity slows nanoparticle diffusion in polymer gels.* The Journal of Chemical Physics, 2017. **146**(20): p. 203318.

103. Zhang, X., J. Hansing, Roland R. Netz, and Jason E. DeRouchey, *Particle Transport through Hydrogels Is Charge Asymmetric.* Biophysical Journal, 2015. **108**(3): p. 530-539.

104. Dirk, d.B., S. Paul, and L. Zbigniew, *Measurement of local diffusion coefficients in biofilms by microinjection and confocal microscopy.* Biotechnology and Bioengineering, 1997. **53**(2): p. 151-158.

105. Cu, Y. and W.M. Saltzman, *Controlled Surface Modification with Poly(ethylene)glycol Enhances Diffusion of PLGA Nanoparticles in Human Cervical Mucus.* Molecular Pharmaceutics, 2009. **6**(1): p. 173-181.

106. Lieleg, O. and K. Ribbeck, *Biological hydrogels as selective diffusion barriers.* Trends in Cell Biology, 2011. **21**(9): p. 543-551.

107. Dirk, d.B., S. Paul, and L. Zbigniew, *Liquid flow in heterogeneous biofilms.* Biotechnology and Bioengineering, 1994. **44**(5): p. 636-641.

108. J., D.W., S.P. S., and C.W. G., *Transport of 1-μm latex particles in pseudomonas aeruginosa biofilms.* Biotechnology and Bioengineering, 1993. **42**(1): p. 111-117.

109. Macierzanka, A., A.R. Mackie, B.H. Bajka, N.M. Rigby, F. Nau, and D. Dupont, *Transport of Particles in Intestinal Mucus under Simulated Infant and Adult Physiological Conditions: Impact of Mucus Structure and Extracellular DNA.* PLoS ONE, 2014. **9**(4): p. e95274.

110. Moschakis, T., A. Lazaridou, and C.G. Biliaderis, *Using particle tracking to probe the local dynamics of barley β-glucan solutions upon gelation.* Journal of Colloid and Interface Science, 2012. **375**(1): p. 50-59.

111. Ma, T.M., J.S. VanEpps, and M.J. Solomon, *Structure, Mechanics, and Instability of Fibrin Clot Infected with Staphylococcus epidermidis.* Biophysical Journal, 2017. **113**(9): p. 2100-2109.

112. Reiß, S., G. Burau, O. Stachs, R. Guthoff, and H. Stolz, *Spatially resolved Brillouin spectroscopy to determine the rheological properties of the eye lens.* Biomedical Optics Express, 2011. **2**(8): p. 2144-2159.

113. Galy, O., P. Latour-Lambert, K. Zrelli, J.-M. Ghigo, C. Beloin, and N. Henry, *Mapping of Bacterial Biofilm Local Mechanics by Magnetic Microparticle Actuation.* Biophysical Journal, 2012. **103**(6): p. 1400-1408.

114. Waters, M.S., S. Kundu, N.J. Lin, and S. Lin-Gibson, *Microstructure and Mechanical Properties of In Situ Streptococcus mutans Biofilms.* ACS Applied Materials & Interfaces, 2014. **6**(1): p. 327-332.

115. Kuo, C.K. and P.X. Ma, *Ionically crosslinked alginate hydrogels as scaffolds for tissue engineering: Part 1. Structure, gelation rate and mechanical properties.* Biomaterials, 2001. **22**(6): p. 511-521.

116. Mullen, Conleth A., Ted J. Vaughan, Kristen L. Billiar, and Laoise M. McNamara, *The Effect of Substrate Stiffness, Thickness, and Cross-Linking Density on Osteogenic Cell Behavior.* Biophysical Journal, 2015. **108**(7): p. 1604-1612.

117. Jung, J.P., M.K. Bache-Wiig, P.P. Provenzano, and B.M. Ogle, *Heterogeneous Differentiation of Human Mesenchymal Stem Cells in 3D Extracellular Matrix Composites.* BioResearch Open Access, 2016. **5**(1): p. 37-48.

118. Haugh, M.G., C.M. Murphy, R.C. McKiernan, C. Altenbuchner, and F.J. O'Brien, *Crosslinking and Mechanical Properties Significantly Influence Cell Attachment, Proliferation, and Migration Within Collagen Glycosaminoglycan Scaffolds.* Tissue Engineering Part A, 2010. **17**(9-10): p. 1201-1208.

119. Lo, C.-M., H.-B. Wang, M. Dembo, and Y.-l. Wang, *Cell Movement Is Guided by the Rigidity of the Substrate.* Biophysical Journal, 2000. **79**(1): p. 144-152.

120. Solon, J., I. Levental, K. Sengupta, P.C. Georges, and P.A. Janmey, *Fibroblast Adaptation and Stiffness Matching to Soft Elastic Substrates.* Biophysical Journal, 2007. **93**(12): p. 4453-4461.

121. Baker, E.L., J. Lu, D. Yu, R.T. Bonnecaze, and M.H. Zaman, *Cancer Cell Stiffness: Integrated Roles of Three-Dimensional Matrix Stiffness and Transforming Potential.* Biophysical Journal, 2010. **99**(7): p. 2048-2057.

122. Doyle, A.D., N. Carvajal, A. Jin, K. Matsumoto, and K.M. Yamada, *Local 3D matrix microenvironment regulates cell migration through spatiotemporal dynamics of contractility-dependent adhesions.* Nature Communications, 2015. **6**: p. 8720.

123. Sapudom, J., S. Rubner, S. Martin, T. Kurth, S. Riedel, C.T. Mierke, and T. Pompe, *The phenotype of cancer cell invasion controlled by fibril diameter and pore size of 3D collagen networks.* Biomaterials, 2015. **52**: p. 367-375.

124. Shin, Y., H. Kim, S. Han, J. Won, H.E. Jeong, E.-S. Lee, R.D. Kamm, J.-H. Kim, and S. Chung, *Extracellular Matrix Heterogeneity Regulates Three-Dimensional Morphologies of Breast Adenocarcinoma Cell Invasion.* Advanced Healthcare Materials, 2013. **2**(6): p. 790-794.

125. Zhu, J., L. Liang, Y. Jiao, L. Liu, and U.S.C.P.S.-O.A. on behalf of the, *Enhanced Invasion of Metastatic Cancer Cells via Extracellular Matrix Interface.* PLOS ONE, 2015. **10**(2): p. e0118058.

126. Winter, H.H. and F. Chambon, *Analysis of Linear Viscoelasticity of a Crosslinking Polymer at the Gel Point.* Journal of Rheology, 1986. **30**(2): p. 367-382.

Chapter 3

A Model Complex Fluid with Controlled Microrheological Heterogeneity

3.1 INTRODUCTION

Complex fluids are found everywhere. They occur naturally in our body, for example blood, mucus and also synovial fluid. Other examples such as polymer matrix of a biofilm or even the extracellular matrix of our organs can also be categorized as complex fluids. Complex fluids also have importance in our everyday lives, as many liquid consumer products are complex fluids. Examples include food, cosmetic or cleaning products as well as materials used in various industrial processes. The characterisation of complex fluids will be critical to understand their design and use. Many diseases are related to the change of biofluid flow properties, and a common example is cystic fibrosis which changes the properties of mucus, making it thicker and stickier than healthy mucus [1]. Complex fluid characterisation helps understand diseases better to help to design drugs for treatments [2]. Characterisation of complex fluids will be useful in industrial processes such as mixing [3] and even the final quality of products [4, 5] are determined by the fluid properties. This means understanding fluid properties will allow us to be able to improve processes and product quality.

Complex fluids have structures that are formed by the molecular interaction between their building blocks, typically polymers, colloids, and/or surfactants. As a result, complex fluids often have viscoelastic properties, making them behave as some combination of elastic solids or viscous fluids. Viscoelasticity usually originates from structure at small, typically micron and submicron, length scales, but conventional bulk rheology characterises these properties at scales much larger than the structural length scale [6]. The method of microrheology is used to characterise local viscoelastic properties of a fluid at meso- or micron length scales, as this is the characteristic size of the fluid microstructure. Microrheology is also needed to characterise rare or biological fluids when only tiny amounts are available. Examples include fluids like cytoskeleton networks [7], cystic fibrosis mucus [8] and bacterial biofilms [9].

The characterisation of fluids *via* microrheology depends on the diffusivity of probe particles in the fluid. The quantification of particle diffusivity is usually

done by microscopic observation of the tracer probes, calculation of the particle mean square displacement, or MSD, for a given time. MSD is defined as:

Equation 3.1 $\text{MSD}(\tau) = \langle \Delta r(\tau)^2 \rangle = \langle [r(t+\tau) - r\,(t)]^2 \rangle$

where r(*t*) is is the position of the particle at time *t*, and τ is the lag time between the two positions of a particle to calculate its MSD. The average MSD is then fitted to a power law equation, where the power law exponent (n) indicates the diffusivity of particles. Particles are fully diffusive when n~1, while n~0 indicates particles are trapped in the structure mesh. Many polymer systems are viscoelastic, thus their n-value usually lies in between these two extremes, meaning that the particles experiencing sub-diffusive motions. When the n~1, the particle diffusivity can also be calculated from the power-law fitting using the intercept of the power law fitting (A), which is defined as:

Equation 3.2 $A = 2dD$

where d is the dimension where the particle tracking is done. For particle tracking that is done on a single plane, the dimension is two, hence the formula will become

Equation 3.3 $A = 4D$

The diffusivity coefficient itself is related to the viscosity of medium based on Stokes-Einstein equation, where it is defined as:

Equation 3.4 $D = \frac{k_B\, T}{6\pi\ \eta\ r}$

kB is Boltzmann's constant, T is sample temperature during experiment, η is the viscosity of the fluid and r is the radius of particle diffusing.

When the particles are sub-diffusive (n<1), moduli are calculated to characterise the fluid. Here, the generalised Stokes-Einstein equation is used, which is defined as:

Equation 3.5 $|G(\omega)| = \frac{k_B\, T}{\pi a \langle \Delta r^2 \left(\frac{1}{\omega}\right) \rangle\ \Gamma\,[1+\,\alpha(\omega)]}$

a is the radius of particle diffusing, Γ is gamma function that is defined as

Equation 3.6 $\Gamma[1+\alpha] \approx 0.457\,(1+\alpha)^2 - 1.36(1+\alpha) + 1.90,$ where $\alpha(\omega)$is:

Equation 3.7 $\alpha(\omega) = \frac{dln\langle r^2(\tau)\rangle}{d\ln\tau}$, with τ=1/ω [10]. This is then used to calculate the elastic (G') and viscous moduli (G"), where it is defined as:

Equation 3.8 $G'(\omega) = |G(\omega)|\cos\left(\frac{\pi\alpha(\omega)}{2}\right)$

Equation 3.9 $G"(\omega) = |G(\omega)|\sin\left(\frac{\pi\alpha(\omega)}{2}\right)$

In many cases, fluid structure and mechanical properties can vary depending on the characteristic length scale of the three-dimensional polymer or particle structure responsible for a fluid's viscoelastic properties. Studies often speak of a "mesh" size, as the microstructure can be quite porous with a background fluid permeating the mesh [11]. When the tracer probe size is smaller than the fluid mesh size, tracer diffusivity will be dependent on the background fluid viscosity. In contrast, particles larger than the fluid mesh size can be used to characterise the bulk rheology of the viscoelastic structure. If the probe size has the same length scale as the fluid structure, it measures the elastic properties of the mesh material [12]. As a result, the characterisation of rheology can be strongly length scale-dependent and a key variable is the relative size of particles to the mesh size [13].

Biological and synthetic complex fluids can be structurally and spatially heterogeneous in their mechanical properties. The formation of heterogeneity can occur naturally as a result of many mechanisms, discussed in greater detail in Chapter 2, but a common one is the interaction of soluble polymers in a fluid, which can be tuned by changes in fluid ionic strength or pH [14, 15]. Heterogeneity in many biopolymer systems is often detected at concentrations typical of the semi-dilute regime [7, 16-19].

Structural heterogeneity is formally defined as the existence of multiple complex fluid microenvironments in a single fluid, and in many polymer solutions it is a mesh of interacting polymers surrounded by a continuous phase fluid, often water,

forming a bulk gel [20-23]. This means that particles inside the microscale polymer network will diffuse in a very constrained environment, while the particles outside the network will diffuse relatively freely, as if in water alone [23]. Variation of structure, length scale, tracer properties, and environmental conditions can create, remove, or vary heterogeneity.

Thus, qualitative assessment of heterogeneity *via* particle displacements alone can be misleading, as experimental variations can affect microrheology measurements. Indeed, it has been shown in the literature that a very large variation in the "MSD *vs* lag time" plot might be observed in glycerol as an example of a homogeneous system [24]. Furthermore, the statistic of these MSD values are limited hence heterogeneity is qualitatively assessed by plotting the van-Hove correlation function of the ensemble-averaged particle displacement at a given lag time. The movement of particles in a purely diffusive system should follow a probability density function of

Equation 3.10 $P(\Delta x,\tau) = (4\pi D\tau)^{-1/2} \exp(\langle \Delta x^2 \rangle / 4D\tau)$ [24].

If particles are diffusing in a homogeneous medium, the van Hove correlation function should fit a single Gaussian function, which indicates that all particles have the same diffusion coefficient. However, in heterogeneous media multiple Gaussian modes are required to describe the behaviour as the particles might have multiple diffusion coefficients. Statistical analysis is also commonly done to quantitatively differentiate two possible microenvironments in a fluid, for example the skewness measure or F-statistic of the data [7, 16, 24]. A third approach is the measurement of non-Gaussian parameters (*N or HR ratio*), which is defined as:

Equation 3.11 $N\ (\text{HR ratio}) = \frac{\langle \Delta x^4 \rangle}{3\langle \Delta x^2 \rangle^2} - 1$

This equation is basically the ratio between the fourth and second moment of the particle displacement distribution [25]. When *N* or the *HR ratio* is equal to or close to zero, it indicates a Gaussian distribution or homogeneity of the system [26]. Heterogeneity is important to characterisation of processes like polymer gel

degradation [27], which can increase [8] or decrease the degree of heterogeneity [28], as well as numerous other biological and medical examples discussed in Chapter 2.

Although common in natural fluids, there are no generally accepted model heterogeneous fluids with a controllable degree of heterogeneity. A model heterogeneous fluid would enable comparison and standardisation of different microrheology techniques, such as dynamic differential microscopy [29, 30] and conventional particle tracking. A more standardised approach to controlling fluid heterogeneity also has numerous applications in design of novel consumer, pharmaceutical, cosmetic, and food product microstructures in order to enhance function and performance [31].

In this chapter, we studied the feasibility of developing a controlled heterogeneous model fluid using gellan gum. Gellan gum is a water-soluble anionic polysaccharide produced by the bacterium *Sphingomonas elodea*. This has been used in literature as a model to mimic mechanical properties of biofilm [33]. The properties can be easily modified by adding different types of salts which creates different gels properties. Therefore, this polymer have a great potential to model heterogeneity in biofilms.

3.2 MATERIALS AND METHODS

3.2.1 | Gellan gel preparation

Gellan solutions were prepared by adding 0.1 g of gellan powder (Gelzan; Sigma Aldrich, Sydney, Australia) to 20 mL of water heated to 80 °C and mixing for 20 minutes. This becomes a stock solution that was used to prepare gellan gels with different polymer and salt concentrations. Potassium chloride (KCl) and sodium chloride (NaCl) (Chem-Supply Pty Ltd, South Australia, Australia) were used as cross-linkers for cross-linked gellan gels. These salts were added to hot gellan solution (80 °C) as a solution and then mixed with stir bar for a further 10 minutes at low speed. Successively, the gels are cooled down to room temperature for at

least 1 hour before use in any experiments. To prepare the mixed gels, the two gels were mixed again using a stir bar at low speeds at 25 °C.

3.2.2 | Bulk rheology experiment

Bulk rheology was performed using a Discovery HR-1 rheometer (TA Instruments) with a 40 mm cone and plate geometry and 2° angle. For all measurements, samples were pre-sheared at 10 s^{-1} for 10 s, and then equilibrated for 120 s. Flow studies were performed by changing the shear rate from 1 to 1000 s^{-1}, while an oscillation stress sweep was done by increasing stress from 0.01 Pa to 50 Pa at a frequency of 1 Hz. A frequency sweep was also performed from 0.1 rad/s to 100 rad/s.

3.2.3 | Microrheology experiments

1-µm carboxylated fluorescent particles (Polysciences inc, Pennsylvania, USA) were used as tracking probes for all microrheology experiments. The particles were added at a concentration 0.0025% w/v during mixing of gellan and salt solutions. The chamber used for microrheology experiments was made from a flat capillary tube with a 0.21 mm wall thickness and an opening width of 3 mm (Vitrocom, New Jersey, USA). The two ends of the capillary were sealed using epoxy glue (Selleys, Australia). This chamber was then glued onto a glass slide.

For microrheology experiment, samples were slowly pipetted into the sample chamber, using a 20 ul air displacement pipette. The shear itself is defined as linear velocity over diameter of minimum pipette. All samples were pipetted into the chamber after they are cooled down, except the gels used for experiments in part 3.3.3, which were pipetted into the chamber when they were still hot. The hot "hard gel" was pipetted first into the chamber and only after they cooled down, the second hot "soft gel" was pipetted into the same chamber to contact the first.

Microrheology experiments were performed using a TIRF Zeiss (Germany) inverted microscope with 63x lens, NA of 1.4. A Leica DM2500M (Germany) with a 50x objective, NA of 0.75 was also used for some studies. The Zeiss

microscope uses a laser at 488 nm to illuminate the sample (relative laser strength 70%). For the Zeiss microscope, image series (movies) were captured with a Hamamatsu camera (Hamamatsu, Japan), with a frame rate of 35 frames per second for 990 frames, with an exposure time of 30 ms and frame size 512x512 pixels. The Leica is connected to a Moticam 10MP (Motic, China) and used to acquire data with a frame rate of 2 frames per second for 1000 frames and a frame size of 800 x 600 pixels. All pictures were analysed using the Python library Trackpy [32]. Due to intrinsic error of particle tracking using Python, the data in the van-Hove correlation plots show variability in the probability range between 1 and 10. This could graphically affect the Gaussian plot, however the majority of the data sets that is found between 10 and 1000 are not affected.

3.3 RESULTS AND DISCUSSIONS

3.3.1 | Effect of salts on gellan rheology

Gellan gum is a biopolymer isolated from *Sphingomonas elodea*. Gellan has been used previously to mimic bulk rheological properties of native biofluids such as biofilms [33]. Gellan polymers undergo a coil-to-helix transformation when they are heated, which starts an aggregation process leading to gel formation [34]. The presence of salt will decrease the repulsion between gellan aggregates, thus stabilising the structure and increasing its elasticity [34]. Higher valence salts have a stronger gelling effect on gellan, allowing manipulation using different types of salts [35-38] at a range of concentrations [38, 39] and pH values [40]. Gellan gels formed with divalent ions are very hard and brittle [37] and also have a higher gelation temperature [41].

The first aim of the work was to prepare two different gels that had different properties when studied by bulk and microrheology. Gellan polymer was chosen because its gelation properties can be modified easily by tuning the concentrations and types of salt solution added to the gel. In addition, the resulting gels are clear and transparent, easing particle observation *via* microscope.

All experiments here used monovalent ions to avoid formation of overly hard, brittle gels. When both KCl and NaCl were used, the resulting properties of the gels are slightly different, although the same concentrations of salts are used. Stress sweep measurements done on the gels made with 20 mM KCl and NaCl show that the two gels' storage moduli were always lower than their loss modulus (G'<G") (Figure 3.1a). This indicates that both of them are primarily viscous, rather than elastic, fluids. But for clarity, this type of system will be referred to as a "soft gel" from now on in this chapter.

The ratio of G" to G', called tan δ, indicates the relative importance of viscous fluid properties to elasticity. In the case of KCl and NaCl, the tan δ of gels made with KCl is lower than those made with NaCl (Figure 3.1b), meaning gels made with NaCl are more viscous than the made with KCl. The influence of salt effects on gellan gelation follows this salt sequence : $Li^+ < Na^+ < K^+ < Cs^+$ [42], with cesium salts producing the strongest gels because of stronger cross-linking [43]. As the gellan concentration used here is quite dilute, the salt plays a very important role in formation of microstructure.

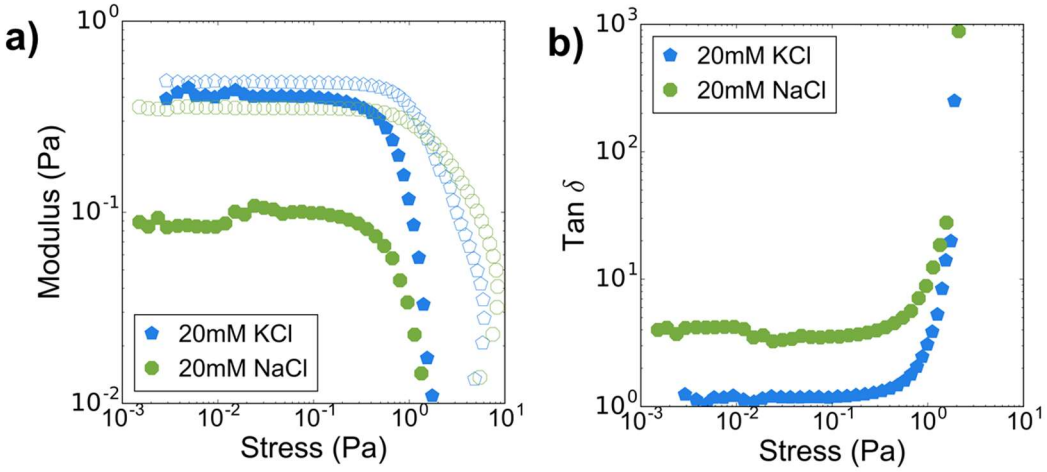

FIGURE 3.1 Bulk rheology of 0.25% gellan with two different salts; a) Stress sweep results at 1Hz, b) calculated tan δ. Closed symbol indicates storage modulus (G'), while open symbol indicates loss modulus (G")

3.3.2 | Heterogeneity of gellan gels with different mixture of salts

We might expect to observe heterogeneity when the KCl and NaCl gels are mixed together and used to produce a single gel. Here, we use different proportions of KCl and NaCl, keeping the actual number of cations available for the gellan chains to form cross-links.

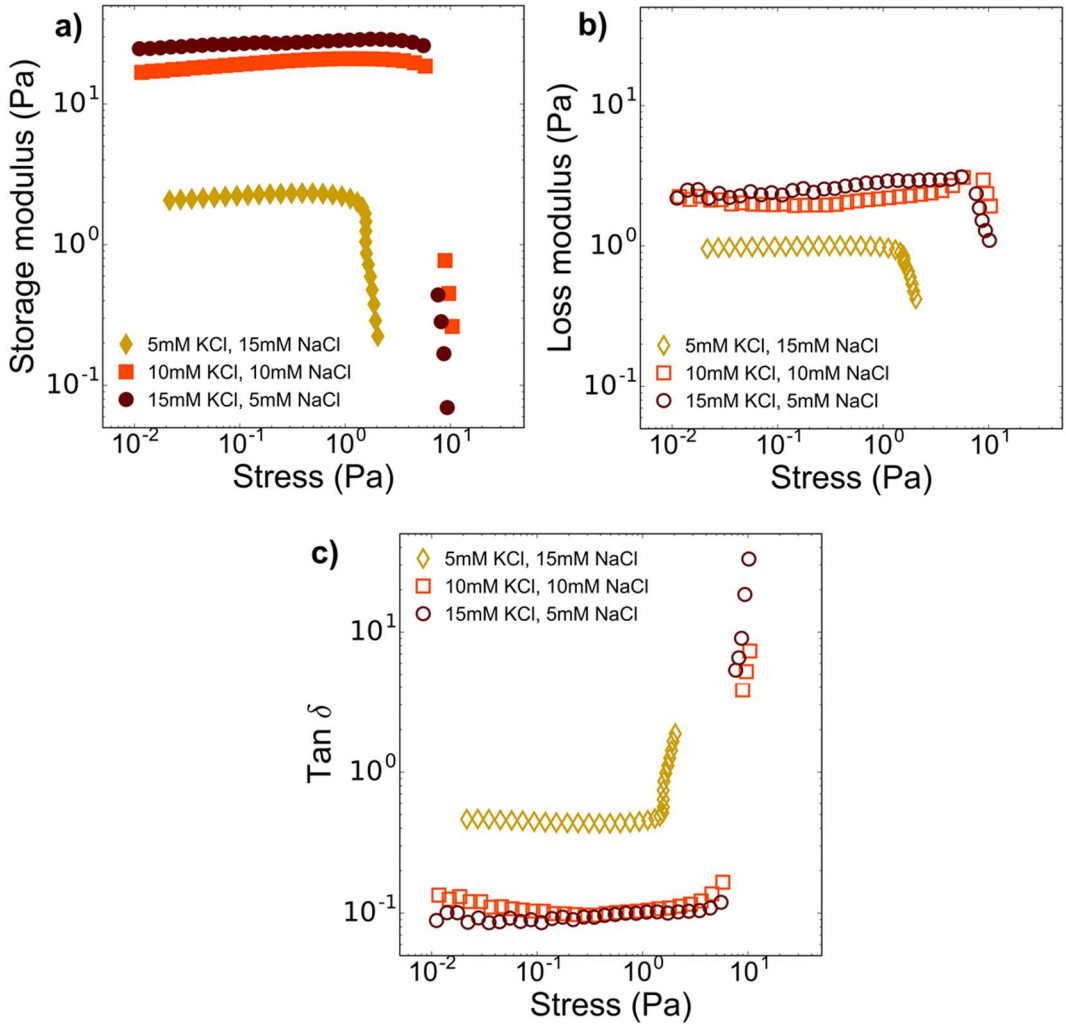

FIGURE 3.2 a) Storage modulus of gels with different proportions of KCl and NaCl, b) Loss modulus of gels with different proportion KCl and NaCl, c) Tan δ of gels with different proportion KCl and NaCl

The results plotted in Figure 3.2 show the bulk rheology results of gels prepared with mixture of two salts. It can be seen that with increasing concentration of KCl from 5mM to 10mM, there is an increase in storage modulus around 10 times (Figure 3.2a). However, by increasing KCl concentration from 10mM to 15mM, there is only a slight change observed (Figure 3.2a). Similarly, for loss modulus and tan delta (Figure 3.2b and Figure 3.2c), the biggest change can only be seen when increasing KCl concentration from 5mM to 15mM. As figure 3.2a shows, the two gels with highest concentration of KCl yield very abruptly, which may be due to the brittleness of the gel. The two gels with highest concentration of KCl have quite low concentrations of NaCl, while the gel with lowest concentration of KCl has the highest amount of NaCl. This also suggests that when two are present concurrently, high concentration of NaCl helps to "soften" the gel, making it yield more gradually, as in the case of low KCl. The result in Figure 3.2c also shows that the tan δ reduces with increasing concentration of KCl, indicating that KCl helps to strengthen the structure. This again supports the information from literature that K^+ ions bind more strongly to gellan chains, which results in stronger cross-linking network than Na^+ ions [42].

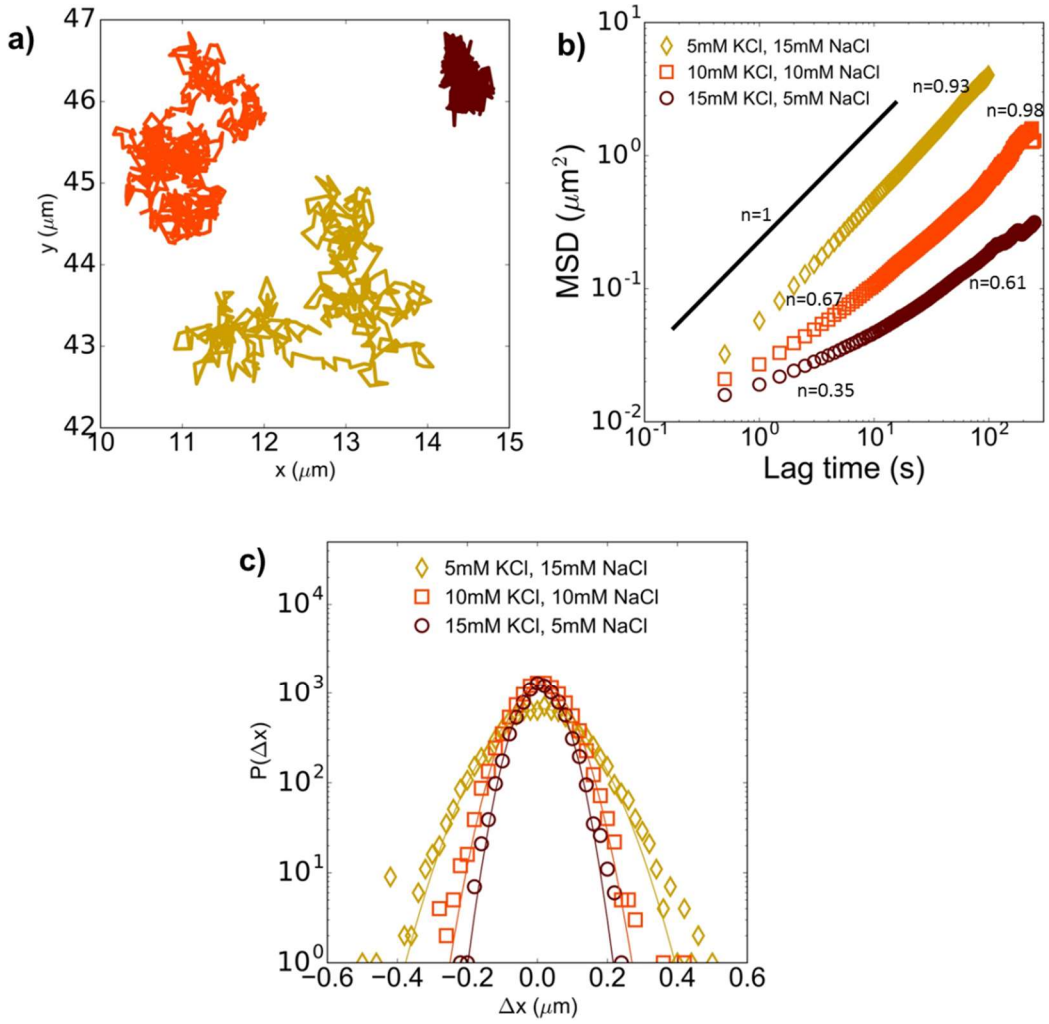

FIGURE 3.3 a) Particle diffusive trajectories in gels with different proportion of KCl and NaCl, b) The average MSDs of particles diffusing in gels with different proportions of salts (black line indicates slope equals to 1), c) van Hove correlation of gels with different proportion of NaCl and KCl at t = 0.5s.

At the microscale, the behaviour of the gellan gels tested here should be different from one another. Additionally, the heterogeneity might also be different as past work indicated that the mesh of gellan gels produced from different single cations are different [44]. In Figure 3.3a, it is shown the representative trajectories in the mixed gels where they decreased in size with increasing concentration of KCl in the system. The particle trajectory becomes more trapped as we increase the concentration of KCl. This is followed by a decrease in slope of the MSD (Figure

3.3b), where gels with higher concentration of NaCl show almost diffusive behaviour (n ~ 1). At 10mM KCl, the MSD shows sub-diffusive behaviour at short time, (indicated by n<1) while at long times they also show diffusive behaviour (n ~1). The sub-diffusive behaviour at short time is a characteristic of particles diffusing in a mesh, but after a while they manage to escape hence there is diffusive behaviour at long time. At 15mM KCl however, the MSD always shows sub-diffusive behaviour at all times. This indicates that the particles are always diffusing in the elastic mesh that traps them. This further confirms the role of KCl in strengthening the structure of gellan gels.

To understand the heterogeneity of a gel structure made with different proportions of salts, van Hove functions of the particle displacement are plotted in Figure 3.3c. As shown in Figure 3.3c, the distribution of displacements of the gels can be fitted with a regular Gaussian distribution, which indicates their homogeneity. Although past work has indicated that the mesh of gellan gels with different single cations might be different [44], the fact is that when the two salts are mixed together, heterogeneity cannot still be observed. This is probably related to the fact that the salt solution itself is a homogeneous solution. Network heterogeneity of gellan gels could not be created with the addition of homogeneous salt solution into the aqueous gellan solution, as a result, the resulting gels are still homogeneous.

3.3.3 | Heterogeneity of two mixed gellan gels

In order to make a heterogeneous fluid with controlled heterogeneity, we mix in bulk two different gels with distinct bulk- and micro-rheological properties using a magnetic stirrer. Figure 3.4 shows the appearance of the gels that were used for experiments. Both gels are able to flow, making them easy to handle. Although that is the case, the slight brittleness of the hard gel possibly cause it to break into microgels particles as documented in Caggioni et al [23]. However, as the initial two gels are different, it is still expected that the resulting gels are heterogeneous.

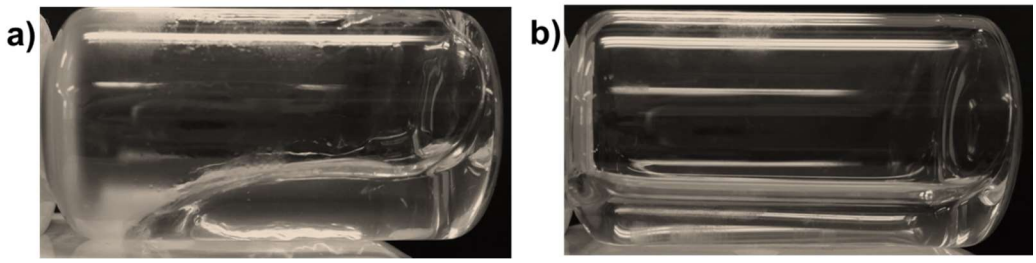

FIGURE 3.4 Bulk appearance of the gels used in the experiments; a) 100% hard gel, b) 100% soft gel (0% hard gel)

Bulk rheology measurements show in Figure 3.5a that both original gels, as well as their mixtures, are shear-thinning fluids. The hard gel is roughly 10 times more viscous than the soft gel at low shear rates. The plateau moduli of the two gels in Figure 3.4b indicate that hard gel is a true gel in the sense that its elastic modulus is larger than its viscous modulus, G' > G", while the soft gel is weaker with G' < G". The microrheology of the two gels is similar, Figure 3.5, although can only be assessed in comparison with the low shear rate data measured with bulk rheologyin Figure 3.5a. The trajectories of tracer particles in these two fluids are different; in hard gel the particles are trapped, while the particles in 100% soft gel are fully diffusive (Figure 3.6a).

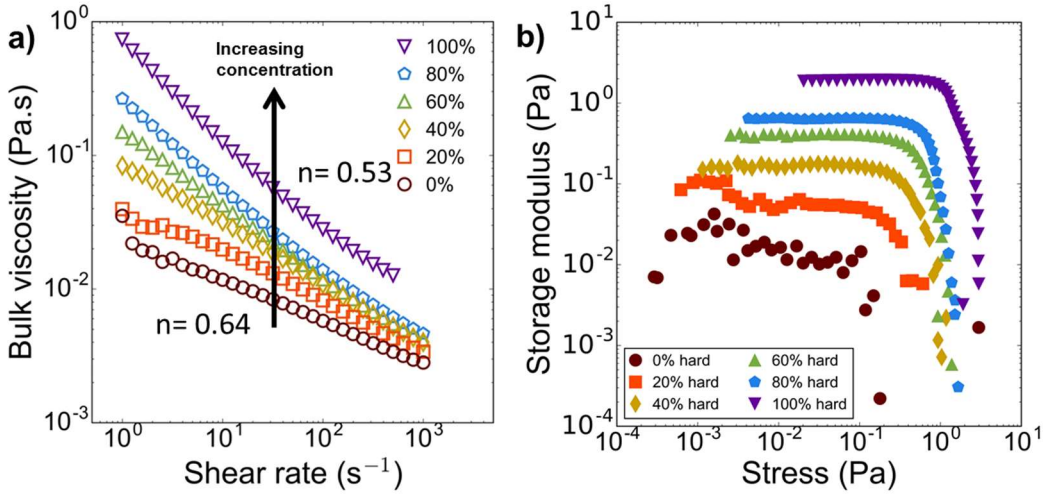

FIGURE 3.5 Bulk rheology of hard gels, soft gels, and their mixtures at a range of concentrations of the hard gel. a) Flow curves of gels and gel mixtures, the n here indicates flow index, b) Storage modulus (G') obtained from stress sweep

As we mixed the two gels, we expected the bulk rheological properties of the mixtures to change. It was hypothesised that the properties of gels with higher proportion of hard gels should become more like the hard gel itself. The results shown in Figure 3.4a prove that this is possibly happening; all viscosities of the mixture are in between the hard and soft gels, the viscosities increase with increasing proportion of hard gels in the mixture. The stress sweep test also showed that with increasing concentration of hard gel, there is an increase in elasticity (G'). From 0% hard gel to 100% hard gel, there is an increase about 100 times in terms of G'.

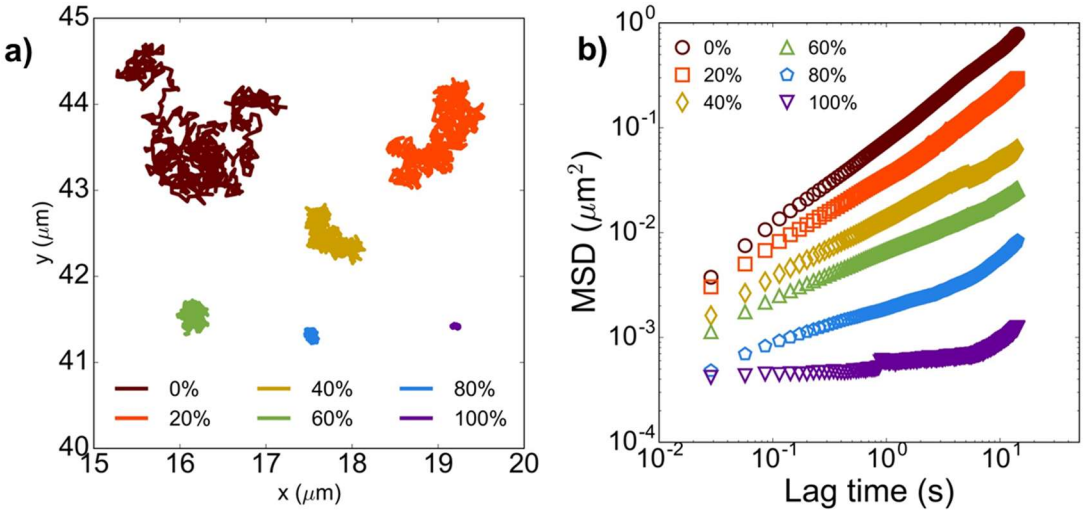

FIGURE 3.6 a) Representative particle trajectories in gels with different % of hard gels, b) Average mean square displacement of particles diffusing in gels with different % of hard gels

In micro scale, the distance that the particles diffuse decreases with increasing concentration of hard gel in the mixture (Figure 3.6a). The maximum distance the particles can diffuse in 0% hard gel is around 2μm, decreasing with increasing concentration. The distance of particles diffusing in 60% hard gel is less than 1μm while in 100% hard gel, it looks just like a dot. So, it is expected that the MSD will also decrease with increasing hard gel concentration (Figure 3.6b). The slope of MSD of 0% hard gel is ~0.8, which indicates that the particles are not diffusing in fully viscous samples, but in samples with elasticity. This slope again decreases with increasing hard gel concentration, where the slope of MSD of particles in 100% hard gel is very close to 0, which indicates that they are trapped.

As the slope for all of these gels is less than 1, the Stokes-Einstein formula to calculate viscosity cannot be applied anymore, thus moduli of the gels in microscale are calculated [10] and the result is presented in Figure 3.7. The magnitude of both bulk (Figure 3.7a) and microrheology (Figure 3.7b) are very similar, which is the case when the mesh size is smaller than the probe size [45].

Both results show that hard gel concentration 60% was the point where the G'>G" (Figure 3.7).

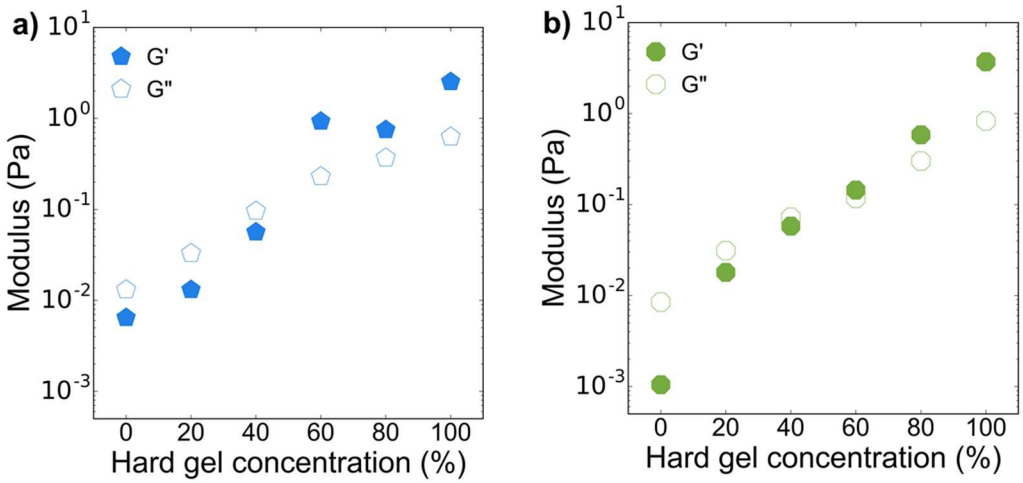

FIGURE 3.7 Moduli as a function of hard gel concentration at ω=1 rad/s. a) Bulk moduli, b) Micro scale moduli

Microrheology detects local rheological properties of the fluid, thus it is expected in heterogeneous mixed gels, the distinct properties of the two gels should be observed using this technique. van-Hove correlation has been used to quantify heterogeneity in the fluid, where the distribution of the particle displacement should display a Gaussian distribution [24]. This is because the particles that diffuse in the homogeneous medium at a lag time should always diffuse similarly but not for particles that are diffusing in a heterogeneous medium. As the mixture gel is made with completely different gels, we should be able to see these differences in microscale.

It was expected that the two starting gels are homogeneous and the van-Hove distribution showed that the displacement distribution of particles in these two gels (Figure 3.8a and Figure 3.8f) are Gaussian. The figures also show that in two different lag times (0.029s and 0.29s), both gels still have Gaussian distributions, which confirms their homogeneity.

Surprisingly, the gel mixtures that are made from two different gels also show Gaussian distributions (Figures 3.8b, 3.8c, 3.8d, and 3.8e). Even when the data are plotted at longer time scale, the Gaussian distribution still persists, which indicates that the samples are always homogeneous.

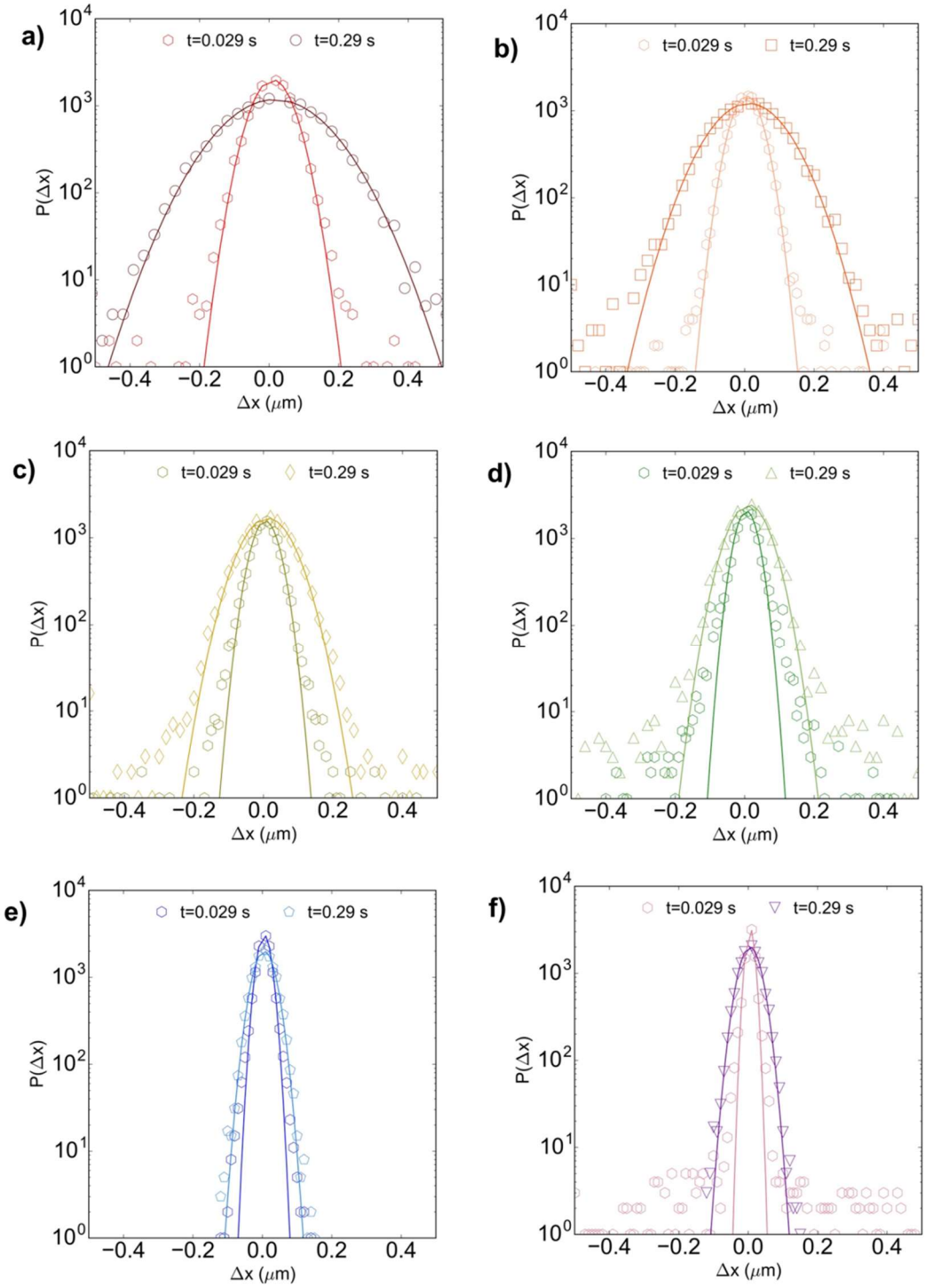

FIGURE 3.8 Plots of van-Hove correlation of gellan samples at short (0.029s) and at long time (0.29s). a) 0% hard gel, b) 20% hard gel, c) 40% hard gel, d) 60% hard gel, e) 80% hard gel, f) 100% hard gel

3.3.4 | Heterogeneity of gellan gels in a capillary

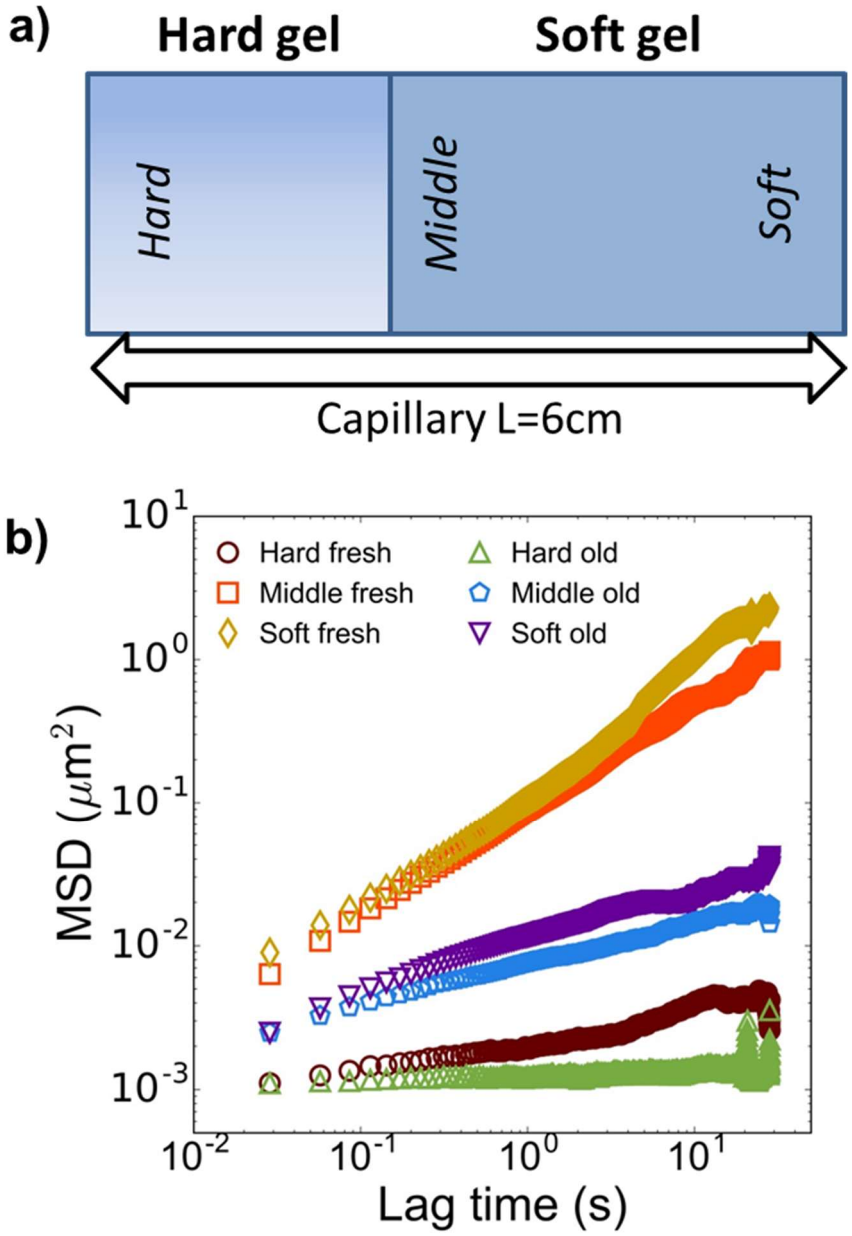

FIGURE 3.9 a) Cartoons showing location of observed particle locations in capillary, b) MSD of particle at different location when fresh and aged

To understand what is happening during mixing, the two gels were placed side by side in a capillary that acts as a sample chamber for microrheology experiments. The length of the capillary was 6 cm (Figure 3.9a). Three different areas were imaged: one in the hard gel region, another one in the soft gel region and the last one is in the middle part where the two gels meet, but on the soft side. For this experiment, particles with different dyes were used. Particles coated with Fluorescein dye (Green) was added into the soft gel, while particles with Rhodamine (Red) dye was added to hard gel to ease the differentiation between the two gels during imaging. Thus, the area where the two gels meet are defined as the middle part, where the images were taken.

As expected, the gels are initially divided into two microenvironments, one that is a hard gel (where all tracers are trapped) and one that is a soft gel (where all tracers are diffusive). The area just at the interface on the side of soft gel shows that the tracers are behaving just like the soft gel. The collated displacement data of the three positions cannot be fitted to a Gaussian distribution, which indicates their heterogeneity (Figure 3.9d, Fresh data). Although that is the case, the particle displacement at each of these positions shows Gaussian distributions (Figure 3.9a, 3.9b, 3.9c, Fresh data).

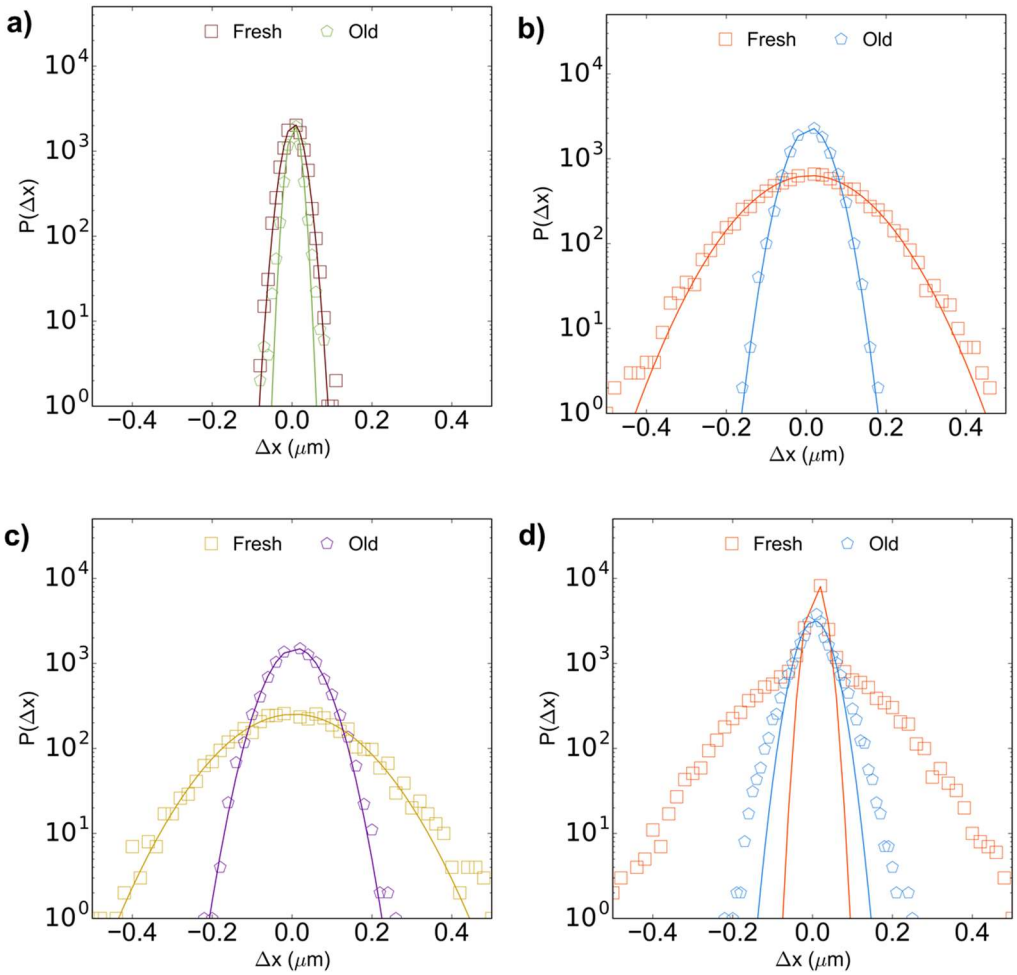

FIGURE 3.10 Plots of van-Hove correlation of particles at different positions in capillary (t=0.29s) for both fresh and aged sample at 15 hrs; a) hard side of capillary, b) middle side of capillary, c) soft side of capillary, d) collated data of all positions

After 15hrs of incubation, the tracers in the hard gel region stay trapped, but the gel in the middle and the soft region change, becoming gels with lower diffusivity (Figure 3.9b). The MSD showed that this gel became more like the 40% hard gel that is bulk mixed (Figure 3.5b). This indicates that, during mixing, the soft gel becomes harder due to the change caused by the hard gel. As the two gels are made by different salt concentrations, it is likely the effect is caused by the two gels equilibrating due to the osmotic gradient. It has been shown that osmotic gradient plays an important role during degradation of cross-linked gellan gels

that are immersed in water, which happens within 8 hours after they are placed in contact with water [46]. Despite this, the displacement of tracers at each position still show homogeneity (Figure 3.10a, 3.10b, 3.10c). Similar to the fresh data, the collated van Hove correlation functions for aged samples shows that the particle movement in whole capillary is still heterogeneous as it cannot be fitted with a single Gaussian distribution (Figure 3.10d).

It is also found that the salt concentration in any of the gels tested here is in excess, which indicates that there are some free salt ions that can easily travel from the hard gel to the soft gel due to the osmotic gradient between two gels. The observed decrease in the slope of MSDs of particles in a soft gel is most probably due to the gel network reinforcement with extra salt [47]. This causes the slope of the MSDs of soft gels to decrease.

This of course is very different than the phenomena observed in the bulk scale, as heterogeneity cannot be observed. In bulk, shear supposedly breaks the hard gel into microgels with length scales smaller than the probe size. But in the capillary experiment, as the hard gel is not sheared, the length scale of the gel is still larger than the probe. Hence, in this case heterogeneity can be observed.

3.4 CONCLUSIONS

The characterisation of structural heterogeneity is very dependent on the length scale of observation. When the molecular structure of gellan gel is varied using two different salts at different levels, heterogeneity is not observed at the length scale studied here. In the case of a mixture of two gels that are bulk- and micro-rheologically different, heterogeneity was also not observed. This is likely because shear during mixing breaks the hard gel into microgel particles. In this case, the size is much smaller than the probe particles used, hence the heterogeneity cannot be resolved. Shear seems to help the microgels of hard gel come into contact with the soft gel. Due to the presence of an osmotic gradient between the two gels, because of a difference in salt concentration, the gels are equilibriated within 10 minutes of mixing. In a capillary experiment where the

gels are not mixed together, no shear breaks the hard gel into small bits so the gels remain intact. Osmotic gradients cause the gel to change slowly over time. The length scale of heterogeneity in this system is on the order of the size of capillary (mm), much larger than the probe particle size (μm), hence why heterogeneity in the system can still be detected, even after 15 hours of incubation.

3.5 REFERENCES

1. Rubin, B.K., *Mucus structure and properties in cystic fibrosis.* Paediatric Respiratory Reviews, 2007. **8**(1): p. 4-7.

2. Henke, M.O. and F. Ratjen, *Mucolytics in cystic fibrosis.* Paediatric Respiratory Reviews, 2007. **8**(1): p. 24-29.

3. Bird;, R.B., G.C. Dai;, and B.J. Yarusso, *The Rheology and Flow of Viscoplastic Materials.* Reviews in Chemical Engineering, Volume 1, Issue 1, Pages 1–70, ISSN (Online) 2191-0235, ISSN (Print) 0167-8299, DOI: https://doi.org/10.1515/revce-1983-0102., 1983. **1**(1): p. 1-70.

4. Torbica, A., M. Hadnađev, and T. Dapčević, *Rheological, textural and sensory properties of gluten-free bread formulations based on rice and buckwheat flour.* Food Hydrocolloids, 2010. **24**(6): p. 626-632.

5. Kristo, E., C.G. Biliaderis, and N. Tzanetakis, *Modelling of rheological, microbiological and acidification properties of a fermented milk product containing a probiotic strain of Lactobacillus paracasei.* International Dairy Journal, 2003. **13**(7): p. 517-528.

6. Amblard, F., A.C. Maggs, B. Yurke, A.N. Pargellis, and S. Leibler, *Subdiffusion and Anomalous Local Viscoelasticity in Actin Networks.* Physical Review Letters, 1996. **77**(21): p. 4470-4473.

7. Apgar, J., Y. Tseng, E. Fedorov, M.B. Herwig, S.C. Almo, and D. Wirtz, *Multiple-Particle Tracking Measurements of Heterogeneities in Solutions of Actin Filaments and Actin Bundles.* Biophysical Journal, 2000. **79**(2): p. 1095-1106.

8. Suk, J.S., S.K. Lai, N.J. Boylan, M.R. Dawson, M.P. Boyle, and J. Hanes, *Rapid transport of muco-inert nanoparticles in cystic fibrosis sputum treated with N-acetyl cysteine.* Nanomedicine, 2011. **6**(2): p. 365-375.

9. Birjiniuk, A., N. Billings, E. Nance, J. Hanes, K. Ribbeck, and P.S. Doyle, *Single particle tracking reveals spatial and dynamic organization of the Escherichia coli biofilm matrix.* New Journal of Physics, 2014. **16**(8): p. 085014.

10. Mason, T.G., *Estimating the viscoelastic moduli of complex fluids using the generalized Stokes–Einstein equation.* Rheologica Acta, 2000. **39**(4): p. 371-378.

11. Levine, A.J. and T.C. Lubensky, *Response function of a sphere in a viscoelastic two-fluid medium.* Physical Review E, 2001. **63**(4): p. 041510.

12. Cai, L.-H., S. Panyukov, and M. Rubinstein, *Mobility of Nonsticky Nanoparticles in Polymer Liquids.* Macromolecules, 2011. **44**(19): p. 7853-7863.

13. Moschakis, T., A. Lazaridou, and C.G. Biliaderis, *Using particle tracking to probe the local dynamics of barley β-glucan solutions upon gelation.* Journal of Colloid and Interface Science, 2012. **375**(1): p. 50-59.

14. Aufderhorst-Roberts, A., W.J. Frith, and A.M. Donald, *Micro-scale kinetics and heterogeneity of a pH triggered hydrogel.* Soft Matter, 2012. **8**(21): p. 5940-5946.

15. Wagner, C.E., B.S. Turner, M. Rubinstein, G.H. McKinley, and K. Ribbeck, *A Rheological Study of the Association and Dynamics of MUC5AC Gels.* Biomacromolecules, 2017. **18**(11): p. 3654-3664.

16. Goodman, A., Y. Tseng, and D. Wirtz, *Effect of Length, Topology, and Concentration on the Microviscosity and Microheterogeneity of DNA Solutions.* Journal of Molecular Biology, 2002. **323**(2): p. 199-215.

17. Tseng, Y. and D. Wirtz, *Mechanics and Multiple-Particle Tracking Microheterogeneity of α-Actinin-Cross-Linked Actin Filament Networks.* Biophysical Journal, 2001. **81**(3): p. 1643-1656.

18. Xu, J., Y. Tseng, C.J. Carriere, and D. Wirtz, *Microheterogeneity and Microrheology of Wheat Gliadin Suspensions Studied by Multiple-Particle Tracking.* Biomacromolecules, 2002. **3**(1): p. 92-99.

19. Xu, J., W. Cheng, G.E. Inglett, P. Wu, S. Kim, S.X. Liu, and Y. Tseng, *Micro-heterogeneity of cellulosic fiber biopolymer prepared from corn hulls.* LWT - Food Science and Technology, 2010. **43**(6): p. 977-981.

20. Oppong, F.K., P. Coussot, and J.R. de Bruyn, *Gelation on the microscopic scale.* Physical Review E, 2008. **78**(2): p. 021405.

21. Oppong, F.K., L. Rubatat, B.J. Frisken, A.E. Bailey, and J.R. de Bruyn, *Microrheology and structure of a yield-stress polymer gel.* Physical Review E, 2006. **73**(4): p. 041405.

22. van den Ende, D., E.H. Purnomo, M.H.G. Duits, W. Richtering, and F. Mugele, *Aging in dense suspensions of soft thermosensitive microgel particles studied with particle-tracking microrheology.* Physical Review E, 2010. **81**(1): p. 011404.

23. Caggioni, M., P.T. Spicer, D.L. Blair, S.E. Lindberg, and D.A. Weitz, *Rheology and microrheology of a microstructured fluid: The gellan gum case.* Journal of Rheology, 2007. **51**(5): p. 851-865.

24. Valentine, M.T., P.D. Kaplan, D. Thota, J.C. Crocker, T. Gisler, R.K. Prud'homme, M. Beck, and D.A. Weitz, *Investigating the microenvironments of inhomogeneous soft materials with multiple particle tracking.* Phys Rev E Stat Nonlin Soft Matter Phys, 2001. **64**(6 Pt 1): p. 061506.

25. Weeks, E.R., J.C. Crocker, A.C. Levitt, A. Schofield, and D.A. Weitz, *Three-Dimensional Direct Imaging of Structural Relaxation Near the Colloidal Glass Transition.* Science, 2000. **287**(5453): p. 627-631.

26. Kegel, W.K., B. van, and Alfons, *Direct Observation of Dynamical Heterogeneities in Colloidal Hard-Sphere Suspensions.* Science, 2000. **287**(5451): p. 290-293.

27. Schultz, K.M. and K.S. Anseth, *Monitoring degradation of matrix metalloproteinases-cleavable PEG hydrogels via multiple particle tracking microrheology.* Soft Matter, 2013. **9**(5): p. 1570-1579.

28. Stewart, E.J., A.E. Satorius, J.G. Younger, and M.J. Solomon, *Role of Environmental and Antibiotic Stress on Staphylococcus epidermidis Biofilm Microstructure.* Langmuir : the ACS journal of surfaces and colloids, 2013. **29**(23): p. 7017-7024.

29. Bayles, A.V., T.M. Squires, and M.E. Helgeson, *Probe microrheology without particle tracking by differential dynamic microscopy.* Rheologica Acta, 2017. **56**(11): p. 863-869.

30. Cerbino, R. and V. Trappe, *Differential Dynamic Microscopy: Probing Wave Vector Dependent Dynamics with a Microscope.* Physical Review Letters, 2008. **100**(18): p. 188102.

31. Lee, J., S. Sung, Y. Kim, J.D. Park, and K.H. Ahn, *A new paradigm of materials processing—heterogeneity control.* Current Opinion in Chemical Engineering, 2017. **16**: p. 16-22.

32. Allan, D.B., Caswell, Thomas, Keim, Nathan C., & van der Wel, Casper M, *trackpy: Trackpy v0.4.1 (Version v0.4.1)*, in *Zenodo*. 2018.

33. Hellriegel, J., S. Gunther, I. Kampen, A.B. Albero, A. Kwade, M. Bol, and R. Krull, *A Biomimetic Gellan-Based Hydrogel as a Physicochemical Biofilm Model.* Journal of Biomaterials and Nanobiotechnology, 2014. **5**(2): p. 83-97.

34. Morris, E.R., K. Nishinari, and M. Rinaudo, *Gelation of gellan – A review.* Food Hydrocolloids, 2012. **28**(2): p. 373-411.

35. Watase, M. and K. Nishinari, *Effect of potassium ions on the rheological and thermal properties of gellan gum gels.* Food Hydrocolloids, 1993. **7**(5): p. 449-456.

36. Moritaka, H., K. Nishinari, M. Taki, and H. Fukuba, *Effects of pH, Potassium Chloride, and Sodium Chloride on the Thermal and Rheological Properties of Gellan Gum Gels.* Journal of Agricultural and Food Chemistry, 1995. **43**(6): p. 1685-1689.

37. Moritaka, H., H. Fukuba, K. Kumeno, N. Nakahama, and K. Nishinari, *Effect of monovalent and divalent cations on the rheological properties of gellan gels.* Food Hydrocolloids, 1991. **4**(6): p. 495-507.

38. Pérez-Campos, S.J., N. Chavarría-Hernández, A. Tecante, M. Ramírez-Gilly, and A.I. Rodríguez-Hernández, *Gelation and microstructure of dilute gellan solutions with calcium ions.* Food Hydrocolloids, 2012. **28**(2): p. 291-300.

39. Yuguchi, Y., H. Urakawa, and K. Kajiwara, *The effect of potassium salt on the structural characteristics of gellan gum gel.* Food Hydrocolloids, 2002. **16**(3): p. 191-195.

40. Picone, C.S.F. and R.L. Cunha, *Influence of pH on formation and properties of gellan gels.* Carbohydrate Polymers, 2011. **84**(1): p. 662-668.

41. Tang, J., M.A. Tung, and Y. Zeng, *Gelling Temperature of Gellan Solutions Containing Calcium Ions.* Journal of Food Science, 1997. **62**(2): p. 276-280.

42. Grasdalen, H. and O. Smidsrød, *Gelation of gellan gum.* Carbohydrate Polymers, 1987. **7**(5): p. 371-393.

43. Ikeda, S., Y. Nitta, T. Temsiripong, R. Pongsawatmanit, and K. Nishinari, *Atomic force microscopy studies on cation-induced network formation of gellan.* Food Hydrocolloids, 2004. **18**(5): p. 727-735.

44. Noda, S., T. Funami, M. Nakauma, I. Asai, R. Takahashi, S. Al-Assaf, S. Ikeda, K. Nishinari, and G.O. Phillips, *Molecular structures of gellan gum imaged with atomic force microscopy in relation to the rheological behavior in aqueous systems. 1. Gellan gum with various acyl contents in the presence and absence of potassium.* Food Hydrocolloids, 2008. **22**(6): p. 1148-1159.

45. Buchanan, M., M. Atakhorrami, J.F. Palierne, and C.F. Schmidt, *Comparing Macrorheology and One- and Two-Point Microrheology in Wormlike Micelle Solutions.* Macromolecules, 2005. **38**(21): p. 8840-8844.

46. Hossain, K.S. and K. Nishinari, *Chain Release Behavior of Gellan Gels*, in *Gels: Structures, Properties, and Functions: Fundamentals and Applications*, M. Tokita and K. Nishinari, Editors. 2009, Springer Berlin Heidelberg: Berlin, Heidelberg. p. 177-186.

47. Nitta, Y., S. Ikeda, and K. Nishinari, *The reinfocement of gellan gel network by the immersion into salt solution.* International Journal of Biological Macromolecules, 2006. **38**(2): p. 145-147.

Chapter 4

Atmospheric air plasma induces increased cell aggregation during the formation of Escherichia coli biofilms

4.1 INTRODUCTION

Biofilms are colonies of microorganisms surrounded by a complex fluid matrix made predominantly of extracellular polysaccharide polymers (EPS). The EPS provides the mechanical stability of biofilms, mediates their adhesion to surfaces and forms a cohesive, 3-dimensional polymer network that interconnects and transiently immobilises biofilm cells [1]. This EPS matrix provides a protective barrier for bacterial colonies in a biofilm [1], increasing the resistance of bacteria to chemical and antibiotic treatments and also reducing the efficacy of physical treatment. Consequently, cells residing within the biofilm matrix demonstrate increased survival to many conventional methods of eradication which are found effective for their freely dispersed, or planktonic, counterparts [2]. Biofilms can form on many surfaces, including the skin of fresh fruits and vegetables, industrial pipe surfaces, in between teeth, and on medical devices [3, 4]. Due to their widespread existence and resilience, biofilms are known to be the main cause of persistent bacterial infections in hospitals [5], contamination of foods in process environments [6], and reduced process cleaning efficiency in manufacturing. Biofilm physical and flow properties have recently been studied as a means of understanding molecular transport through the matrix and to better enable destruction [7, 8]. New approaches are being developed to more aggressively treat biofilms during formation, for example, to interfere with the attachment of these bacteria to surfaces and disturb their structure [9].

One novel treatment currently being investigated for this purpose is atmospheric plasma, which is essentially an ionized gas that is generated at ambient temperatures and under atmospheric conditions that allows treatment of sensitive biological matter [10, 11]. Numerous recent studies have demonstrated the anti-microbial efficacy of atmospheric plasma for planktonic bacteria or cells embedded in biofilms [12]. Plasma species are reported to be capable of penetrating into the biofilm structure [13]. Plasma can inactivate biofilms with treatment times of less than 60 s [14] and cause a five log reduction in biofilm viability [15], while longer treatments can decrease viable cells to undetected levels [15-17]. This ability of plasma to inactivate bacteria is thought to be an effect of its production of short- and long- lived reactive species [18], such as

ozone and other radicals [19]. Direct or indirect plasma discharges in air to water creates an acidified, nitrogen-oxide containing solutions known as plasma-activated water (PAW), which remains antibacterial for long periods. Such long-lived species have been shown to be effective to treat *Escherichia coli* suspensions even after a 7 days period, following plasma liquid generation [20].

Apart from its ability to inactivate bacteria in a biofilm, atmospheric air plasma has been shown to change the overall biofilm structure by disrupting and degrading the EPS biofilm components [21]. For example, separation of initially aggregated bacteria has been observed during EPS degradation due to plasma treatment [22]. Plasma-induced EPS degradation causes a decrease in biofilm thickness [21, 23] and volume [21] as well as an increase in its roughness and porosity [21]. Plasma treated biofilms are also known to have reduced adhesion to surfaces [23, 24].

In model systems, monolayers of surface-deposited *Listeria innocua* responded to plasma treatment by forming cell aggregates of damaged cells, into which viable cells were then moved, affecting plasma inactivation kinetics [25]. Bayliss *et al*. [25] suggested such sheltering of cells extends the treatment time needed for bacterial inactivation and is driven by plasma gas flow-induced drying and the resultant fluid shear stresses. Although the work was carried out on a manually-deposited layer of cells, it likely has relevance for more developed biofilm community environments as well. This work examines the effects of short duration plasma treatments on young biofilm structures and how modification of those structures affects bacterial resilience to subsequent plasma treatments.

4.2 MATERIALS AND METHODS

4.2.1 | Preparation of biofilm sample

Single *E. coli* MG1655 (CSIRO Food Research Ryde Bacteriology Culture Collection) colonies were inoculated in nutrient broth (1 g L^{-1} 'Lab-Lemco' powder, 2 g L^{-1} 170 yeast extract, 5 g L^{-1} peptone, 5 g L^{-1} sodium chloride, pH 7.4; Oxoid, Adelaide, Australia) and grown in a shaking incubator (Bioline

Global, South Australia) at 37° C and 100 rpm for 12 to 15 h. One single colony was used per experiment and it came from the same plate; no differences in biofilm production was observed between colonies. To produce biofilm, the protocol of Ziuzina et al [17] was used where it was modified slightly, where in this chapter, a Fluorodish was used instead of 96-well plate to act as dielectric barrier of plasma treatment. The cultures contained approximately 10^9 CFU mL which was diluted to 10^7 CFU mL^{-1}. From this diluted culture, 2 mL samples were transferred to a FluoroDish™ cell culture dish (World Precision Instruments). These dishes were incubated at 37 °C to allow biofilm formation. After 24 h, the medium was exchanged for fresh medium. The biofilms were grown for a period of 48 h total for time-dependent and liquid coverage experiments or 24, 48, and 72 h for cell regrowth and multiple treatment studies, after which the medium was removed and the biofilm washed twice with phosphate buffered saline (PBS) prior to treatment and analysis. Details of the regrowth studies are provided in section 4.2.3.1.

4.2.2 | Plasma setup

The power supply used to drive the plasma discharge was an HV half bridge resonant inverter circuit (PVM2000, Information Unlimited, New Hampshire, USA). The power source has a power of 2 kW, a high-frequency power driver from 20 to 100 kHz, a peak to peak voltage up to 40 kV (load dependent) and a duty cycle control from 10 to 90%. The plasma setup consists of a FluoroDish™ used to grow the biofilm (see section 4.2.1) that is placed in between the electrodes of the Dielectric Barrier Discharge (DBD), consisting of a 2 mm thick poly(methyl methacrylate) single layer dielectric and a top electrode that is partially recessed within the imaging dish to reduce the discharge gap to 6 mm (Figure 4.1a). The discharges were induced in open atmospheric air conditions.

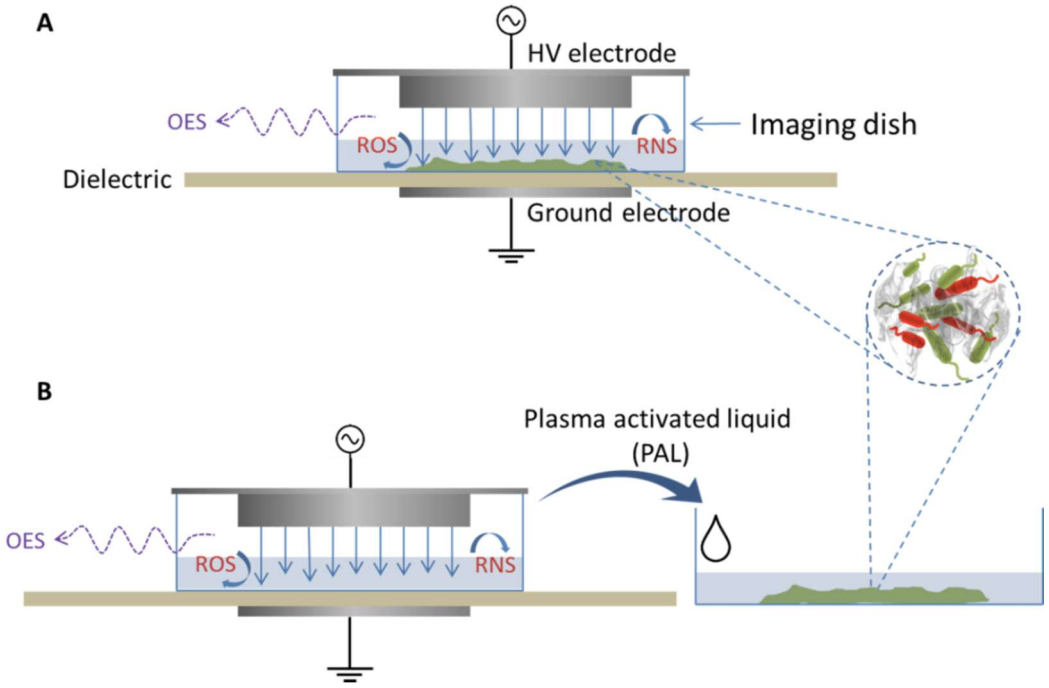

FIGURE 4.1 a) DBD design incorporating the glass bottom imaging dish containing the growing biofilm within the discharge gap, b) Schematic of air discharge in contact with liquid and addition of PAL to growing biofilm

4.2.3 | Plasma-biofilm treatment conditions

4.2.3.1 | Direct treatment

The growing biofilms were exposed to direct plasma treatment, Figure 4.1a, after 24 or 48 h of growth, while only biofilms aged 48 h were exposed to plasma-activated liquid (see section 4.2.3.2 below, Figure 4.1b). Plasma treatment was performed at 6 kV and 60 kHz with treatment time varied from 10s to 60s The optical emission spectra, OES, for the discharge were mainly in the UV region, the OES are not included, the reader is referred to Lu *et al.* [26] for characterisation of discharges with this power source. The DBD design incorporating the dish used to grow the biofilm allows for non-invasive sample preparation, as the biofilm could be imaged directly in its growth dish before and after plasma treatment, which is critical for imaging of a biofilm's structure. The design also offers the added benefit of a relatively controlled discharge in terms of spatial homogeneity and treatment time when compared to plasma jets. Precise

control of treatment time (±1s) allows the effects of short plasma treatment times on biofilm behaviour to be investigated.

For time-dependent studies, biofilms aged 48 h were exposed to direct plasma for times ranging from 0 to 60 s. The biofilm was kept wet by adding 200 μL of PBS into the dish. For liquid coverage studies, different amounts of PBS were added to the cell culture dish, from 200 to 1000 μL, and biofilms aged 48 h were used. In the regrowth study, biofilms aged 24 and 48 h were used and exposed to plasma for 30s. On each day, biofilms were compared to untreated controls (Table 4.1). After exposure to plasma, biofilms were incubated again with fresh nutrient broth at 37 °C. All nutrients were changed every 24 h until the final day (72 h).

4.2.3.2 | Indirect (liquid) treatment

Plasma-treated liquid was generated by treating 1 mL of PBS in the same setup as direct treatment, as indicated in Figure 4.1b. After treatment, 200 μL of the liquid was removed from the dish and transferred to another dish containing the biofilm, and subsequently incubated for 1 hr prior to imaging. Commercial hydrogen peroxide (Chem-Supply Pty Ltd, South Australia, Australia) was employed for comparison to the plasma-treated liquid via addition to PBS. Similarly, 200 μL of these peroxide-PBS solutions were also incubated for 1 hr with the biofilm prior to imaging.

TABLE 4.1 Design of regrowth experiment where U indicates untreated and T treated samples

Biofilm age (h)	**Control**	**Treatment**		
24	U	T24		
48	U	T48	T24+48	
72	U	T24+48	T24	T48

4.2.4 | Confocal Laser Scanning Microscopy (CLSM)

Before imaging, the biofilm was dyed with Live/Dead BacLight™ Bacterial Viability Kits (Thermo Fisher Scientific, Victoria, Australia), which contains SYTO9 and Propidium Iodide (PI), following supplier's instructions. The dishes were then incubated in the dark for about 15 min before imaging. Biofilm imaging was performed on a Leica TCS SP5 STED inverted confocal microscope with oil objective 63×, NA 1.4. The lasers used for imaging were at 488 nm for SYTO9 and 498 nm for PI.

4.2.5 | Image analysis

All images were analyzed using Image-J [27]. Green (alive) and red (dead) channels from CLSM data were separated and then analyzed individually to calculate biofilm coverage area. From the literature, it is known the approximate size of one *E. coli* cell is $1 \times 3\mu m^2$ [28]. No shape variation was observed during experiment; thus the area of the cells here is calculated based on their oval shape. This means that the area of one *E. coli* cell is 2.35 μm^2. Hence, any number that is less than this value is disregarded in the calculation. The percentage of red cells

was calculated from the total area covered by red cells divided by the total area covered by both green and red cells. Each data set contains at least six fields of view that are used for data quantification.

4.2.6 | Hydrogen peroxide (H_2O_2) measurement

Quantification of H_2O_2 concentration in the plasma liquid was performed following the protocol of Pick and Keisari [29]. Briefly, 5 g of horseradish peroxidase Type II (Sigma Aldrich, Sydney, Australia) powder was dissolved in 0.05M phosphate buffer. Phenol red dye is used to detect colour change due to the presence of H2O2, using a concentration of 0.28 mM. Standard curves were then prepared by measuring spectra of milli-Q water containing various concentrations of H_2O_2 from 0 to 60 μM. The solution was taken out of the dish, transferred into a small glass vial, and incubated for 1 h before spectra measurement. Just before spectra measurement, 10 μL of the horseradish peroxidase solution and 10 μL of the phenol red solution were added into the standard samples and plasma-treated liquid. These vials were then incubated again at 25 °C for 5 min. After incubation, NaOH was added to the solution to change its colour from orange to purple and keep the colour stable [29]. Spectra of samples at 610 nm were then recorded using a UV–VIS spectrophotometer (Shimadzu Corporation, Kyoto, Japan).

4.3 RESULTS AND DISCUSSIONS

4.3.1 | The effect of plasma treatment on biofilm structure

Plasma treatment has been reported previously to destabilize biofilm structures [21]. Here we use an *E. coli* biofilm that is in a younger state than the previously studied biofilms of *Pseudomonas aeruginosa* or *Staphylococcus aureus* [21]. The latter two usually show thicker and more complex biofilms. The early stage here is defined when the bacteria starts to stick to the surface, where no big microcolonies have been formed yet. The size of big microcolonies are determined here to be bigger than 10μm^2. Figure 4.2a shows the microscopic initial state of these young biofilms, with green live cells visible throughout the

field of view at t = 0 s. Figure 4.2a also shows micrographs of the biofilm after different plasma exposure times, enabling tracking of the kinetic progression of cell death by following the increase in red, or dead, cells and the survival of the green, or living, cells and the formation of cell clumps. These effects are contrary to those reported by Ferrell *et al.* [21] with plasma treatment inducing aggregation and forming a new structure rather than structure breakdown. This plasma-induced structural re-arrangement has been observed previously in surface-deposited planktonic bacteria [25].

Figure 4.2a shows that cell aggregation occurred for all treatment times tested. However, quantitative analysis via cell imaging revealed that there was only a slight increase in the percentage of larger aggregates (>10 μm^2) as a function of treatment time (Figure 4.2b). An aggregate area cut-off value of 10 μm^2 was chosen to differentiate aggregates from cells in sufficient proximity to be classified as an aggregate. An increase was only observed between the untreated and the shortest treatment time of 10 s (around 20% increase), indicating that cell aggregation occurs rapidly and is not significantly governed by treatment time.

Figure 4.2b shows that although plasma treatment causes cell aggregation, it also inactivates bacterial cells in the biofilm. This behaviour has been observed in many studies that study the effect of treatment on bacterial viability [15-17]. However, for the current system, it is found that after 40 s the number of dead cells reaches a plateau of 40%, Figure 4.2b. This indicates that there is a limit to the number of bacteria that can be killed with plasma treatment, perhaps because aggregation offers some form of protection.

Of particular interest is that the aggregation of the cells and the mortality effects of the plasma appear to both plateau, although on different time scales, after 40 s for cell viability and after 10 s for cell aggregation (Figure 4.2b). Live-dead staining was used in this instance to visualize aggregation of bacterial cells and effectiveness of plasma treatment; aggregation was not used as an indicator of biofilm formation.

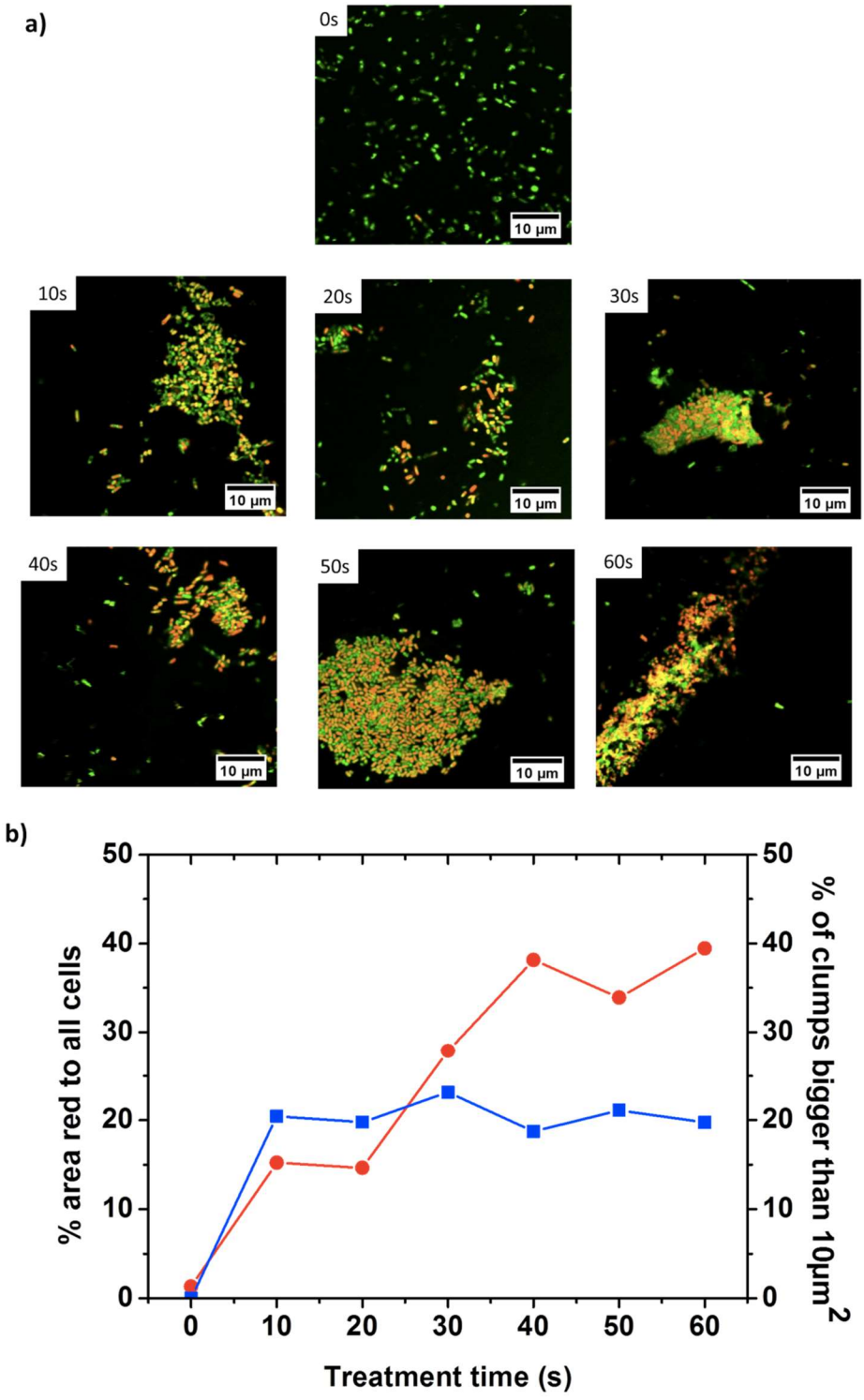

FIGURE 4.2 Effect of treatment time on biofilm structure a) Confocal images of biofilm structure before and after plasma treatment, b) quantification of dead cells (symbol ●) and cell clumps larger than 20 μm^2 (symbol ■)

The biofilms used in this study are considered mature once they are 48 h old, but we also examined the effects of biofilm age on aggregation and mortality response to plasma treatment. This is because the amount of EPS increases with biofilm age and it may play a role in protecting cells from plasma and aggregation induced by plasma. When subjected to the same plasma treatment for 30 s, both biofilms aged 24 h and 48 h form aggregates (Figure 4.3a). The percentage of big aggregates formed in these two samples is quite similar, although the actual percentage of bigger clumps is slightly higher for the treated younger biofilm. The older biofilm is expected to have more EPS, which might explain why there is a slight discrepancy between the two values. Aggregation requires both attractive interactions between cells and sufficient mobility to bring cells together for collision. The cells in the older biofilm might move less than the cells in younger ones, resulting in the current observation.

Figure 4.3 also shows that older biofilms have increased resistance to plasma treatment. In Figure 4.3c, the percentage of dead cells after treatment increased compared to the control. For biofilms aged 24 h, the percentage of dead cells increases from around 2–40% upon treatment. The efficacy of plasma decreases with increasing age of biofilm, as the percentage of dead cells only increases from 2 to 25% upon treatment, about half of the impact seen for biofilms aged 24 h. This might be due to different compositions of biofilm EPS during aging. Indeed, it has been shown in literature that the latest stage of biofilm growth has the highest EPS composition. This could possibly increase protection of bacterial

cells against plasma treatment.

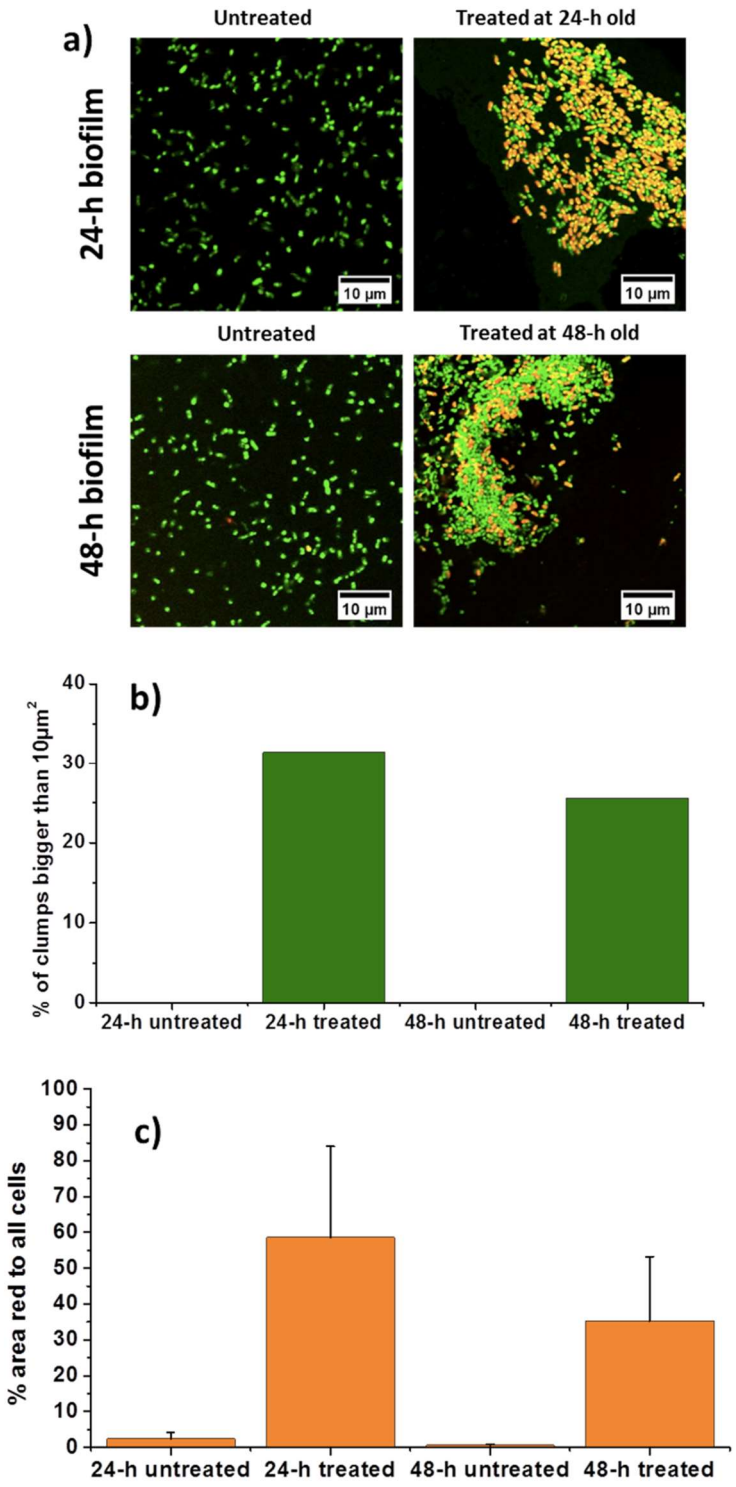

FIGURE 4.3 Effect of biofilm maturity on plasma clumping a) confocal images of 24-h and 48-h of untreated and plasma treated biofilm, b) percentage of clumps bigger than 20 μm^2, c) quantification of red cells

4.3.2 | Regrowth of surviving bacteria

When plasma treatment does not inactivate all bacterial cells in a biofilm, the surviving cells may be able to grow and reproduce when given sufficient nutrients. Under these circumstances, we are interested in how these bacterial cells regrow in their restructured environment. To answer this question, both younger and more mature biofilms were exposed to plasma treatment and then regrown, until the biofilm reached an age of 72 h, before being imaged. Biofilms that have been treated at least once after regrowth have distinct structures when compared to previously untreated biofilms with the same treatment. Figure 4.4a indicates that biofilms treated at least once during their growth have clearly aggregated structures compared to untreated biofilms that retain a fully dispersed structure. Indeed, after plasma treatment of biofilms either 24 or 48 h old, bacteria keep growing in the aggregates instead of growing separately as in the untreated samples. This indicates that the surviving bacteria are able to reproduce and grow in this newly formed structure.

Yet, these aggregated structures that occur after treatment at 24 and 48 h, or treated twice at 24 and 48 h old, are hardly distinguishable from each other. Quantitative analysis of the aggregates (Figure 4.4b) reveals that biofilms treated at 24 h have a higher percentage of aggregates larger than 10 μm^2 than a biofilm treated at 48 h or treated at 24 and 48 h. This may be due to fact that biofilms treated at 24 h have more time to expand the size of their colonies as longer growth time increases cell cluster size [30]. In addition, as seen from Figure 4.4a, a plasma-treated biofilm consists of only living cells. Analysis shows that despite 30 s of plasma treatment causing cell death of a significant proportion of cells (Figure 4.4c), only a very small number (<10%) of dead cells could be detected after biofilm re-growth. However, it is likely that some dead cells are hidden within the new structure. However, the percentage of these red cells is still quite low, less than 10%, which is not significant.

4.3.3 | The effect of plasma-induced biofilm structure on subsequent treatment

In section 4.3.2, it was found that after plasma treatment, bacteria in a biofilm can utilize the new structure to reproduce and grow. In previous work by Ferrell *et al.* [21], a mature biofilm with large aggregates was shown to change structure by increasing the porosity of the biofilm structure. In this kind of mature biofilm, the high amount of EPS should prevent the aggregation of bacteria as this EPS provides elastic resistance to deformation by the flow. The plasma-treated biofilm has a structure more similar to the mature biofilm used by Ferrell *et al.* [21]. It is interesting to know if this plasma-mediated structure has a similar behaviour to a mature biofilm.

To answer this, biofilms were exposed to plasma after 24 h of growth. This sample is incubated again for another 24 h before exposing this to the second plasma treatment. Figure 4.5a shows that clumping is still apparent in this system. However, quantitative analysis shows that the relative amount of aggregates decreases after the second plasma treatment instead of increasing. This observation agrees with Ferrell *et al.*'s [21] work. This also indicates that after a certain point, aggregation is not possible anymore as biofilms might produce

enough EPS to resist deformation by plasma. Another explanation is that subsequent plasma treatments can destroy structures formed by previous treatments. Interestingly, Figure 4.5a also indicates that biofilms that have been previously treated mainly consist of live cells. This result is unexpected as when the sample is treated twice, it is likely that the percentage of red cells should be higher compared to 24 or 48 h old biofilms. As can be seen from Figure 4.5c, the percentage of dead cells in the sample treated both at 24 and 48 h is about 5% which is much lower than the percentage of cells inactivated by single treatment when they were 24 h (by six times) or 48 h old (by four times). This suggests that the bacteria developed resistance after the first treatment that reduced efficacy of the second treatment, consistent with other reports of resistant colonies induced by plasma treatment [16, 31].

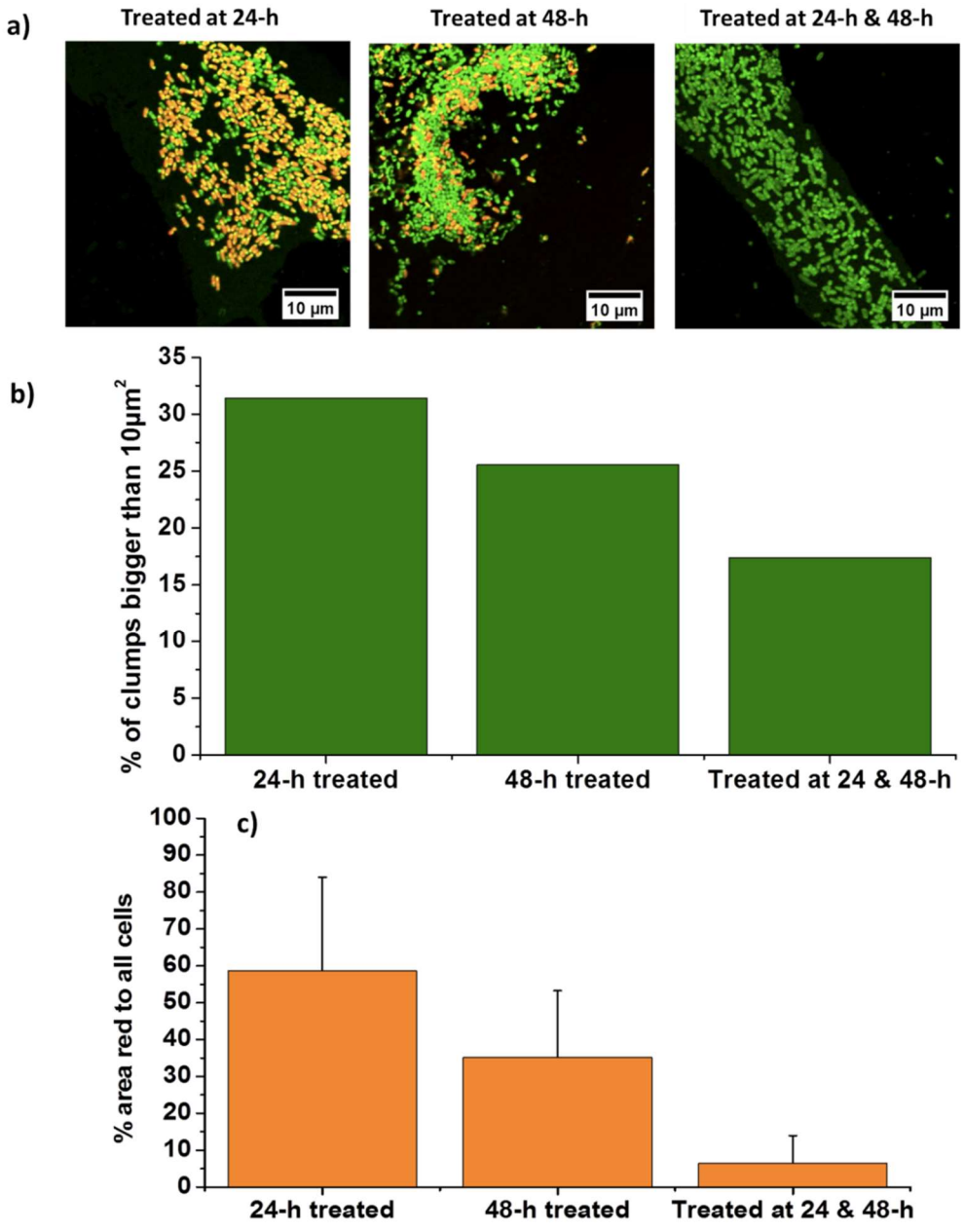

FIGURE 4.5 a) Confocal imaging of plasma-treated samples that were imaged right after treatment where fewer cells are killed after treated twice, b) the percentage of aggregates bigger than 10 μm^2, c) quantification of red cells

4.3.4 | The effect of plasma chemicals on biofilm structure

In the literature, the death of bacterial cells induced by plasma is usually associated with the presence of reactive species produced by plasma treatment. It is plausible that such chemicals could also cause clumping, as bacteria are known to respond to chemicals present via chemotaxis. Chemotaxis is the phenomenon

by which motile cells move towards or away from a chemical by altering their swimming pattern. Bacteria such as *E. coli* have several flagella per cell which facilitate some directional control over their motion to either find favourable locations with high concentrations of attractants or to avoid repellents [32], such as chemicals produced by plasma. Although chemotaxis traditionally is known only for motile cells, recent finding shows that chemotaxis might also occur in surface-attached cells [33].

One of the chemicals often found in atmospheric plasma-treated liquid is H_2O_2 [19, 34]. For this work only H_2O_2 is measured, for a more comprehensive species diagnostic of PAW using this power source, the reader is referred to our recent publications [26, 35]. Figure 4.6b indicates that the concentration of H_2O_2 in the liquid increases with increasing treatment time. This behaviour has been seen in plasma-treated water previously, where initially the concentration of peroxide increases linearly before reaching a plateau[26].

If the aggregation observed previously is related to the presence of chemicals produced by plasma reactive species, we should be able to induce such aggregation by adding commercial H_2O_2, or plasma-treated water, to the biofilms and comparing the result to plasma-treated biofilms. The concentration of H_2O_2 added to the liquid is the same as the concentration of H_2O_2 in water treated in plasma for 60 s, which is 30 μM.

Figure 4.7a shows that biofilms that were exposed to plasma-treated liquid or 30 μM peroxide solutions are similar to the control. Data analysis (Figure 4.7b) reveals that there are actually changes in clumping after addition of peroxide or incubation with plasma water compared to control. Figure 4.7b also shows that compared to peroxide only, plasma water increases the extent of clumping by two times (from 3 to 6%), which might suggest that presence of other chemicals that also give rise to cell clumping. However, the change in clumping caused by chemicals (~6%) is not as much as the clumping caused by direct treatment (~20%). This suggests that aggregate formation might be slightly affected by chemicals present in plasma-treated water, but it is not the main mechanism.

Movement of bacteria is also required for aggregation and is likely controlled by plasma discharge induced flow [25].

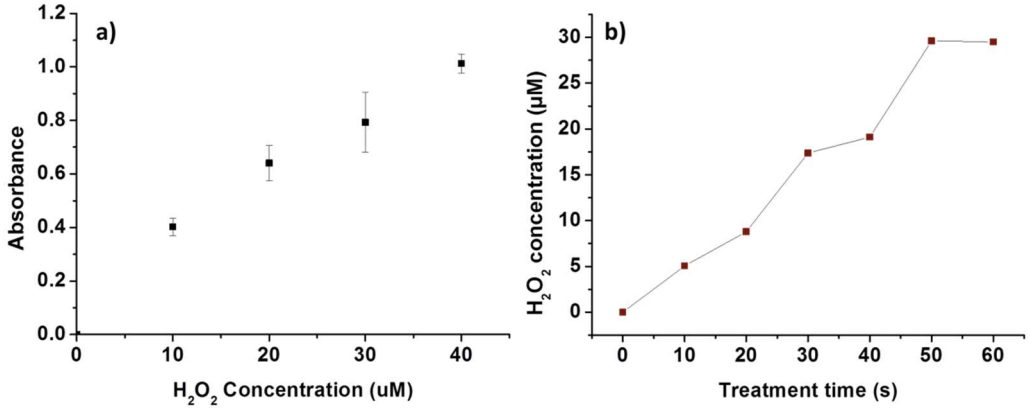

FIGURE 4.6 a) Calibration curve for H_2O_2 by spectrometer at 610 nm, b) The H_2O_2 concentration in plasma treated liquid

Additionally, the use of hydrogen peroxide and plasma liquid here does not cause significant cell death. The fact that hydrogen peroxide cannot kill bacteria cells is probably due to the secretion or upregulation of ferritin in biofilm. As shown in Figure 4.7b, the percentage of cells killed by treatment is very small, less than 2%. These values are similar to the levels in untreated biofilms. This means there is very little effect of plasma-treated water, which is not in agreement with literature as plasma-treated liquid has been shown to inactivate bacteria in biofilms [36, 37]. But, literatures [38, 39] have indicated that in order for plasma-treated liquid to be effective in inactivating bacteria, acidified conditions are required. Naïtali *et al*.[38] showed that in plasma-treated water, a bacterial population was reduced from eight log CFU to two log CFU. However, the effect was diminished for buffered plasma liquid where only a minimal reduction was observed. As all experiments here use a buffer solution, PBS, the pH of the solution is not expected to change and become acidified.

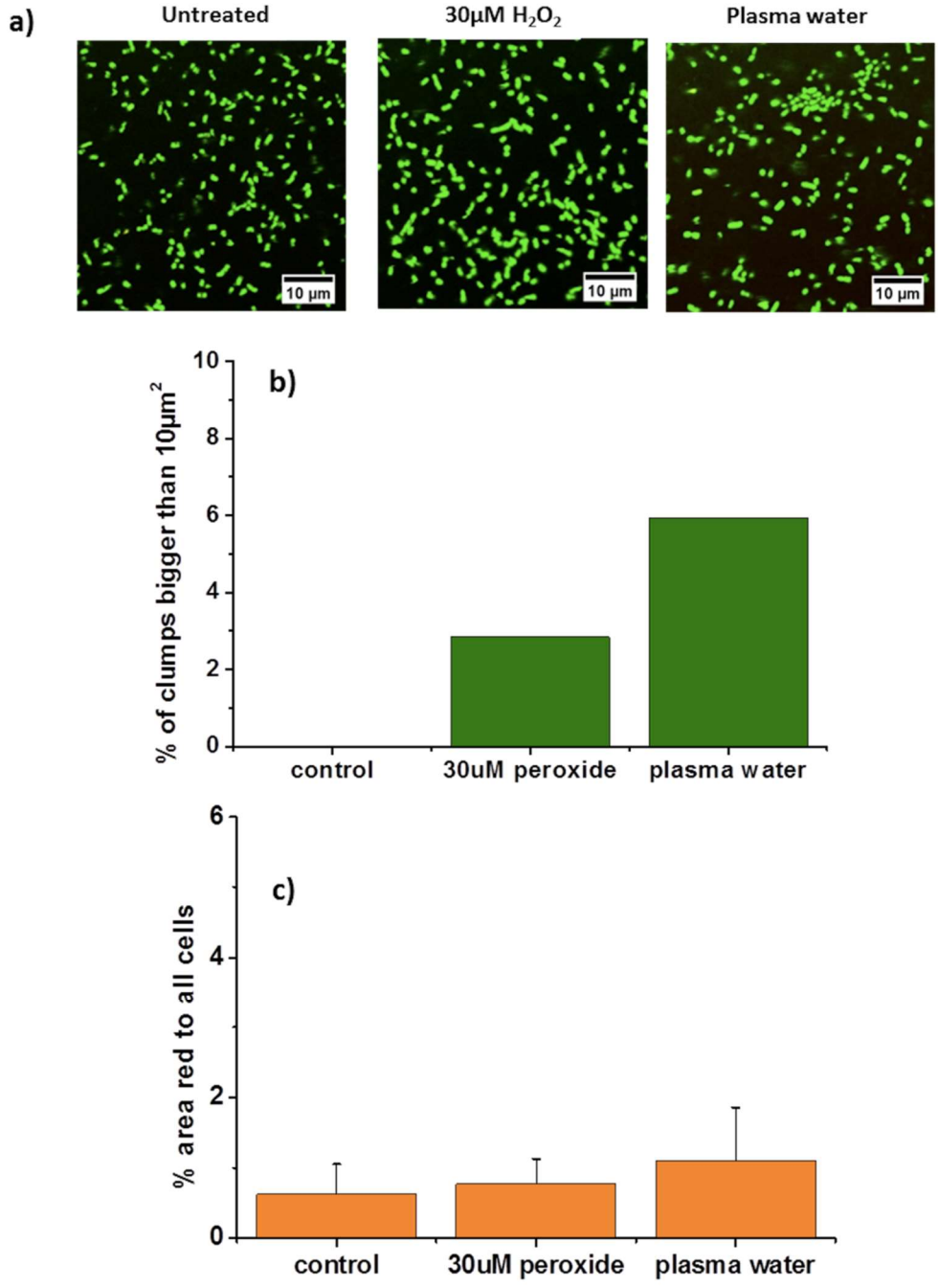

FIGURE 4.7 A) Confocal images of untreated biofilm, incubated with 30 µM H2O2 and incubated with plasma liquid treated for 60 s, b) percentage of aggregates bigger than 10 µm^2, c) red cells quantification of samples

4.3.5 | Dilution effect on biofilm structure

As mentioned before, the formation of ring structure has been observed in surface deposited bacteria, which is said due to drying by plasma jet [25]. This means that there is high possibility that the structure here is also caused by drying. To understand better the drying by our plasma system, we measured how much water removed when exposed to plasma.

TABLE 4.2 The amount of water removed by plasma treatment

Amount of water in dish (g)	Amount of water removed (g)	Percentage of water removed (%)
0.2	0.064 ± 0.024	32.9±2.7
0.4	0.053 ± 0.007	13.3±1.7
0.6	0.044 ± 0.011	7.4±1.9
0.8	0.060 ± 0.019	7.5± 2.3
1	0.051 ± 0.013	5.1 ± 1.3

Table 4.2 shows that for 30 s treatment time, plasma treatment removes between 0.04–0.06 g water from the system by evaporation regardless of the starting amount of water. From this result, it appears that there is a maximum amount of water that can be removed by plasma for the same treatment time. On the other hand, Table 2 also indicates that the percentage of water removed changes depending on the amount of initial liquid covering biofilm. In this case, the maximum of water removed is 32.9% for a biofilm covered with 200 μL of water (Table 4.2). Additionally, this suggests that after plasma treatment for 30 s, biofilms will not completely dry out. Thus, from this observation, it is therefore

likely that larger volumes of water could reduce the drying and convective effects of plasma treatment in a specified treatment time. Interestingly, we have observed that biofilms that were completely dried in an oven overnight have a similar structure to these plasma-treated samples (data not shown).

The above experiments were repeated with biofilms present in varying amounts of water and a constant plasma exposure time of 30 s. Figure 4.8 summarizes the results obtained from this experiment. It is clear that biofilms can aggregate in liquid volumes up to 600 µl. However, when biofilms are in larger liquid volumes (>600 µl) no aggregation was observed, presumably due to a protective effect from the liquid against drying.

Figure 4.8b also indicates that aggregation and cell death was steadily reduced with increasing amounts of liquid. Increasing the amount of water by 200 µL lowers the percentage of dead cells and also reduces the extent of clumping by around 10%. For biofilms that are covered by 800 and 1000 µL, the clumping effect and amount of cell death is very small. This confirms the hypothesis that extra liquid protects biofilms during plasma treatment and reduces the drying effect imposed by plasma discharge. Although plasma drying is not mentioned much in the literature as a mechanism of plasma inactivation, it is an important factor governing cell death. Due to this, the effect of plasma drying during treatment has to be taken into account when treating bacteria or biofilms, as this effect is apparent even when biofilms are treated for very short times.

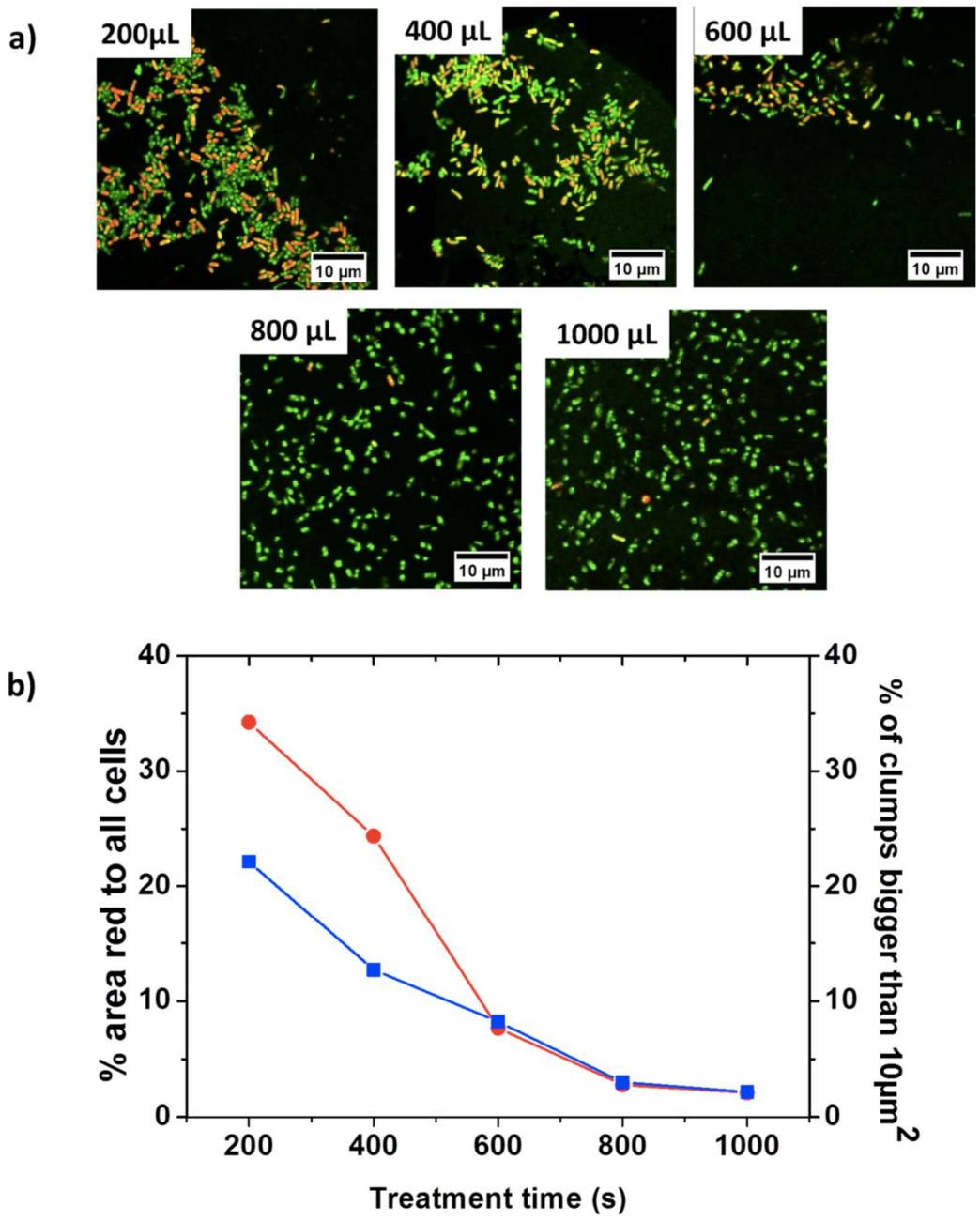

FIGURE 4.8 The effect of liquid volume covering biofilm during plasma treatment on aggregation and cell death a) confocal images of different structures observed, b) quantification of dead cells (symbol ●) and cell clumps larger than 10 μm^2 (symbol ■)

4.3.6 | Explanation of structure formation

Our results from the previous section indicate that the structure generated by plasma treatment is mainly due to a drying effect. There is a difference in the convection produced by plasma and standard oven, as Figure 4.9a & b indicates treatment with a conventional oven at 50 °C (average temperature of cold plasma) for the same time scale (30 or 60 s) could not cause the same effect of aggregation. In addition, as can be seen from Figure 4.9c, even prolonged dehydration for 90 s using the oven could not cause the same clumping effect as plasma treatment, although there is indication of some cell death.

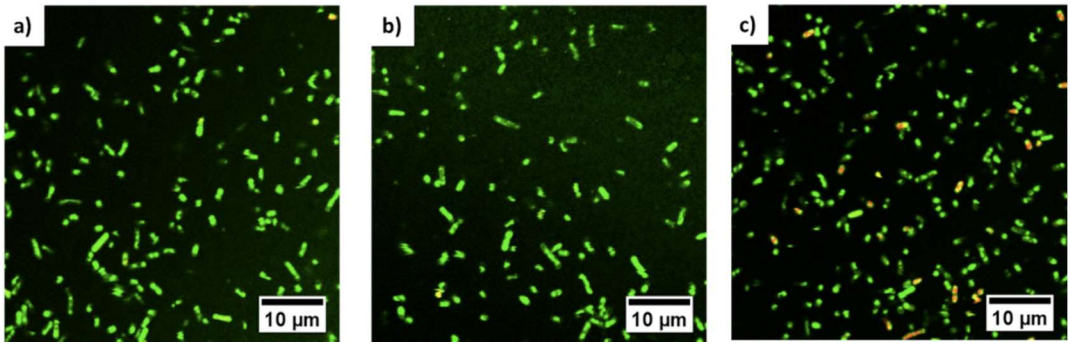

FIGURE 4.9 The drying effect on structure of biofilm by oven at 50 °C for different treatment time. a) Treated for 30 s, b) treated for 60 s, c) treated for 90 s

The circular pattern observed in Figure 4.10a resembles Benard cells, hexagonally-ordered structures that spontaneously form in fluids with a convection flow during heating or evaporation [40]. The length scale of this structure is on the order of µm and is similar to structures formed by surface deposited bacteria [25], as depicted in Figure 4.10c. Deegan *et al.* [41] showed that various patterns can be created by changing the conditions of evaporation. Apart from the formation of Benard cells where the deposit forms a ring, Deegan *et al.* [41] also observed the formation of compact structures as we observed in our biofilm (Figure 4.10b). As biofilms are known to have a heterogeneous spatial structure, the plasma jets are also generally heterogeneous in their effects on targets, resulting in the two distinct structures observed. Fischer [42] reported the

formation of such ring structures only occurs when there is outward flow to replenish liquid evaporating from the edges.

The fact that there is a limit of maximum liquid coverage of biofilms for significant convective effects may be related to the conditions required for Benard cell formation in thin films, namely that the thickness be less than 1 mm [43]. In our experiments, water mainly covered the inner area of the FluoroDish™, which has an overall diameter of 23.5 mm. Assuming that liquid covers the inner area uniformly and the area is in a cylindrical shape, the volume of liquid added to each system allows us to calculate the height of liquid covering the biofilm. It was found that only biofilm containing 200 and 400 µL liquid is covered by water layer which is less than 1 mm thick. This agrees with the finding that aggregation of cells is more apparent in those samples. Drying of 200 µL water for 30s by oven only removed 1.6 ± 0.25% water, which is around 20 times lower than drying the same amount of water by plasma (Table 4.2). Probstein [43] also indicates that for thin films around 0.5–1 mm deep, the cell spacing should be around three times the liquid depth. The difference between the two might relate to the different rate of drying of plasma, oven or natural convection. In addition, the fact that biofilms have polymeric gels that encapsulate them might reduce the rate of bacterial cell migration during drying, hence smaller size structures were observed.

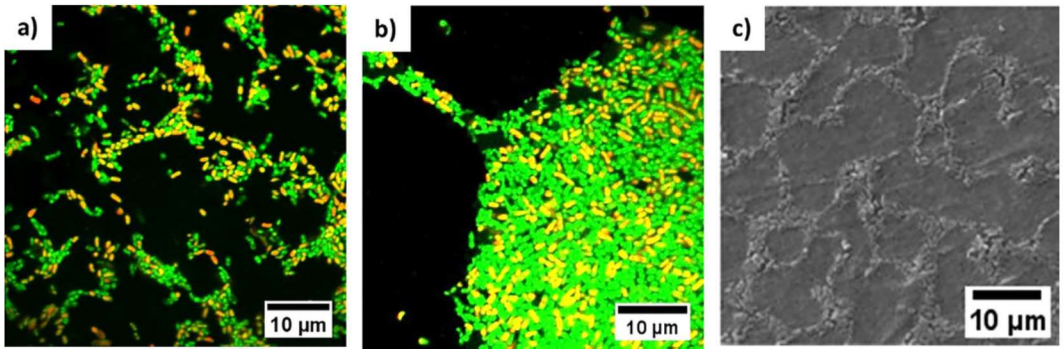

FIGURE 4.10 a) Circular pattern ring structure formed by bacteria after plasma treatment, b) Compact structure formed by bacteria after plasma treatment, c) pattern rings formed by surface-deposited bacteria after plasma treatment reproduced from ref [25] with permission

4.4 CONCLUSIONS

Plasma can be an effective treatment for biofilm eradication. However, this study found that plasma can also induce new structures within the biofilm, which can persist after treatment during regrowth. This phenomenon was evident for both young and more mature biofilms. Once such structures form, subsequent treatments are less effective in terms of efficacy, likely due to the surviving bacteria becoming increasingly resistant to plasma. The structures induced for the biofilms tested are similar to those observed previously for plasma-treated surface-deposited bacteria.[29] The observed structures are reminiscent of Benard cells, whose main mechanism of formation is convection. Secondary plasma species formed in the liquid phase were not found to induce the formation of such structures. Finally, future studies should try to transfer plasma technology, presented here, to biofilm produced by other bacteria. Indeed, EPS compositions (and survival mechanisms) can vary a lot between intra and inter bacterial species. It would be interesting to see how different biopolymers and biofilms would rearrange and react after plasma treatment.

4.5 REFERENCES

1. Flemming, H.-C. and J. Wingender, *The biofilm matrix.* Nat Rev Micro, 2010. **8**(9): p. 623-633.

2. Mah, T.-F.C. and G.A. O'Toole, *Mechanisms of biofilm resistance to antimicrobial agents.* Trends in Microbiology, 2001. **9**(1): p. 34-39.

3. Donlan, R.M., *Biofilms and Device-Associated Infections.* Emerging Infectious Disease journal, 2001. **7**(2): p. 277.

4. Donlan, R.M., *Biofilms: Microbial Life on Surfaces.* Emerging Infectious Diseases, 2002. **8**(9): p. 881-890.

5. Hall-Stoodley, L., J.W. Costerton, and P. Stoodley, *Bacterial biofilms: from the Natural environment to infectious diseases.* Nat Rev Micro, 2004. **2**(2): p. 95-108.

6. Srey, S., I.K. Jahid, and S.-D. Ha, *Biofilm formation in food industries: A food safety concern.* Food Control, 2013. **31**(2): p. 572-585.

7. Birjiniuk, A., N. Billings, E. Nance, J. Hanes, K. Ribbeck, and P.S. Doyle, *Single particle tracking reveals spatial and dynamic organization of the Escherichia coli biofilm matrix.* New Journal of Physics, 2014. **16**(8): p. 085014.

8. Stewart, E.J., M. Ganesan, J.G. Younger, and M.J. Solomon, *Artificial biofilms establish the role of matrix interactions in staphylococcal biofilm assembly and disassembly.* Scientific Reports, 2015. **5**: p. 13081.

9. Chen, M., Q. Yu, and H. Sun, *Novel Strategies for the Prevention and Treatment of Biofilm Related Infections.* International Journal of Molecular Sciences, 2013. **14**(9): p. 18488–18501.

10. Misra, N.N., B.K. Tiwari, K.S.M.S. Raghavarao, and P.J. Cullen, *Nonthermal Plasma Inactivation of Food-Borne Pathogens.* Food Engineering Reviews, 2011. **3**(3): p. 159-170.

11. Tendero, C., C. Tixier, P. Tristant, J. Desmaison, and P. Leprince, *Atmospheric pressure plasmas: A review.* Spectrochimica Acta Part B: Atomic Spectroscopy, 2006. **61**(1): p. 2-30.

12. Joshi, S.G., M. Paff, G. Friedman, G. Fridman, A. Fridman, and A.D. Brooks, *Control of methicillin-resistant Staphylococcus aureus in planktonic form and biofilms: A biocidal efficacy study of nonthermal dielectric-barrier discharge plasma.* American Journal of Infection Control, 2010. **38**(4): p. 293-301.

13. Xiong, Z., T. Du, X. Lu, Y. Cao, and Y. Pan, *How deep can plasma penetrate into a biofilm?* Applied Physics Letters, 2011. **98**(22): p. 221503.

14. Alkawareek, M.Y., Q.T. Algwari, G. Laverty, S.P. Gorman, W.G. Graham, D. O'Connell, and B.F. Gilmore, *Eradication of Pseudomonas aeruginosa Biofilms by Atmospheric Pressure Non-Thermal Plasma.* PLOS ONE, 2012. **7**(8): p. e44289.

15. Ziuzina, D., S. Patil, P.J. Cullen, D. Boehm, and P. Bourke, *Dielectric Barrier Discharge Atmospheric Cold Plasma for Inactivation of Pseudomonas aeruginosa Biofilms.* Plasma Medicine, 2014. **4**(1-4): p. 137-152.

16. Mai-Prochnow, A., M. Bradbury, K. Ostrikov, and A.B. Murphy, *Pseudomonas aeruginosa Biofilm Response and Resistance to Cold Atmospheric Pressure Plasma Is Linked to the Redox-Active Molecule Phenazine.* PLOS ONE, 2015. **10**(6): p. e0130373.

17. Ziuzina, D., D. Boehm, S. Patil, P.J. Cullen, and P. Bourke, *Cold Plasma Inactivation of Bacterial Biofilms and Reduction of Quorum Sensing Regulated Virulence Factors.* PLOS ONE, 2015. **10**(9): p. e0138209.

18. Liu, D.X., Z.C. Liu, C. Chen, A.J. Yang, D. Li, M.Z. Rong, H.L. Chen, and M.G. Kong, *Aqueous reactive species induced by a surface air discharge: Heterogeneous mass transfer and liquid chemistry pathways.* Scientific Reports, 2016. **6**: p. 23737.

19. Gaunt, L.F., C.B. Beggs, and G.E. Georghiou, *Bactericidal Action of the Reactive Species Produced by Gas-Discharge Nonthermal Plasma at Atmospheric Pressure: A Review.* IEEE Transactions on Plasma Science, 2006. **34**(4): p. 1257-1269.

20. Matthew, J.T., J.P. Matthew, K. Sharmin, H. Pritha, S. Yukinori, S.C. Douglas, and B.G. David, *Long-term antibacterial efficacy of air plasma-activated water.* Journal of Physics D: Applied Physics, 2011. **44**(47): p. 472001.

21. Ferrell, J.R., F. Shen, S.F. Grey, and C.J. Woolverton, *Pulse-based non-thermal plasma (NTP) disrupts the structural characteristics of bacterial biofilms.* Biofouling, 2013. **29**(5): p. 585-599.

22. Khan, M.S.I., E.-J. Lee, and Y.-J. Kim, *A submerged dielectric barrier discharge plasma inactivation mechanism of biofilms produced by Escherichia coli O157:H7, Cronobacter sakazakii, and Staphylococcus aureus.* Scientific Reports, 2016. **6**: p. 37072.

23. Zelaya, A.J., G. Stough, N. Rad, K. Vandervoort, and G. Brelles-Mariño, *Pseudomonas aeruginosa Biofilm Inactivation: Decreased Cell Culturability, Adhesiveness to Surfaces, and Biofilm Thickness Upon High-Pressure Nonthermal Plasma Treatment.* IEEE Transactions on Plasma Science, 2010. **38**(12): p. 3398-3403.

24. Vandervoort, K.G. and G. Brelles-Mariño, *Plasma-Mediated Inactivation of Pseudomonas aeruginosa Biofilms Grown on Borosilicate Surfaces under Continuous Culture System.* PLoS ONE, 2014. **9**(10): p. e108512.

25. Bayliss, D.L., J.L. Walsh, F. Iza, G. Shama, J. Holah, and M.G. Kong, *Complex Responses of Microorganisms as a Community to a Flowing Atmospheric Plasma.* Plasma Processes and Polymers, 2012. **9**(6): p. 597-611.

26. Lu, P., D. Boehm, P. Bourke, and P.J. Cullen, *Achieving reactive species specificity within plasma-activated water through selective generation using air spark and glow discharges.* Plasma Processes and Polymers, 2017: p. e1600207-n/a.

27. Schneider, C.A., W.S. Rasband, and K.W. Eliceiri, *NIH Image to ImageJ: 25 years of image analysis.* Nat Meth, 2012. **9**(7): p. 671-675.

28. Reshes, G., S. Vanounou, I. Fishov, and M. Feingold, *Cell Shape Dynamics in Escherichia coli.* Biophysical Journal, 2008. **94**(1): p. 251-264.

29. Pick, E. and Y. Keisari, *A simple colorimetric method for the measurement of hydrogen peroxide produced by cells in culture.* Journal of Immunological Methods, 1980. **38**(1): p. 161-170.

30. Beyenal, H., Z. Lewandowski, and G. Harkin, *Quantifying Biofilm Structure: Facts and Fiction.* Biofouling, 2004. **20**(1): p. 1-23.

31. Sladek, R.E.J., S.K. Filoche, C.H. Sissons, and E. Stoffels, *Treatment of Streptococcus mutans biofilms with a nonthermal atmospheric plasma.* Letters in Applied Microbiology, 2007. **45**(3): p. 318-323.

32. Adler, J., *Chemotaxis in Bacteria.* Science, 1966. **153**(3737): p. 708-716.

33. Oliveira, N.M., K.R. Foster, and W.M. Durham, *Single-cell twitching chemotaxis in developing biofilms.* Proceedings of the National Academy of Sciences, 2016. **113**(23): p. 6532-6537.

34. Oehmigen, K., J. Winter, M. Hähnel, C. Wilke, R. Brandenburg, K.-D. Weltmann, and T. von Woedtke, *Estimation of Possible Mechanisms of Escherichia coli Inactivation by Plasma Treated Sodium Chloride Solution.* Plasma Processes and Polymers, 2011. **8**(10): p. 904-913.

35. Lu, P., D. Boehm, P. Cullen, and P. Bourke, *Controlled cytotoxicity of plasma treated water formulated by open-air hybrid mode discharge.* Applied Physics Letters, 2017. **110**(26): p. 264102.

36. Ercan, U., Joshi, S. , Yost, A. , Gogotsi, N. , O'Toole, S. , Paff, M. , Melchior, E. and Joshi, S., *Inhibition of Biofilms by Non-Thermal Plasma Treated Novel Solutions.* Advances in Microbiology, 2014. **4**: p. 1188-1196.

37. Kamgang-Youbi, G., J.M. Herry, T. Meylheuc, J.L. Brisset, M.N. Bellon-Fontaine, A. Doubla, and M. Naïtali, *Microbial inactivation using plasma-activated water obtained by gliding electric discharges.* Letters in Applied Microbiology, 2009. **48**(1): p. 13-18.

38. Naïtali, M., G. Kamgang-Youbi, J.-M. Herry, M.-N. Bellon-Fontaine, and J.-L. Brisset, *Combined Effects of Long-Living Chemical Species during Microbial Inactivation Using Atmospheric Plasma-Treated Water.* Applied and Environmental Microbiology, 2010. **76**(22): p. 7662-7664.

39. Oehmigen, K., M. Hähnel, R. Brandenburg, C. Wilke, K.D. Weltmann, and T. von Woedtke, *The Role of Acidification for Antimicrobial Activity of Atmospheric Pressure Plasma in Liquids.* Plasma Processes and Polymers, 2010. **7**(3-4): p. 250-257.

40. Rayleigh, L., *LIX. On convection currents in a horizontal layer of fluid, when the higher temperature is on the under side* Philosophical Magazine, 1916. **32**(192): p. 529-546.

41. Deegan, R.D., O. Bakajin, T.F. Dupont, G. Huber, S.R. Nagel, and T.A. Witten, *Contact line deposits in an evaporating drop.* Physical Review E, 2000. **62**(1): p. 756-765.

42. Fischer, B.J., *Particle Convection in an Evaporating Colloidal Droplet.* Langmuir, 2002. **18**(1): p. 60-67.

43. Probstein, R.F., *Surface Tension*, in *Physicochemical Hydrodynamics*. 1993, Wiley: New York. p. 267-318.

Chapter 5

Engineering bacterial cellulose fiber structure and mechanical properties with growth medium rheology

5.1 INTRODUCTION

Cellulose is one of the main polysaccharides produced in biofilms by cells of many different bacteria species, usually in conjunction with other extracellular polymeric substances, or EPS. Numerous studies of bacterial cellulose have focused on behavior of *Acetobacter* species, where the cellulose is the main polysaccharide material excreted by the bacteria [1].

Acetobacter species form biofilms at the air-liquid interface of a bacterial growth medium in the form of a pellicle, a porous mat made of many interconnected cellulose nanofibers. The diameter of each of the cellulose fibres is around 15-25 nm, while they can reach lengths as large as 10 μm [1]. In the native bacterial cellulose pellicle, the cellulose fibres are entangled [2] and are stabilized by hydrogen bonding, forming a supramolecular network with a Young's modulus >15 GPa across the dried sheets [1]. Due to its mechanical strength, the material is useful as a cell scaffold [3-5] and bandage or dressing [6]. Even when the fibers are dispersed from a coherent pellicle into a pulp dispersion, the paper produced from the dispersion has a Young's modulus that is nearly one third of the original pellicle's value [1]. Dispersed bacterial cellulose has also found application as a rheology modifier for consumer products [7] and for pharmaceutical nasal sprays [8]. Due to their useful properties, people are trying to increase the cellulose yield by modifying the growth process.

There are two most common growing methods that people use which are static culture or agitated culture. The standard pellicle that grows in air-liquid interface usually forms in a static culture, whereas the agitated culture instead forms aggregated cellulose clumps that vary in size [9]. In general, agitated cultures produce less cellulose than static cultures [9] and the cellulose has less crystallinity [10], and a lower degree of polymerization [11]. This results in a decrease of Young's modulus and tensile strength of the cellulose pellicle [10, 11], which could be undesirable for certain applications if too dramatic a change.

Other factors like growth medium properties, or culture temperature, will also affect the cellulose yield. When sucrose, glucose, mannitol or glycerol is used as a carbon source for the bacteria, the amount of cellulose produced is around 1.2 to 2 times higher than other carbon sources such as galactose or fructose [12-14]. Changing the carbon source might also increase or decrease the overall crystallinity of the cellulose produced, but not its structure [12, 14]. For example, by using mannitol, Mikkelsen *et al* found that the cellulose crystallinity is increased by 10% than when glucose is used [12]. The addition of a nitrogen source, such as yeast extract and peptone into the growth medium will also increase production of bacterial cellulose than when only carbon source is present[13]. Some chemicals such as ethanol or ammonium sulphate can act as additional nutrient sources, which will also improve cellulose production [15]. Growing *Acetobacter* culture at certain pH increase the production of cellulose [15], although Hutchens *et al.* [16]found that actually it's the interaction between pH and carbon source is the key factor.

To improve the productivity of cellulose in agitated culture, some researchers added polymeric additives into the bacterial culture. The addition of polymeric additives increases medium viscosity and reduce shear stress during agitation, allowing bacteria to form more homogeneous pellets which in turn will increase its productivity [17-20]. However, studies have shown that this also changes the microstructure of pellicles, where the polymeric additives form a composite with cellulose [19, 21-23]. The interaction seems to be affected by the type of polymeric additives. The polymer, sodium alginate for example, might incorporates into the pellicle through both chemical and physical interactions with cellulose fibers. It has been shown that cellulose fibers and alginate might form hydrogen bonding [19] as well as weak physical interaction between carbonyl group of cellulose and alginate based on FT-IR spectra [22]. Both studies saw changes in the structure of the alginate-cellulose network.

Zhou *et al.* [17] reported more open structure in the cellulose-alginate pellicle compared to the highly compact fibres in a regular pellicle, with alginate commonly deposited on the fibre surfaces. Kanjanamosit *et al*. [22] showed that,

if left inside the pellicle, alginate occupies most of the pore volume in the cellulose network, reducing the pore size, resulting in a 20% lower tensile strength and Young's modulus versus normal pellicle material. Alginate-cellulose composite networks made by mechanically blending the two materials also showed a decrease in Young's modulus by about 20% at alginate compositions of 20% in the blend [25].

Other polysaccharides, like carboxymethyl cellulose (CMC), reduce the size of pellicle pores and were thought to increase the diameter of cellulose fibrils [21, 24], likely because of adsorption [17]. Seiffert *et al*. [26] found deposition of CMC on cellulose pellicles can reduce the density of a pellicle and increase pore size [17]. However, all studies found an order of magnitude reduction in Young's modulus [15, 19] and elastic modulus [20] of cellulose pellicles after addition of CMC. Addition of CMC also improves the ability to rehydrate dried pellicles [21, 26], partially as a result of higher water affinity and retention by CMC [23]. Differences in ultimate locations and disposition of added polysaccharides onto the fibers can vary the properties of the resulting pellicles [20], so more information is needed about specific physicochemical mechanisms behind such effect in order to properly harness any benefits to engineering the bacterial products.

Though well-studied as composite systems, the mechanisms behind some of the interesting effects on pellicle structure have not been fully explained. Some of the simple approaches to modifying the final pellicle properties hold promise for robust processes to produce a wide array of properties in the final materials. We study here the quantitative physical mechanisms of pellicle modification using simple approaches like modification of the growth medium rheology and explain the effects of the medium on the resultant growth. This holds promise for design of biomaterials and engineering of complex bacterial growth processes with simple process changes.

5.2 MATERIALS AND METHODS

5.2.1 | Preparation of alginate solution

TRIS buffer solution (1 M) was prepared by dissolving 60.6g tris(hydroxymethyl)aminomethane (Sigma-Aldrich, Sydney, Australia) in 400 mL of distilled water and the pH was adjusted to neutral with HCl. Sodium Alginate (FD155, Danisco, Sydney, Australia) solution was prepared by adding sodium alginate powder in 0.1 M TRIS buffer, the mixture was stirred using a magnetic stirrer (Ika-Works,VWR, Sydney, Australia) at 600RPM for 24 hours or until all the solids were dissolved.

5.2.2 | Bacterial cellulose production

A mixed culture of *Acetobacter xylinum* and *Saccharomyces cerevisiae*, maintained by our lab from commercial sources (Nourishme Organics, Australia) was used to produce all pellicles. The growth medium was made by first adding black tea (Coles, Australia) into boiling water and letting it steep for 10 minutes. Into this tea, sucrose (Coles, Australia) was added at 10% w/v concentration. The solution was then added to a bacterial starter culture that was grown for 5 days prior.

The culture was then combined with an equal volume of aqueous sodium alginate solution sufficient to produce alginate concentrations from 0 - 1% w/v. The solutions were then incubated at 25 °C for up to 10 days.

After a certain growth time, the cellulose pellicles that grew at the air-liquid interface were harvested and washed with water to remove any loosely attached fibrous materials from the pellicles. The pellicles were then washed in 0.5 M NaOH (Chem-Supply Pty Ltd, Australia) at 90 °C for 90 minutes to kill the bacteria. The pellicles were then washed with water until the rinse pH becomes neutral. The cleaned pellicles were stored at 4 °C immersed in 100mL water preserved with 2 drops of an aqueous 1.5% solution of methylchloroisothiazolinone (Sigma Aldrich, Sydney, Australia), which acts as preservative for the pellicles before any experiments.

5.2.3 | Preparation of cellulose dispersion

To make cellulose dispersion, the clean pellicles were blended using DI water using a food blender (Breville: Model BBL405, Australia) in batches at the highest speed (speed 4), according to internal procedure. Each time the cycle lasts for ~2 minutes. Then, the concentration of the cellulose dispersion is determined using gravimetric analysis. The known amount of cellulose dispersion is weighed into small petri dish and dried using a food dehydrator (Sunbeam: Model DT6000, Australia) at 70 °C for 19 hours. The dried cellulose is then weighed and concentration is determined by dividing dry cellulose weight with the initial weight of the cellulose dispersion.

5.2.4 | Measurement of pellicle properties

The wet weight was obtained by patting the pellicles on paper towel for one minute to remove excess water, but preserve any absorbed within the structure, before weighing. For dry weight measurement, the pellicles were placed in a food dehydrator (Sunbeam: Model DT6000, Australia) and dried at 70 °C for 19 hours before weighing. The pellicle thickness was measured by image analysis, using ImageJ [27], of calibrated digitized microscopic observations of the pellicle edge, using an average of five radial locations.

5.2.5 | Rheological measurement

Rheological measurements were carried out on a DHR-1 Rheometer (TA Instruments) using a 40mm parallel plate geometry. Clean pellicles obtained from cultures after 10 days of growth were placed into the rheometer and the gap between measurement plates was adjusted accordingly depending on sample heights and desired test strain between 0 to 70% strain. Mechanical testing of pellicles was performed via compressional deformation using a frequency of 1Hz.

5.2.6 | Zeta potential measurement

Different concentration of alginate is added to cellulose dispersion, until the desired concentrations of both alginate and cellulose were reached. The samples were then briefly mixed using a rotor mixer (Ratek: Model VM1, Australia) for around 30s. The zeta potential measurement was performed using phase analysis light scattering using Malvern Zetasizer Nano ZSP (Malvern Instruments Ltd., Malvern, UK). Zeta potential values were presented as means of triplicate runs (size sub-runs) per sample (n=9±SD).

5.2.7 | Confocal Laser Scanning Microscopy (CLSM)

Full pellicles are 70 mm disks, so samples for confocal imaging were cut into small cubes with dimensions of 5 mm x 5 mm x initial pellicle height. The samples were then incubated in 0.5% w/v Congo Red dye (Sigma Aldrich, Sydney, Australia) for 15 minutes before imaging. The imaging was performed on a Leica TCS SP5 WLL STED (Germany) inverted confocal microscope with a 63X oil objective with an NA = 1.4. The wavelength of the laser used for imaging was 461 nm. The structure of pellicles was scanned from the top, or air-facing side, bottom or water-immersed side, and side surface to a depth of 100 μm, the working limit of the objective used. The pellicles were also imaged on each side at two positions: one close to the outer edge and the other one towards the pellicle centre.

5.2.8 | Calculation of intermolecular forces

The intermolecular forces acting in the system are calculated by assuming cellulose fibres to be two flat parallel plates, following the method of Boluk *et al* [28]. The actual cellulose fibres are assumed to be cylindrical in shape, with dimensions of 50nm width and 1μm length.

The electrostatic interaction (V_{ele}) is estimated by using

Equation 5.1 $$V_{ele} = 64(\pi)^{0.5} nKT\gamma^2 L \frac{(\kappa a)^{0.5}}{\kappa^2} \exp(-\kappa H)$$

The n is the number density of ions, k is the Boltzmann constant, T is the absolute temperature of 25°C, κ is the Debye length, a is the radius of cellulose, L is the length of cellulose, while γ in the equation is defined as:

Equation 5.2 $$\gamma = \tanh\left(\frac{e\psi_0}{4kT}\right)$$

The e in the equation refers to charge of the electron and ψ_0 is the surface potential.

The van der Waals interaction potential is calculated by:

Equation 5.3 $$V_{vdw} = -\frac{3}{8}\pi A \frac{L}{a} a^5 U_5$$

where A is the Hamaker constant of cellulose in TRIS buffer, which is calculated from $A=(\sqrt{A\ cellulose} - \sqrt{A\ Tris})^2$

The Hamaker constant of cellulose is given by Boluk *et al* [28] as 1.1 x 10^{-20} J, but the Hamaker constant of TRIS buffer is from Onuma & Kanzaki [29] where the value 5.2kT is 2.1372x10^{-20} J. The calculated Hamaker constant that was used in the calculations was 1.706x10^{-21} J. Here a is the distance between cylinder axes which is defined as R=H+2a, while U_5 is a function of cylinder radius, defined as [30]:

Equation 5.4

$$U_5 = \frac{1}{R^5}\left\{1 + 6.25\left(\frac{a}{R}\right)^2 + 31.9\left(\frac{a}{R}\right)^4 + 150.7\left(\frac{a}{R}\right)^6 + 684\left(\frac{a}{R}\right)^8 + 2200\left(\frac{a}{R}\right)^{10}\right\}$$

The depletion potential experienced by the fibres (V_{dep}) is estimated using:

Equation 5.5 $$V_{dep} = -\pi S\left[\frac{4Rg}{\sqrt{\pi}} - H - H\chi(H)\right]$$

where Π is the osmotic pressure of alginate solution and Rg is the radius of gyration of alginate. Rg was calculated from the molecular weight of alginate, which is 140,000 Da. Π is calculated using:

Equation 5.6 $$\Pi = n_p kT \left(1 + 1.2\frac{c}{c^*}\right)$$

and $\chi(H)$ is calculated by using equation:

Equation 5.7 $$\chi(H) = \frac{8}{\pi^2}\sum_{p=1,3,5}\frac{1}{n^2}\, exp\left(-\frac{p^2\pi^2 Rg^2}{h^2}\right)$$

5.2.9 | Calculation of cellulose surface area exposed to alginate

Here it is assumed that a single cellulose fibre is cylindrical in shape, with 50nm width (d) and 1μm length (h), in agreement with SEM images. The surface area of a single fibre is the calculated surface area of a cylinder:

Equation 5.8 $$surface\ area = 2\pi rh + \pi r^2$$

The r is calculated half the width (d), or 25 nm. In addition, the volume of a single fibre is found using:

Equation 5.9 $$volume = \pi r^2 h$$

The total volume of the cellulose fibres is calculated by using the dry weight of washed pellicles grown in 1% alginate (data from Figure 5.6b) and substituted into:

Equation 5.10 $$volume = \frac{pellicle\ dry\ wei}{density\ of\ cellulose}$$

where the density used is 1.5g/cm^3. This total volume is then divided with the volume of a single fibre of cellulose. Then the estimated total number of cellulose fibres can be obtained, which is then multiplied by the surface area of a single cellulose fibre.

5.3 RESULTS AND DISCUSSIONS

5.3.1 | The growth of bacterial cellulose pellicle

Bacterial growth in the aqueous medium initially occurs throughout the container volume. Once cellulose growth becomes significant, however, pellicle formation

becomes visible at the bottom of the culture container. Fibrous mass formation can be observed within 24 hours of the start of the bacteria cultivation (Figure 5.1b). Over time, however, the small fibrous masses slowly move up to the top of the growth medium, despite being denser than water with $\rho_{cellulose}$ ~1.5 g/cm^3 [31], and remain at the air-liquid interface for all later growth (Figure 5.1). Schramm & Hestrin [9] suggest the decreased density of the fibres this is due to carbon dioxide molecules produced by the bacteria forming bubbles that adsorb to the surface of the cellulose fibres. The cellulose agglomerates are then buoyant and able to float to the air-liquid interface.

The fibre agglomerates form and accumulate at the interface, then consolidate into the final pellicle after about 60 hours of growth, as shown in Figure 5.1c. At this stage, Figure 5.1d, some fibrous masses still hang underneath the initial pellicle, but are also eventually incorporated into the main fibrous mass after around 100 hours of incubation time, Figure 5.1e. After this point, the main growth of cellulose is within the pellicle at the top of the culture, increasing and strengthening the interconnections between the previously separate fibre masses, Figure 5.1f.

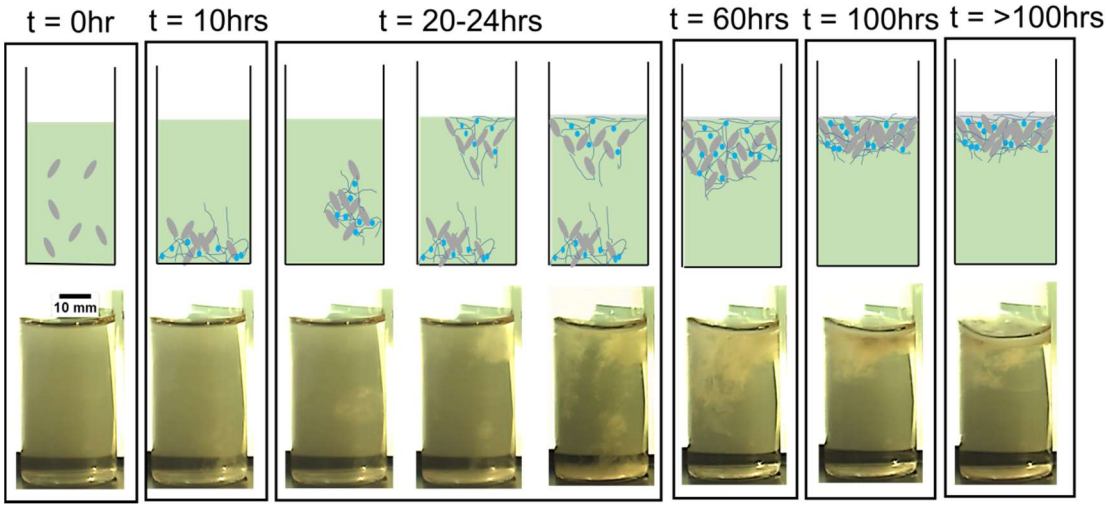

FIGURE 5.1 a) Early incubation, and bacterial multiplication, b) Formation of fibrous masses, c) Flotation of fibrous masses to air-liquid interface and full coverage of the interface, d) Formation of pellicle starter, e) Compaction of fibrous masses below pellicle starter, f) Thickening of pellicle.

5.3.2 | Effect of growth medium rheology on properties of pellicle

Past studies of added polymer effects on bacterial cellulose growth have largely focused on creating composite polymer-cellulose structures, or only studied specific traits of the final pellicle. We are interested here in possible physical mechanisms of pellicle growth modification, in order to easily engineer changes at large scales, and two key aspects of polymer addition to a bacterial cellulose system are polymer adsorption onto fibre surfaces and polymer modification of the growth medium rheology. We expect both factors to play some role in pellicle structure formation, and we study them by incubating the bacterial cultures in medium that contains sodium alginate, a water-soluble polysaccharide. At the concentrations used in this study, alginate is always Newtonian at shear rates between 1 s^{-1} and 100 s^{-1} (Figure 5.2). As a result, only the viscosity of the growth medium is changed by varying alginate concentration.

Alginate is able to form alginic acid gels when the pH of the environment is less than the pKa of the uronic acid formed by the alginate molecule itself [32]. As the metabolism of the bacteria forms acetic acid which and lowers the pH, the alginate powder is dissolved in TRIS buffer to prevent the formation of alginic acid gels and allow us to study just viscosity, rather than elasticity, effects. TRIS buffer was chosen as other buffers tested reduced the viscosity by a factor of 10 to 20 in water.

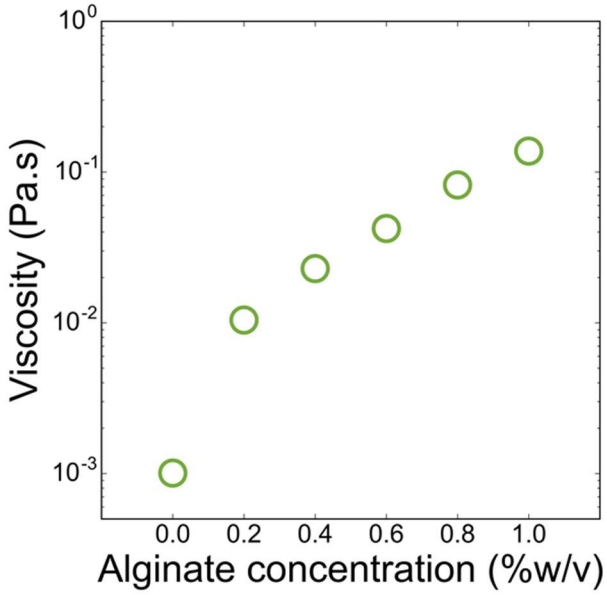

FIGURE 5.2 Viscosities of alginate solution at the different concentrations used in pellicle growth experiments.

The pellicles can grow in all media, both water and alginate solutions with different concentrations. The highest alginate concentration studied here, 1% w/v, increases the viscosity to 100 times that of water, Figure 5.2. The pellicles are harvested after 10 days of incubation. After washing, the pellicles were photographed, showing they look quite similar from the top (Figure 5.3a). However, from the side the pellicles have significantly different heights, with the pellicles grown in the presence of alginate decreasing in thickness as alginate concentration increases (Figure 5.3). The thickness of the pellicles grown in 0.2% alginate decreased by around 30% compared to the pellicles grown in water, Figure 5.3b, so even small concentrations can have a significant effect. The reduction in thickness continues as alginate is added until 0.6% alginate, after which pellicle thickness is similar but represent a roughly 66% reduction in pellicle height at 1% alginate (Figure 5.3). This suggests that with the addition of alginate into the media, the resulting pellicles are denser than the ones grown in water. Measurements of the pellicle mass will enable determination of whether the effect is based on cellulose yield or other factors.

Dry weights of carefully washed pellicles were measured to ascertain the actual mass of cellulose produced by the bacteria. If the growth of bacteria is slowed down, or in some way hindered by the presence of alginate, the change in pellicle thickness observed in Figure 5.3 could be the result of decreased production. Surprisingly, the dry weights of the pellicles across all viscosity media are essentially the same within experimental variation, Figure 5.3c. The consistency of cellulose mass production indicates that the metabolic process of these bacteria is not impaired by changing the rheology of the growth medium.

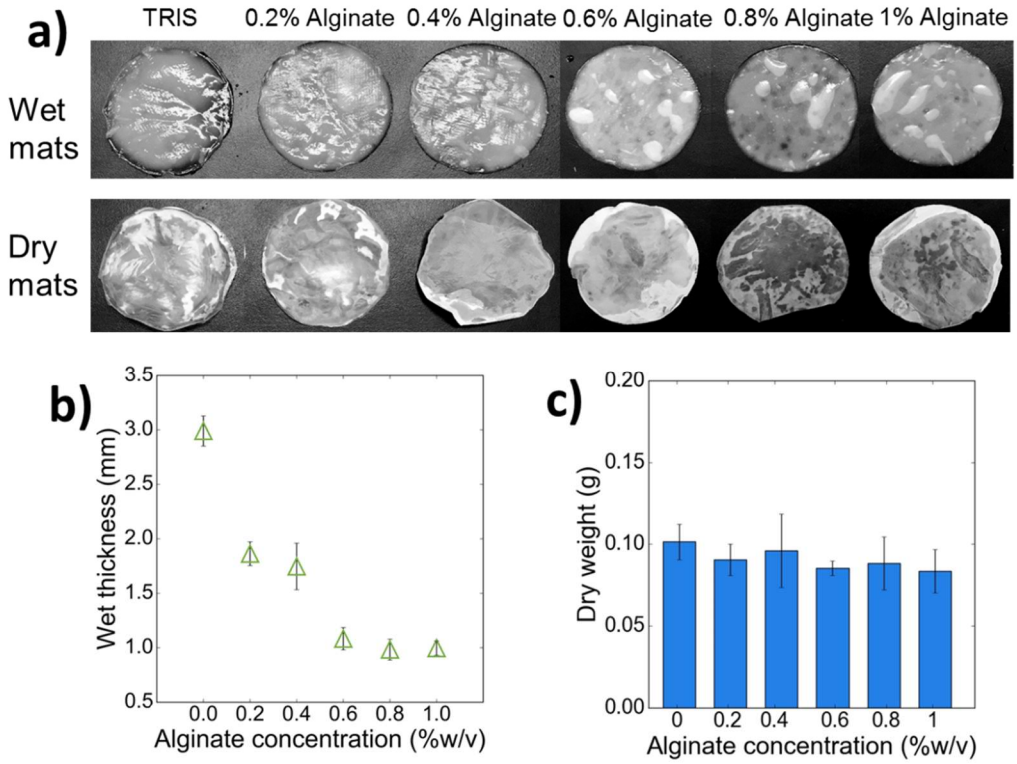

FIGURE 5.3 a) Top view of wet and dry pellicles; b) The change of thickness of wet pellicles with alginate concentration; c) The dry weight of pellicles with alginate concentration

The pellicles are like sponges that absorb and retain water, thus as the thickness of the pellicles changed, but the dry weights remain constant, it implies that the amount of water retained there should be different. Figure 5.4a summarizes the calculated water weight in the pellicles by subtracting the dry weight of the

pellicles from the total weight. It can be seen that with increasing alginate in the medium, the amount of water retained in the pellicles decreased consistently. The amount of water retained in pellicles grown in 1% alginate is around three times lower than the one grown without alginate. Although past work found increased affinity of water for pellicles grown in polymers like alginate [26], we see no significant enhancement of water holding capacity because the decreased pellicle volume effect dominates the growth behaviour. The significant densification of the pellicles is of interest to compare these materials with other systems and to better understand mechanisms behind the densification effect.

Figure 5.4b shows a plot of cellulose pellicle density as a function of alginate solution viscosities. As growth medium viscosity increases, so does pellicle density, following a general power-law behaviour shown in Figure 5.4b, reaching a value at 1% alginate that is three times higher than that for the pellicle grown in water. The observed increased density and constant cellulose mass indicates the dominant effect of growth medium viscosity increase is a change in microstructural packing of the nanofibers. Because a number of applications of nanofiber meshes involve imparting mechanical strength, it is also of interest to see how the apparent structural changes affect deformation response of the pellicles.

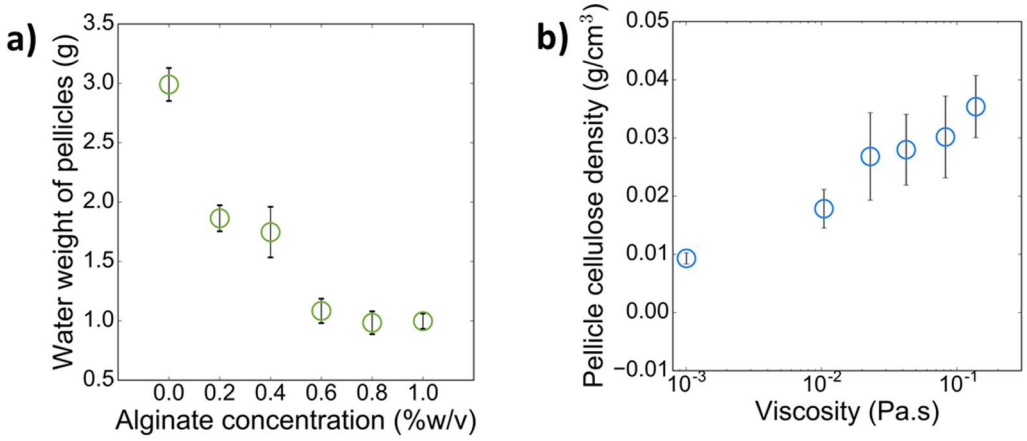

FIGURE 5.4 The change in a) water weight retained in each pellicle with alginate concentration, b) pellicle density with viscosity of alginate solutions

5.3.3 | Effect of medium viscosity on mechanical properties of a cellulose pellicle

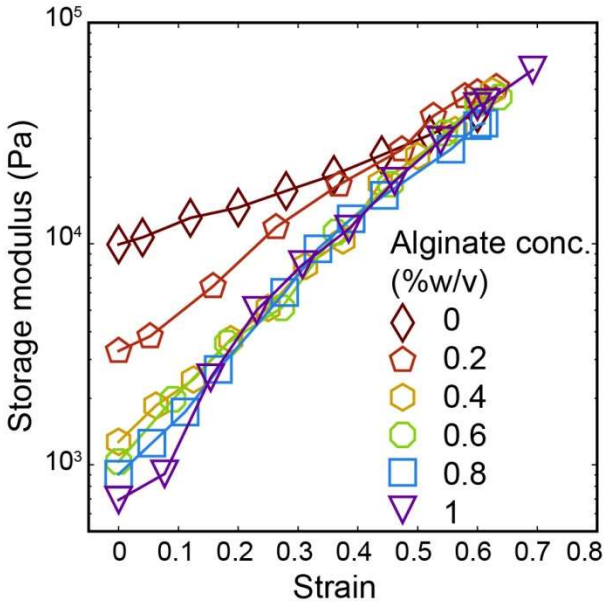

FIGURE 5.5 The change in elastic or storage modulus (G') of pellicles as a function of strain for pellicles grown with different alginate concentrations.

Anisotropic fibres, because of their strong ability to orient during deformation, can often form networks with large variations in nonlinear rheology. An example is actin fibres that form the cytoskeleton of many mammalian cells [33]. Actin networks have been found to exhibit strong strain-stiffening response during extensional deformation, a key mechanism in protection of cells against damage during movement [33, 34]. Here we study the response of the different pellicles produced when they experience a compressional deformation during measurement of viscoelastic properties.

Oscillatory shear of the different pellicles was performed as a measure of dynamic response as well as a means of characterization of network properties like cross-link density [35]. Because the pellicles have different heights, the gap between testing plates is adjusted to the actual height of the pellicles. The deformation, or strain, the pellicles experience is then a normalized ratio of the change in height to

the original height of the pellicle: $\varepsilon = \frac{h_0 p - h_{gap}}{h_0 p}$, where h_0p refers to pellicle height and h_{gap} is the rheometer gap when the measurement is done.

Figure 5.5 shows the measured shear elastic modulus of the different pellicles as a function of applied strain and alginate concentration. As alginate concentration is increased from 0% to 0.2%, an order of magnitude decrease in the zero-strain modulus is observed. Further increases above 0.4% to 1% alginate cause smaller, but still significant, changes in the low-strain modulus, ultimately reducing to about 800 Pa, Figure 5.5. The magnitude of the elastic modulus of polymer networks typically scales with the degree of network cross-linking [35], so Figure 5.5 indicates a potential reduction in cross-linking as a result of alginate-fibre interactions.

The pellicles are also found to exhibit strong strain-hardening for all samples, with Figure 5.5 showing that the modulus of the pellicles increases with increasing applied strain. The increase is significant: more than two orders of magnitude for the highest alginate concentrations. Strain-hardening has also been observed in high aspect ratio actin fibres [34] as well as spun fibres made from regenerated cellulose [36]. The effect of strain hardening is particularly apparent in the samples produced in media containing alginate. As shown in Figure 5.5, the modulus of samples at zero-strain decreases with alginate concentration, but at 60% strain the modulus values are similar (Figure 5.5). This means that the effect of strain-hardening of the pellicles is lower in the samples that were not grown in alginate-contained medium. Strain hardening indicates that structure of a polymer is more entangled or denser, consistent with our finding in Figure 5.4 that pellicles produced in more viscous media are significantly denser.

5.3.4 | Time-dependent properties of pellicles during growth

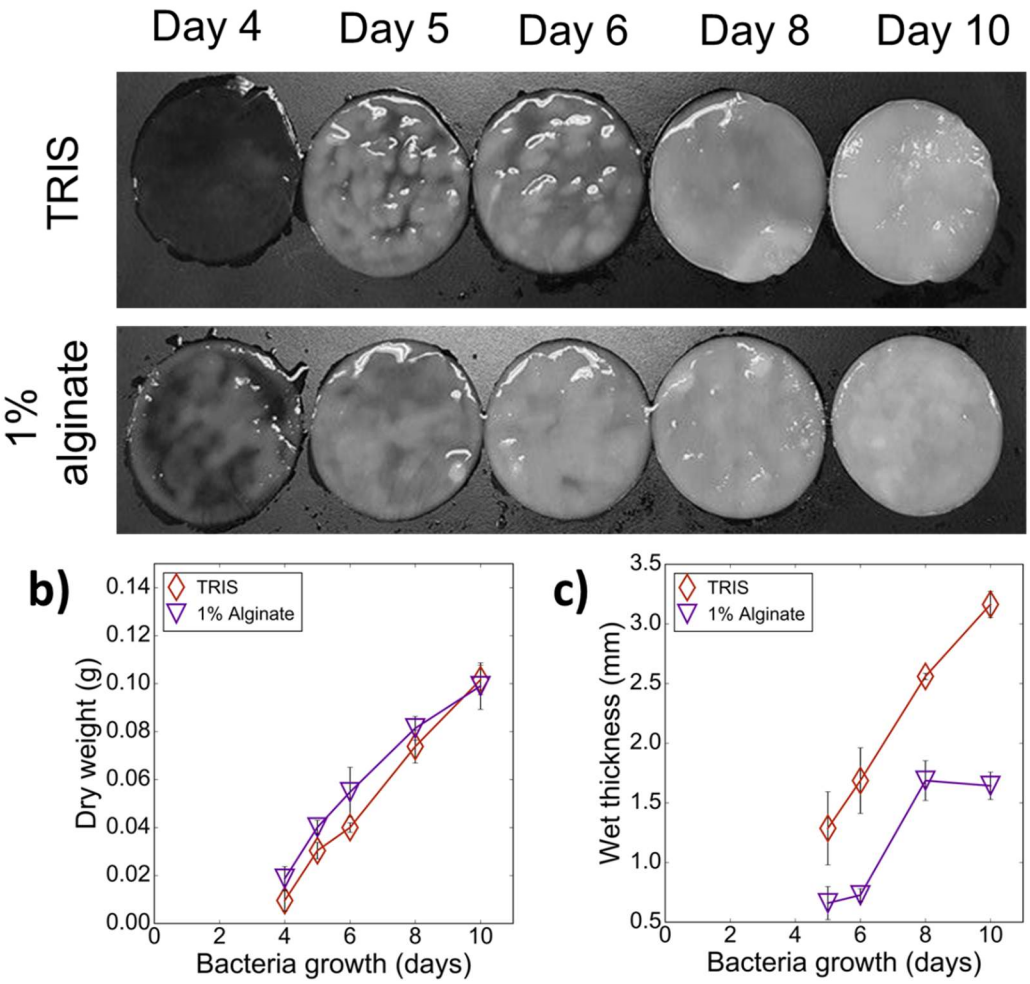

FIGURE 5.6 a) The appearance of pellicles grown in TRIS and 1% alginate at different days; b) the change of dry weight in respect to incubation time (days); c) the change of wet thickness as a function of incubation time.

We also examine the time-dependent properties of pellicles grown in water and in 1% alginate, where the effects of the growth medium are most significant. Figure 5.6a shows the progression of the washed pellicles that are harvested at different stages of growth. Note that below day 4, the pellicles were either incoherent or too thin to be harvested, as observed in Figure 5.1. The day 4 pellicles that were grown in water are essentially transparent, indicating a low density of fibres. As the incubation time progresses, the pellicles become increasingly opaque as the

fibre density increases and scatters more light. Differences for pellicles grown in 1% alginate solution are immediately apparent, as they appear denser from day 4. When the dry weights of the pellicles are compared in Figure 5.6b it is clear that the two cultures produce cellulose at the same rate (Figure 5.6b). The dry weight of both pellicles increases linearly with incubation time.

Thickness measurements of the pellicles in Figure 5.6c, however show that the wet thickness of the pellicles in water increases linearly with time while the thickness of pellicles in 1% alginate increases more slowly and quickly plateaus around day 8. For all samples over the course of the growth process, the wet thickness of the pellicles in 1% alginate never exceeds the thickness of pellicles grown in water (Figure 5.6c).

All of these imply that the main difference between the productions of pellicles in the two media is a result of differences during the growth of the final pellicle. The transport to the air-liquid interface from the bulk volume appears to be unaffected by medium rheology, as the dry weight does not significantly vary with alginate concentration. However, after the initial pellicle forms, the pellicles grown in alginate experience decreasing height expansion.

When pellicles are thickening at the latter stages of growth, the extent of cellulose fibre growth is a function of the bacterial mobility. Hydrodynamic drag on movement of bacteria is directly proportional to the viscosity of the surrounding fluid medium. As alginate increases medium viscosity, the bacteria move shorter distances in a given time than culture at lower viscosity levels. The amount of difference in height, however, does not scale directly with the change in viscosity, as height is decreased by a factor of three, while viscosity is increased by a factor of 100. Other effects might contribute such as the attraction between alginate and cellulose that will be described in the next section.

5.3.5 | The attraction between alginate and cellulose, and its effect on pellicle final structure

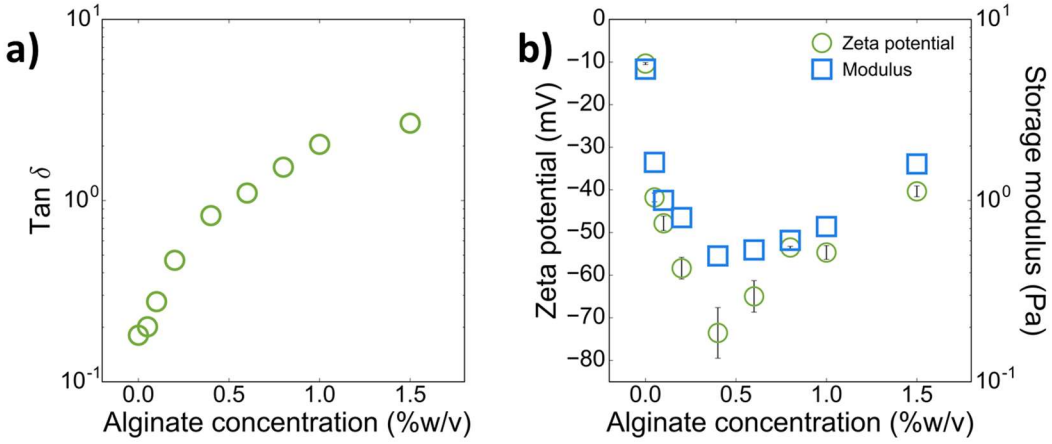

FIGURE 5.7 a) Change in tan δ of cellulose dispersion with alginate concentration, b) Change in storage modulus and yield stress of cellulose dispersion with alginate concentration.

When alginate solutions with the same concentration as the ones used in the study are added to the same concentration of dispersed fibres, there is an increase in tan delta (Figure 5.7a). At lower concentration of alginate (less than 0.5%), there is a decrease in storage modulus, however at higher concentration (larger than 0.5%) there is an increase in storage modulus (Figure 5.7b). This suggests there is a change in the attractive interaction between cellulose fibres as a result of the alginate.

To understand types of interaction that might occur between the cellulose fibres in the presence of alginate, total intermolecular forces were calculated by assuming the cellulose fibres as two parallel plates, according to two flat plates model [28] (See Materials and Methods, part 5.2.7). From the calculation, it is found that at very small distances, electrostatic repulsion dominates in all systems (including the one with no alginate). At around 15nm, the electrostatic force quickly diminishes to zero. For samples with 0.2% alginate, at this point onwards we can see (Figure 5.8) that depletion force becomes the dominant force in the system. A

four-fold increase of total depletion energy from 0.2% (Figure 5.8a) to 1% alginate (Figure 5.8f) is predicted.

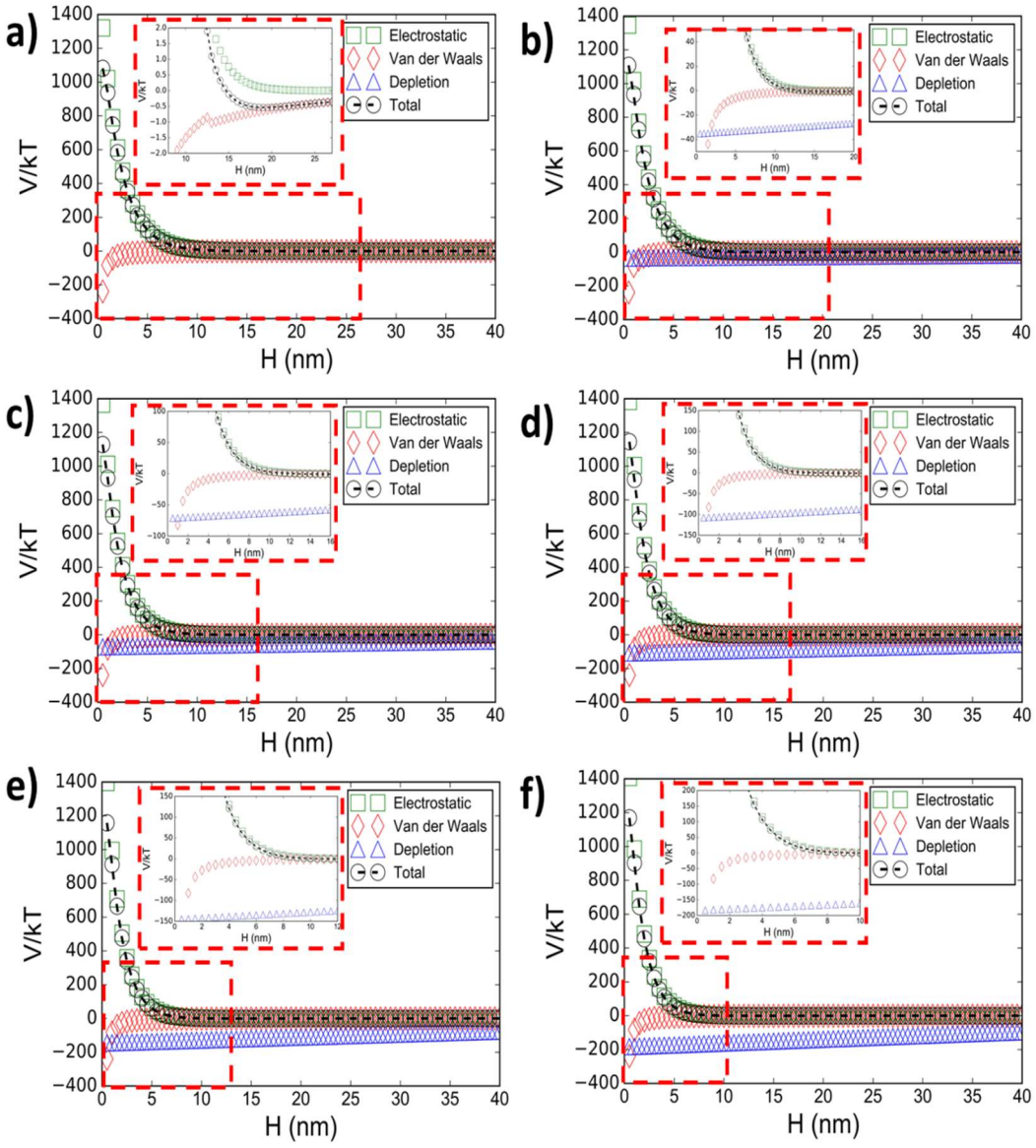

FIGURE 5.8 The calculation of intermolecular forces in the system with different concentration of alginate, a) 0% alginate, b) 0.2% alginate, c) 0.4% alginate, d) 0.6% alginate, e) 0.8% alginate, f) 1% alginate. The insets show zoom-in area of the part of figures in the red squares.

Although Figure 5.7 shows the behaviour of dispersed cellulose fibres in alginate solution, during bacteria growth/pellicle formation, the amount of alginate stays

the same while the cellulose being produced increases overtime. This means that the actual concentration of alginate exposed to fibres decreases as more cellulose forms. Therefore, here we use ratio of moles of alginate to surface area of cellulose, as this should reflect more precisely the conditions during cellulose production (See Materials and Methods part 5.2.8).

Figure 5.9a shows the calculated ratio of dispersed cellulose in alginate that is converted into the ratio of moles of alginate to surface area of cellulose against the actual alginate concentration. It shows that with increasing alginate concentration, the ratio increases from 10^{-5} to $5x10^{-3}$. Figure 5.9b shows the calculated ratio of moles of alginate to surface area of cellulose against the day of growth (See material and method). Figure 5.9c shows the zeta potential data against the ratio of moles of alginate to surface area of cellulose. Here, it can be seen that the relevant zeta potential data are the first five data points. This also indicates that at the early days (day 4), the ratio is around 10^{-4} (Figure 5.9b) and at final days it decreases to around 10^{-5} (Figure 5.9b). In figure 5.9c, this refers to zeta potential from around -80mV (day 4) to around -10mV (day 10). This also suggests the fact that, during growth, cellulose becomes more colloidally unstable and prone to aggregation.

As there is an increasing instability of fibres with higher concentrations of alginate, this likely explains why the pellicle height becomes compressed. Also, the change in the fibre interaction should also change the microstructure of the pellicles. Therefore, confocal microscopy study was performed to examine the pellicle structures in more detail.

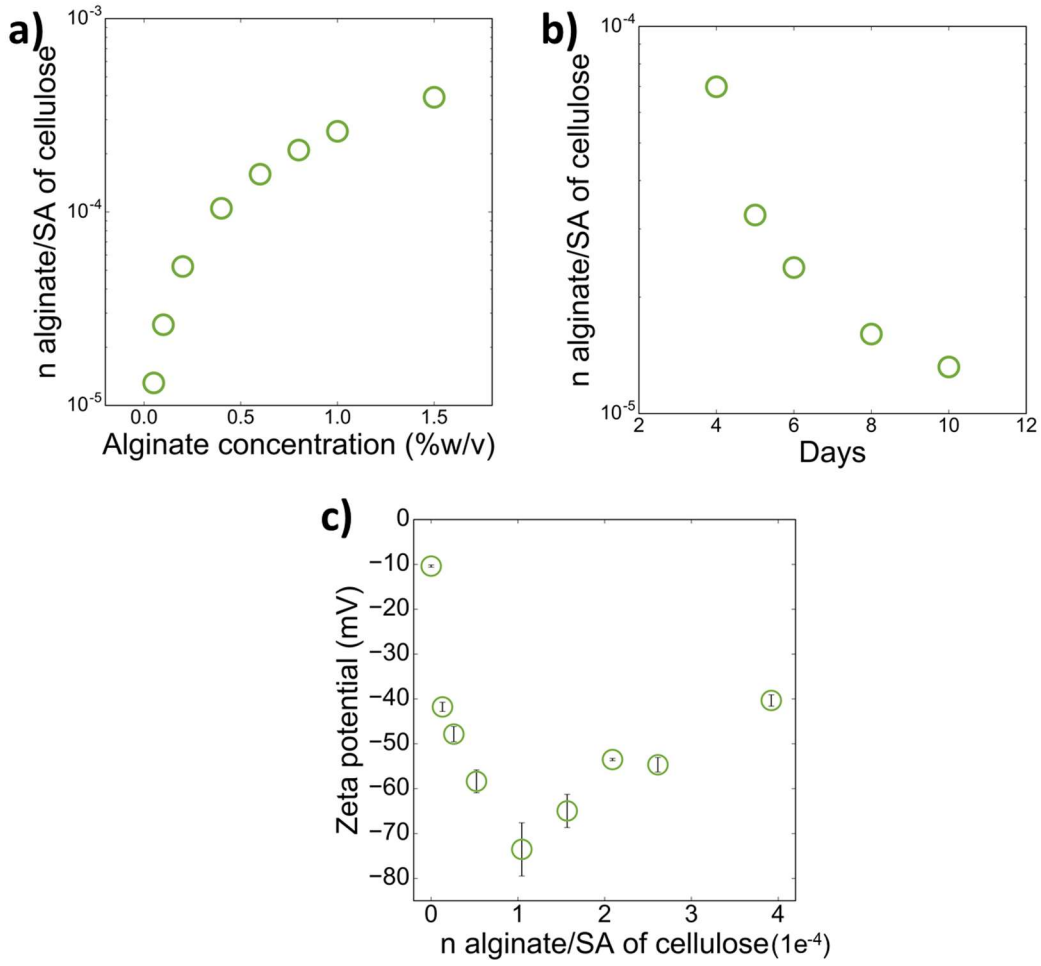

FIGURE 5.9 a) The change of ratio of alginate to surface area of cellulose fibres in respect to alginate concentration (%w/v), b) The change of ratio of alginate to surface area of cellulose fibres in respect to days of growth (data from dry weight of pellicles grown in 1% alginate), c) The change zeta potential in respect of ratio of moles of alginate to surface area of cellulose fibres (data from dispersed fibres).

Figure 5.10 shows that the orientation of fibres in pellicles grown with no alginate is largely random, while the systems containing alginate show increased alignment and local orientation. The effect of alginate is observed whether scanning from either side, the top (facing the air interface) or bottom of the pellicle (facing the liquid interface), although overall orientation varies because of differences in the bulk pellicle assembly process.

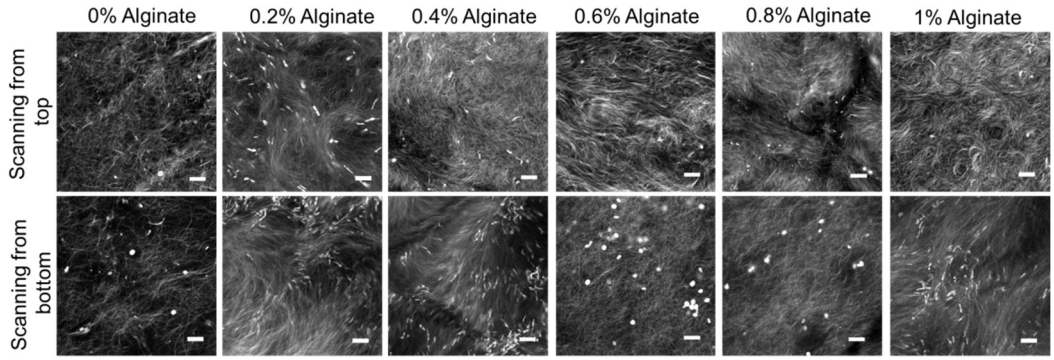

FIGURE 5.10 Confocal images of the structure of pellicles grown in medium with different viscosity. Increasing alginate levels constrain growth and increase attraction between fibres, leading to increased alignment at higher concentrations, though the random nature of pellicle folding, assembly, and continued growth can make quantification difficult. Scale bar is 10 μm.

5.4 CONCLUSIONS

The growth of biofilm in media with systematically varied viscosity causes a significant change in the mechanical properties of the bacterial cellulose structure produced by *Acetobacter xylinum*, though we find no significant change in the cellulose production rate. The production of cellulose by the bacteria is similar in all media studied. As viscosity increases, the mobility of the bacteria is reduced, focusing their growth on a progressively smaller volume as alginate concentration steadily increases the viscosity of the growth medium. The alginate polymers are also shown to increase the attractive interactions between cellulose fibres as they grow, causing them to bundle more tightly together and further hinder expansion of the cellulose pellicle, increasing its final density. The combined effects are a simple physical mechanism that allows engineering of the final mechanical and structural properties of a nanofiber mesh, with benefits envisioned for control of pore size, transport, adhesion, and tissue interactions.

5.5 REFERENCES

1. Yamanaka, S., K. Watanabe, N. Kitamura, M. Iguchi, S. Mitsuhashi, Y. Nishi, and M. Uryu, *The structure and mechanical properties of sheets prepared from bacterial cellulose.* Journal of Materials Science, 1989. **24**(9): p. 3141-3145.

2. Mühlethaler, K., *The structure of bacterial cellulose.* Biochimica et Biophysica Acta, 1949. **3**: p. 527-535.

3. Sanchavanakit, N., W. Sangrungraungroj, R. Kaomongkolgit, T. Banaprasert, P. Pavasant, and M. Phisalaphong, *Growth of Human Keratinocytes and Fibroblasts on Bacterial Cellulose Film.* Biotechnology Progress, 2006. **22**(4): p. 1194-1199.

4. Bäckdahl, H., G. Helenius, A. Bodin, U. Nannmark, B.R. Johansson, B. Risberg, and P. Gatenholm, *Mechanical properties of bacterial cellulose and interactions with smooth muscle cells.* Biomaterials, 2006. **27**(9): p. 2141-2149.

5. Svensson, A., E. Nicklasson, T. Harrah, B. Panilaitis, D.L. Kaplan, M. Brittberg, and P. Gatenholm, *Bacterial cellulose as a potential scaffold for tissue engineering of cartilage.* Biomaterials, 2005. **26**(4): p. 419-431.

6. Foster, L. and P. Moore, *The application of a cellulose-based fibre dressing in surgical wounds.* Journal of Wound Care, 1997. **6**(10): p. 469-473.

7. Emady, H., M. Caggioni, and P.T. Spicer, *Colloidal microstructure effects on particle sedimentation in yield stress fluids.* Journal of Rheology, 2013. **57**(6): p. 1761-1772.

8. Young, P.M., D. Traini, H.X. Ong, A. Granieri, B. Zhu, S. Scalia, J. Song, and P.T. Spicer, *Novel nano-cellulose excipient for generating non-Newtonian droplets for targeted nasal drug delivery.* Drug Development and Industrial Pharmacy, 2017. **43**(10): p. 1729-1733.

9. Schramm, M. and S. Hestrin, *Factors affecting Production of Cellulose at the Air/ Liquid Interface of a Culture of Acetobacter xylinum.* Microbiology, 1954. **11**(1): p. 123-129.

10. Krystynowicz, A., W. Czaja, A. Wiktorowska-Jezierska, M. Gonçalves-Miśkiewicz, M. Turkiewicz, and S. Bielecki, *Factors affecting the yield and properties of bacterial cellulose.* Journal of Industrial Microbiology and Biotechnology, 2002. **29**(4): p. 189-195.

11. Watanabe, K., M. Tabuchi, Y. Morinaga, and F. Yoshinaga, *Structural Features and Properties of Bacterial Cellulose Produced in Agitated Culture.* Cellulose, 1998. **5**(3): p. 187-200.

12. Mikkelsen, D., B.M. Flanagan, G.A. Dykes, and M.J. Gidley, *Influence of different carbon sources on bacterial cellulose production by*

Gluconacetobacter xylinus strain ATCC 53524. Journal of Applied Microbiology, 2009. **107**(2): p. 576-583.

13. Mohammadkazemi, F., M. Azin, and A. Ashori, *Production of bacterial cellulose using different carbon sources and culture media.* Carbohydrate Polymers, 2015. **117**: p. 518-523.

14. Ruka, D.R., G.P. Simon, and K.M. Dean, *Altering the growth conditions of Gluconacetobacter xylinus to maximize the yield of bacterial cellulose.* Carbohydrate Polymers, 2012. **89**(2): p. 613-622.

15. Jagannath, A., A. Kalaiselvan, S.S. Manjunatha, P.S. Raju, and A.S. Bawa, *The effect of pH, sucrose and ammonium sulphate concentrations on the production of bacterial cellulose (Nata-de-coco) by Acetobacter xylinum.* World Journal of Microbiology and Biotechnology, 2008. **24**(11): p. 2593.

16. Hutchens, S.A., R.V. León, H.M. O'Neill, and B.R. Evans, *Statistical analysis of optimal culture conditions for Gluconacetobacter hansenii cellulose production.* Letters in Applied Microbiology, 2007. **44**(2): p. 175-180.

17. Cheng, K.-C., J.M. Catchmark, and A. Demirci, *Effect of different additives on bacterial cellulose production by Acetobacter xylinum and analysis of material property.* Cellulose, 2009. **16**(6): p. 1033.

18. Bae, S., Y. Sugano, and M. Shoda, *Improvement of bacterial cellulose production by addition of agar in a jar fermentor.* Journal of Bioscience and Bioengineering, 2004. **97**(1): p. 33-38.

19. Zhou, L.L., D.P. Sun, L.Y. Hu, Y.W. Li, and J.Z. Yang, *Effect of addition of sodium alginate on bacterial cellulose production by Acetobacter xylinum.* Journal of Industrial Microbiology & Biotechnology, 2007. **34**(7): p. 483.

20. Chao, Y., M. Mitarai, Y. Sugano, and M. Shoda, *Effect of Addition of Water-Soluble Polysaccharides on Bacterial Cellulose Production in a 50-L Airlift Reactor.* Biotechnology Progress, 2001. **17**(4): p. 781-785.

21. Huang, H.-C., L.-C. Chen, S.-B. Lin, C.-P. Hsu, and H.-H. Chen, *In situ modification of bacterial cellulose network structure by adding interfering substances during fermentation.* Bioresource Technology, 2010. **101**(15): p. 6084-6091.

22. Kanjanamosit, N., C. Muangnapoh, and M. Phisalaphong, *Biosynthesis and characterization of bacteria cellulose–alginate film.* Journal of Applied Polymer Science, 2010. **115**(3): p. 1581-1588.

23. Tokoh, C., K. Takabe, M. Fujita, and H. Saiki, *Cellulose Synthesized by Acetobacter Xylinum in the Presence of Acetyl Glucomannan.* Cellulose, 1998. **5**(4): p. 249-261.

24. Dayal, M.S. and J.M. Catchmark, *Mechanical and structural property analysis of bacterial cellulose composites.* Carbohydrate Polymers, 2016. **144**: p. 447-453.

25. Phisalaphong, M., T. Suwanmajo, and P. Tammarate, *Synthesis and characterization of bacterial cellulose/alginate blend membranes.* Journal of Applied Polymer Science, 2008. **107**(5): p. 3419-3424.

26. Seifert, M., S. Hesse, V. Kabrelian, and D. Klemm, *Controlling the water content of never dried and reswollen bacterial cellulose by the addition of water-soluble polymers to the culture medium.* Journal of Polymer Science Part A: Polymer Chemistry, 2004. **42**(3): p. 463-470.

27. Schneider, C.A., W.S. Rasband, and K.W. Eliceiri, *NIH Image to ImageJ: 25 years of image analysis.* Nat Meth, 2012. **9**(7): p. 671-675.

28. Boluk, Y., L. Zhao, and V. Incani, *Dispersions of Nanocrystalline Cellulose in Aqueous Polymer Solutions: Structure Formation of Colloidal Rods.* Langmuir, 2012. **28**(14): p. 6114-6123.

29. Onuma, K. and N. Kanzaki, *Size Distribution and Intermolecular Interaction of Laminin-1 in Physiological Solutions.* The Journal of Physical Chemistry B, 2003. **107**(42): p. 11799-11804.

30. Buining, P.A., A.P. Philipse, and H.N.W. Lekkerkerker, *Phase Behavior of Aqueous Dispersions of Colloidal Boehmite Rods.* Langmuir, 1994. **10**(7): p. 2106-2114.

31. Sun, C., *True Density of Microcrystalline Cellulose.* Journal of Pharmaceutical Sciences, 2005. **94**(10): p. 2132-2134.

32. Draget, K.I., G. Skjåk-Bræk, and B.T. Stokke, *Similarities and differences between alginic acid gels and ionically crosslinked alginate gels.* Food Hydrocolloids, 2006. **20**(2): p. 170-175.

33. Gardel, M.L., J.H. Shin, F.C. MacKintosh, L. Mahadevan, P.A. Matsudaira, and D.A. Weitz, *Scaling of F-Actin Network Rheology to Probe Single Filament Elasticity and Dynamics.* Physical Review Letters, 2004. **93**(18): p. 188102.

34. Xu, J., Y. Tseng, and D. Wirtz, *Strain Hardening of Actin Filament Networks: Regulation by the Dynamic Cross-linking Protein α-Actinin.* Journal of Biological Chemistry, 2000. **275**(46): p. 35886-35892.

35. Calvet, D., J.Y. Wong, and S. Giasson, *Rheological Monitoring of Polyacrylamide Gelation: Importance of Cross-Link Density and Temperature.* Macromolecules, 2004. **37**(20): p. 7762-7771.

36. Gindl, W. and J. Keckes, *Strain hardening in regenerated cellulose fibres.* Composites Science and Technology, 2006. **66**(13): p. 2049-2053.

CHAPTER 6

Conclusions & Recommendations

6.1 GENERAL CONCLUSION

The study presented in this thesis aimed to improve the understanding of microstructural characteristics of biological fluids, specifically biofilms. The study also expands the knowledge of how biological fluid microstructure can be modified by engineering growth or external treatments.

The literature review chapter summarises current knowledge of microstructural heterogeneity in biological fluids and the importance of heterogeneity characterisation. Biological fluid heterogeneity often occurs as a result of heterogeneous interaction between the fluid building blocks, which can include different polysaccharides, proteins, DNA and even cells. Different techniques are available to study heterogeneity, including microscopy techniques such as confocal or SEM as well as passive and active microrheology.

The first study her developed a model system with controllable degrees of heterogeneity using gellan gels. At most of the length scales studied, gellan gels are always homogeneous even when two different salts were mixed together to create a single gel. To control the degree of heterogeneity, two gellan gels (called hard and soft gel) with different concentration of polymer and salts were prepared and get mixed together. However, it seems that the difference in the salt concentration created an osmotic gradient between the two gels, and shear from the mixing helped them to quickly equilibrate to become a single gel. This can be observed in all concentrations of hard gels studied here. When these two gels were placed side-by-side, although osmotic gradients still exist, the salts diffuse slowly to gels with lower concentrations of salt. As no mixing occurs, heterogeneity can be observed even at later times after the soft gel hardened to have the same properties as the one observed in bulk. Even though gellan is able to mimic bulk rheological properties of a biofilm, however the mixture of two different gellan gels with different properties could not mimic the heterogeneity found in biofilm at microscale.

The second study investigated the effect of treatment on the microstructure of *E. coli* biofilm. The initial *E. coli* structure is relatively dispersed and after plasma treatment, the structure changed into a more aggregated structure. This

phenomenon can be observed even at the shortest treatment time. The interesting finding is that this structure is retained after regrowth of the biofilm, and due to this aggregated structure the regrown biofilm is more resistant than before treatment. The change of structure observed here was mostly due to the drying effect of plasma jet rather than to chemicals produced by plasma.

In the third study, the effect of environmental conditions on the microstructure of *A. xylinum* biofilm is studied. *A. xylinum* produced cellulose pellicles at the air-liquid interface. Alginate, a polysaccharide, was then added to the growth medium to increase its viscosity. The production of cellulose was not changed, but the bulk properties such as pellicle thickness and bulk modulus and the pellicle microstructure were changed. As the amount of cellulose produced was the same, the pellicles grown in alginate were denser than those grown in normal growth medium. The addition of alginate causes depletion attraction between cellulose fibres, and limits bacterial mobility, causing the change in the microstructure.

6.2 RECOMMENDATIONS FOR FUTURE STUDY

In future study, some aspects presented in this thesis should be explored more. This could be:

- The mixture of polysaccharides from another source such as carrageenan or alginate with gellan could be explored as another heterogeneity model of biofilm presented in Chapter 3. In addition, it is also possible to use the mixture of different types of gellan, in particular the one with different acyl contents. These gellan derivatives give different type of gels, which are relatively less brittle.
- In Chapter 4, to better understand the effect of plasma on structural properties of biofilm, different plasma condition can be explored such as changing the gas source. This to assure if other purer gases (such as pure helium) can cause drying and gives the same effect.
- Evaluate the effect of plasma on mechanical properties and heterogeneity of biofilm using other techniques, such as AFM. The preliminary studies

done here show that plasma causes the beads used for tracking aggregate. Hence, particle tracking cannot be used in the system.

- Future studies for plasma effects on biofilm structure, should also elucidate the different polysaccharide compositions and ratios at different biofilm ages. This will clarify whether the increase resistance is due to actual EPS formation (different polysaccharides composition) or is due to fibrial adhesion.
- Alginate is a negatively charged (anionic) polysaccharides, which in Chapter 5 was found to change attraction of the cellulose fibers. It could be interesting for future studies to evaluate the effect of polysaccharides with positive charges (cationic) to change the viscosity of the medium and at the same time cause different types of interaction with cellulose fibers.
- Future studies should focus on further quantification (in more detail) of structural changes of the fiber mat. Techniques, such AFM, FTIR and confocal coupled with Fourier Transformation are the suggested approaches to improve the studies performed in this thesis.
-

Appendices

Copyright statements

SPRINGER NATURE LICENSE
TERMS AND CONDITIONS

Aug 27, 2018

This Agreement between UNSW -- Goldina Kwandou ("You") and Springer Nature ("Springer Nature") consists of your license details and the terms and conditions provided by Springer Nature and Copyright Clearance Center.

License Number	4417330838482
License date	Aug 27, 2018
Licensed Content Publisher	Springer Nature
Licensed Content Publication	Nature Reviews Microbiology
Licensed Content Title	The biofilm matrix
Licensed Content Author	Hans-Curt Flemming, Jost Wingender
Licensed Content Date	Aug 2, 2010
Licensed Content Volume	8
Licensed Content Issue	9
Type of Use	Thesis/Dissertation
Requestor type	academic/university or research institute
Format	print and electronic
Portion	figures/tables/illustrations
Number of figures/tables/illustrations	2
High-res required	no
Will you be translating?	no
Circulation/distribution	<501
Author of this Springer Nature content	no
Title	Characterisation and control of biofilm and biofluid microstructure and rheology
Instructor name	n/a
Institution name	UNSW
Expected presentation date	Aug 2018
Portions	figure 1c, d
Requestor Location	UNSW Building F10 (chemical science Building) High St Kensington, NSW 2052 Australia Attn: UNSW
Billing Type	Invoice
Billing Address	UNSW Building F10 (chemical science Building) High St

SPRINGER NATURE LICENSE
TERMS AND CONDITIONS

Aug 28, 2018

This Agreement between UNSW -- Goldina Kwandou ("You") and Springer Nature ("Springer Nature") consists of your license details and the terms and conditions provided by Springer Nature and Copyright Clearance Center.

License Number	4417650555241
License date	Aug 28, 2018
Licensed Content Publisher	Springer Nature
Licensed Content Publication	Nature Materials
Licensed Content Title	Fractal heterogeneity in minimal matrix models of scars modulates stiff-niche stem-cell responses via nuclear exit of a mechanorepressor
Licensed Content Author	P. C. Dave P. Dingal, Andrew M. Bradshaw, Sangkyun Cho, Matthew Raab, Amnon Buxboim et al.
Licensed Content Date	Jul 13, 2015
Licensed Content Volume	14
Licensed Content Issue	9
Type of Use	Thesis/Dissertation
Requestor type	academic/university or research institute
Format	print and electronic
Portion	figures/tables/illustrations
Number of figures/tables/illustrations	1
High-res required	no
Will you be translating?	no
Circulation/distribution	<501
Author of this Springer Nature content	no
Title	Characterisation and control of biofilm and biofluid microstructure and rheology
Instructor name	n/a
Institution name	UNSW
Expected presentation date	Aug 2018
Portions	figure 5a
Requestor Location	UNSW Building F10 (chemical science Building) High St Kensington, NSW 2052 Australia Attn: UNSW
Billing Type	Invoice
Billing Address	UNSW Building F10 (chemical science Building)

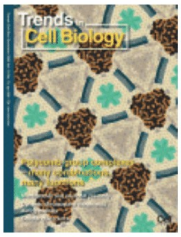

Title: Biological hydrogels as selective diffusion barriers
Author: Oliver Lieleg,Katharina Ribbeck
Publication: Trends in Cell Biology
Publisher: Elsevier
Date: September 2011

Order Completed

Thank you for your order.

This Agreement between UNSW -- Goldina Kwandou ("You") and Elsevier ("Elsevier") consists of your license details and the terms and conditions provided by Elsevier and Copyright Clearance Center.

Your confirmation email will contain your order number for future reference.

printable details

License Number	4418660310351
License date	Aug 30, 2018
Licensed Content Publisher	Elsevier
Licensed Content Publication	Trends in Cell Biology
Licensed Content Title	Biological hydrogels as selective diffusion barriers
Licensed Content Author	Oliver Lieleg,Katharina Ribbeck
Licensed Content Date	Sep 1, 2011
Licensed Content Volume	21
Licensed Content Issue	9
Licensed Content Pages	9
Type of Use	reuse in a thesis/dissertation
Portion	figures/tables/illustrations
Number of figures/tables/illustrations	1
Format	both print and electronic
Are you the author of this Elsevier article?	No
Will you be translating?	No
Original figure numbers	Figure 2
Title of your thesis/dissertation	Characterisation and control of biofilm and biofluid microstructure and rheology
Publisher of new work	UNSW
Expected completion date	Aug 2018
Estimated size (number of pages)	180
Requestor Location	UNSW Building F10 (chemical science Building) High St

Many thanks for sending the permissions request below. The Royal Society of Chemistry hereby grants permission for the use of the material specified below in your thesis.

Please note that if the material specified below or any part of it appears with credit or acknowledgement to a third party then you must also secure permission from that third party before reproducing that material.

Please ensure that the published article carries a credit to The Royal Society of Chemistry in the following format:

[Original citation] – Reproduced by permission of The Royal Society of Chemistry

and that any electronic version of the work includes a hyperlink to the article on the Royal Society of Chemistry website.

Best wishes,

Chloe Szebrat
Contracts and Copyright Executive
Royal Society of Chemistry
Thomas Graham House
Science Park, Milton Road
Cambridge, CB4 0WF, UK
Tel: +44 (0) 1223 438329
www.rsc.org

From: noreply@rsc.org <noreply@rsc.org>
Sent: 30 August 2018 09:11
To: CONTRACTS-COPYRIGHT (shared) <Contracts-Copyright@rsc.org>
Cc: g.kwandou@unsw.edu.au
Subject: Permission Request Form: Goldina Kwandou

Name : Goldina Kwandou
Address :

HIgh Street

Kensington 2052 NSW Australia

Tel : 0293854806
Fax :
Email : g.kwandou6@unsw.edu.au

I am preparing the following work for publication:

Article/Chapter Title : Characterization and control of biofilm and biofluid microstructure and rheology

Journal/Book Title : Thesis
Editor/Author(s) : Goldina Kwandou
Publisher : Thesis Dissertetion - University of New South Wales

I would very much appreciate your permission to use the following material:

Journal/Book Title : Structure and dynamics of cross-linked actin networks/ Soft Matter
Editor/Author(s) : Oliver Lieleg, Mireille M. A. E. Claessens and Andreas R. Bausch
Volume Number : 6
Year of Publication : 2010
Description of Material : Figure 3B
Page(s) : 222

Any Additional Comments :

I'd like to use and cite the above mention figure in the introduction of my thesis

American Physical Society
Reuse and Permissions License

29-Aug-2018

This license agreement between the American Physical Society ("APS") and Goldina Kwandou ("You") consists of your license details and the terms and conditions provided by the American Physical Society and SciPris.

Licensed Content Information

License Number:	**RNP/18/AUG/007270**
License date:	29-Aug-2018
DOI:	10.1103/PhysRevE.64.061506
Title:	Investigating the microenvironments of inhomogeneous soft materials with multiple particle tracking
Author:	M. T. Valentine et al.
Publication:	Physical Review E
Publisher:	American Physical Society
Cost:	USD $ 0.00

Request Details

Does your reuse require significant modifications: No

Specify intended distribution locations:	UK & Commonwealth (excluding Canada)
Reuse Category:	Reuse in a thesis/dissertation
Requestor Type:	Student
Items for Reuse:	Figures/Tables
Number of Figure/Tables:	2
Figure/Tables Details:	Figure 3a and 4a
Format for Reuse:	Print and Electronic
Total number of print copies:	Up to 1000

Information about New Publication:

University/Publisher:	UNSW
Title of dissertation/thesis:	Characterization and control of biofilm and biofluid microstructure and rheology
Author(s):	Goldina Kwandou
Expected completion date:	Aug. 2018

License Requestor Information

Name:	Goldina Kwandou
Affiliation:	Individual
Email Id:	g.kwandou@unsw.edu.au
Country:	Australia

JOHN WILEY AND SONS LICENSE TERMS AND CONDITIONS

Aug 27, 2018

This Agreement between UNSW -- Goldina Kwandou ("You") and John Wiley and Sons ("John Wiley and Sons") consists of your license details and the terms and conditions provided by John Wiley and Sons and Copyright Clearance Center.

License Number	4417400370996
License date	Aug 27, 2018
Licensed Content Publisher	John Wiley and Sons
Licensed Content Publication	Plasma Processes and Polymers
Licensed Content Title	Complex Responses of Microorganisms as a Community to a Flowing Atmospheric Plasma
Licensed Content Author	Danny L. Bayliss, James L. Walsh, Felipe Iza, et al
Licensed Content Date	Mar 20, 2012
Licensed Content Volume	9
Licensed Content Issue	6
Licensed Content Pages	15
Type of use	Dissertation/Thesis
Requestor type	University/Academic
Format	Print and electronic
Portion	Figure/table
Number of figures/tables	1
Original Wiley figure/table number(s)	Figure 6a
Will you be translating?	No
Title of your thesis / dissertation	Characterisation and control of biofilm and biofluid microstructure and rheology
Expected completion date	Aug 2018
Expected size (number of pages)	180
Requestor Location	UNSW Building F10 (chemical science Building) High St Kensington, NSW 2052 Australia Attn: UNSW
Publisher Tax ID	EU826007151
Total	0.00 USD
Terms and Conditions	

TERMS AND CONDITIONS

This copyrighted material is owned by or exclusively licensed to John Wiley & Sons, Inc. or one of its group companies (each a"Wiley Company") or handled on behalf of a society with which a Wiley Company has exclusive publishing rights in relation to a particular work